8-2011

Spatially Resolved Laser and Thermal Desorption/ Ionization Coupled with Mass Spectrometry

Olga Sergeevna Ovchinnikova
University of Tennessee - Knoxville, oovchinn@utk.edu

To the Graduate Council:

I am submitting herewith a dissertation written by Olga Sergeevna Ovchinnikova entitled "Spatially Resolved Laser and Thermal Desorption/Ionization Coupled with Mass Spectrometry." I have examined the final electronic copy of this dissertation for form and content and recommend that it be accepted in partial fulfillment of the requirements for the degree of Doctor of Philosophy, with a major in Physics.

Robert N. Compton, Major Professor

We have read this dissertation and recommend its acceptance:

Gary J. Van Berkel, Joseph H. Macek, Hanno H. Weitering, David C. Joy

Accepted for the Council:
Dixie L. Thompson

Vice Provost and Dean of the Graduate School

(Original signatures are on file with official student records.)

To the Graduate Council:

I am submitting herewith a dissertation written by Olga Sergeevna Ovchinnikova entitled "Spatially Resolved Laser and Thermal Desorption/Ionization Coupled with Mass Spectrometry." I have examined the final electronic copy of this thesis for form and content and recommend that it be accepted in partial fulfillment of the requirements for the degree of Doctor of Philosophy, with a major in Physics.

Robert N. Compton , Major Professor

We have read this dissertation
and recommend its acceptance:

Gary J. Van Berkel

Joseph H. Macek

Hanno H. Weitering

David C. Joy

Accepted for the Council:

Carolyn R. Hodges
Vice Provost and Dean of the Graduate School

(Original signatures are on file with official student records.)

Spatially Resolved Laser and Thermal Desorption/Ionization Coupled with Mass Spectrometry

A Dissertation Presented for the
Doctor of Philosophy
Degree
The University of Tennessee, Knoxville

Olga Sergeevna Ovchinnikova
August 2011

ACKNOWLEDGEMENTS

I would like to thank my advisor, Dr. Gary J. Van Berkel. His support and guidance of my work throughout my studies has allowed me to develop the necessary skills of an independent researcher within a cutting edge laboratory environment. I thank him for opportunity to work in his laboratory and learn from him. Also, I would like to thank, Dr. Robert Compton. His advice and counsel over the years have been of equal importance. I would further like to thank Dr. Vilmos Kertesz for his effort on teaching me the necessary skills needed to conduct quality independent research and to succeed in science. I would also like to thank Dr. Soren Sorensen and the Department of Physics for allowing me to take a two month maternity leave after the birth of my daughter Elizabeth; that time was invaluable to both my family and I. Additionally, I would like to thank my committee members Dr. Robert Compton, Dr. Joseph Macek, Dr. David Joy and Dr. Hanno Weitering. I greatly appreciate their time and input to this dissertation. Furthermore, I would like to thank Dr. Sergei Kalinin, for all the useful scientific discussion regarding atomic force microscopy. Finally, I would like to thank my fellow laboratory co-workers, Mathew Walworth, Dr. Mariam ElNaggar, Dr. Whitney Parson, Dr. James Bradshaw and Joe Stankovich for their help, support, laughter and scientific dialogue throughout the years which have made the research environment absolutely awesome. Especially, I would like to thank Mariam for being world's best office mate, by making everyday at work interesting.

Most importantly I would like to thank my family, my father Dr. Serguei Ovchinnikov and mother Alexandra and brother Oleg for their constant support through out my career. Especially, I would like to thank my husband Dr. Stephen Jesse for his

constant belief and encouragement, and tireless support throughout my career. I would not have been able to succeed without his love and support. Also, I am grateful to my daughter Elizabeth for her ability to make every day worthwhile through her smile and laughter.

ABSTRACT

The work discussed in this dissertation is aimed at creating novel approaches to chemical imaging that ultimately allow for submicron resolution. This goal has been approached from two direction using laser based desorption and coupling it with an AFM using apertureless tip-enhanced laser ablation/ionization. The second direction was through the development a new approach to thermal desorption based mass spectrometry experiments by using a proximal probe to spatially desorb the surface and ionizing the plume of neutrals using a secondary ionization source at atmospheric pressure. The thermal desorption approach allows for the easy scaling of the technique all the way from the millimeter to the nanometer regime. In the nanometer regime an AFM platform with silicon based heating AFM probes is used to locally desorb material from nanometer sized craters. The final work in this thesis focused on trying to improve laser based desorption through a secondary ionization of the neutrals plume by capturing the laser desorption plume into a liquid and then electrospaying the solution into a MS. The added benefit of being able to capture the desorption plume into a liquid is the ability to carry out post sampling processing of the captured analyte via high performance liquid chromatography. The ability to clean up a sample via HPLC also allow for the detection of isobaric compounds as well as trace level materials which otherwise would be obscured by matrix effects in complicated sample matrixes like tissues. This application of laser desorption with a secondary ionization by capture into a liquid could be envisioned to be applied to AFM based laser desorption techniques where boosting the ionization efficiency is crucial for signal detection.

TABLE OF CONTENTS

Chapter Page

LIST OF TABLES

Table Page

LIST OF FIGURES

Figure Page

CHAPTER I
INTRODUCTION

Basic and Applied Needs for Spatially Resolved Chemical Information

There exists a clear need to extend the limits of our understanding of chemical and physical phenomena of materials and biosystems to the nanoscale. Chemical analysis on the nanometer scale has become necessary in many fields of biology, medicine, and material science. Understanding processes like signal transduction in a single cell[1,2], elemental distribution in single cells and organelles[3], characterization of nanoelectronics with respect to trace impurities[4], and the study of pharmaceuticals[5] require nanometer-resolved chemical analysis. The chemical analysis of compounds in complex mixtures or specimens such a biological tissue requires highly specific and sensitive analytical methods, that require little or no sample preparation and can be studied *in vivo*. The ability to chemically image fragile biological systems at atmospheric pressure is a growing field of interest because preparation of biological samples for analysis in vacuum is often difficult, time-consuming, and even at times not possible.

An analytical tool with high sensitivity that can provide detailed molecular information with high spatial resolution has been the goal behind the development of different chemical imaging techniques. In mass spectrometry, the desorption and ablation of material from surfaces in vacuum is a well established field. Techniques like secondary ion mass spectrometry (SIMS)[6] and matrix-assisted laser desorption ionization (MALDI)[7,8] have become common tools for surface sampling and imaging. Each approach has advantages and disadvantages depending on the particular application. In SIMS, surface species are desorbed by keV particle bombardment[9] while the ionization

of the particles occurs during their desorption by intrinsic processes. SIMS can yield images with lateral resolution on the order of 100 nm.[10] Laser based desorption systems like MALDI are capable of routinely achieving 20 μm spatial resolution and have the advantage of minimal fragmentation of the molecules of interest.[3] However, both of these imaging techniques have the drawback that they are carried out in vacuum, which limits the type of sample that can be studied because of the constraints of placing the sample into the vacuum system. Atmospheric pressure (AP) sampling mass spectrometry (MS) is especially suited for this with its high degree of chemical specificity and its minimal or no sample preparation. The ability to carry out AP-MS experiments largely depends on the desorption and ionization mechanisms. Techniques like atmospheric pressure chemical ionization (APCI)[11], electrospray ionization (ESI)[12] and inductively coupled plasma ionization (ICP)[13] that have the ability to ionize samples at atmospheric or reduced pressures in combination with highly localized sample desorption techniques, like near-field laser desorption[14] and micro-thermal desorption [15] are opening the door for mass spectrometry to carry out nanometer scale chemical imaging at atmospheric pressure.

Overview of Current Chemical Imaging Techniques in MS

Mass spectrometric imaging (MSI) is a powerful technique that uses molecular surface sampling to generate images that correlate the physical features on a surface with the presence of chemical species. MSI has been in use for approximately 20 years, starting with the development and implementation of high resolution chemical imaging with secondary ion mass spectrometry (SIMS) and matrix assisted laser desorption

ionization mass spectrometry (MALDI-MS).[16,17,18] However, recent growth in the number of atmospheric pressure (AP) sampling/ionization techniques[19,20,21] has led to an exponential increase in the number of publications using MSI for the identification of small molecule pharmaceuticals, metabolites, lipids, peptides, and proteins in biological tissues *in vivo* as well from surfaces for forensic applications .[22,23,24]

Effectively sampling surfaces with high spatial resolution is critical for visualizing the physical distribution of a molecular species present in a sample. Presently, a majority of AP sampling/ionization techniques are focused on achieving micrometer scale MSI resolutions.[25,26,27,28,29,30,31,32,33,34] From these techniques the achievable spatial resolution of methods employing a liquid/gas desorption process is related to the size of the liquid/gas jet cross section impacting the surface and has been found to be around 50 μm and 250 μm for desorption electrospray ionization (DESI) and using a low temperature plasma probe (LTP), respectively.[27,28] The laser based techniques have demonstrated, spatial resolutions between 2 μm and 400 μm depending on the laser spot size, wavelength and repetition rate.[29,30,32,33] Finally, solid sampling probes have also used for imaging purposes with a spatial resolution of about 60 μm, determined by the actual size of the needle probe, have been demonstrated.[34]

Herein I will discuss in detail the different approaches to desorption and ionization of laser and thermal based experiments for AP surface sampling MS.

Laser Desorption with a Secondary Ionization Mass Spectrometry

Laser desorption/ablation experiments that couple laser ionization with a mass spectrometer were introduced in the 1960's. In some of the first laser ionization

experiments, Vastola et al[35] used a 694.3 nm ruby laser to ionize organic salts in vacuum. These early laser desorption experiments provided a new technique for desorbing material that decomposed from direct heating, like organic salts. Although, direct laser desorption ionization has been used to examine larger molecules like peptides, it is much better suited for small molecule analysis like organic dyes, porphyrins, organic salts, and UV-light absorbing synthetic polymers[36]. However, laser desorption produces a greater number of neutrals over ions, and therefore can be successfully coupled with many different secondary ionization sources. For laser desorption and ionization at AP these techniques include: inductively coupled plasma (ICP), and various forms of APCI, ESI, as well as AP-MALDI.

Introduced by Alan Gray[13] in 1985, ***Laser Ablation Inductively Coupled Plasma (LA-ICP)*** is one of the most established atmospheric pressure laser ablation techniques. In the LA-ICP-MS technique material is ablated from the surface by a laser; and then atomized and ionized in the high temperature plasma, Figure 1. In LA-ICP-MS experiments, the sample is placed in a closed ablation chamber which is flushed with argon or helium as a carrier gas and the laser beam is focused on the sample surface through a cell window.[37] When the laser irradiance is high enough the material is ablated and carried in the carrier gas to the plasma of the ICP-MS. The ICP is a separate excitation source where laser-generated particles are vaporized, atomized and ionized. The ions are then extracted into a vacuum interface and guided into a mass analyzer. The advantages of LA-ICP-MS analysis are high sensitivity, large dynamic range, and simple spectra.

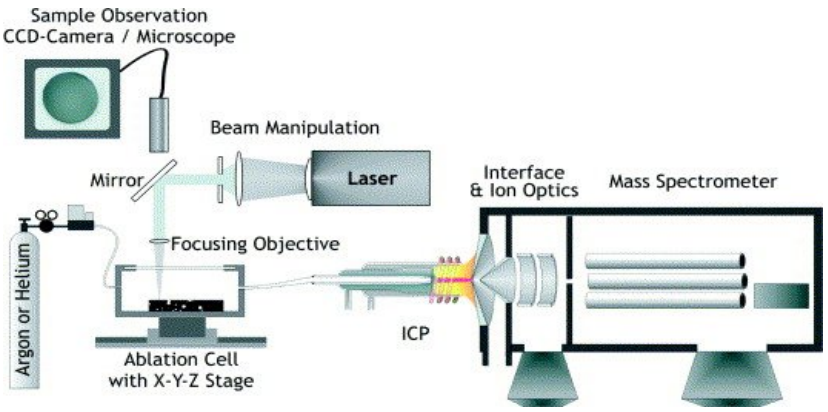

Figure 1. Schematic of LA-ICP-MS setup. Used with permission for reference 37.

The LA-ICP-MS technique's biggest merit is its sensitivity, achieving a sub-ng/g detection limit for spot sizes that are above 100 μm[37]. Combining high spatial resolution that is achieved with laser ablation with the high sensitivity in the ICP allow for trace-element determination at the μm scale. This makes the LA-ICP-MS a tool that is widely used in geology for the detection of trace elements in minerals, as a screening tool in geochemical studies of (U/Th/Pb), and for the elemental analysis of fluid inclusions for studies of ore-formation processes.[38] Forensics is another area where the LA-ICP-MS is heavily used; within this field fingerprinting of gemstones seems to be a fast growing areas.[37]

The LA-ICP technique has also recently been used by Becker et al. to image elements in thin cross section of human brain samples.[39,40,41] The tissue samples were ~ 20 μm thick and the ablation of the sample was preformed with a 266 nm frequency quadrupled Nd:YAG laser. The ablated material was carried by argon gas into the ICP. Laboratory standards were created by spiking the brain tissue with known solutions of the selected elements such as Cu. The signal was then normalized to the maximum ion intensity of $^{63}Cu^{+}$ using the laboratory standards. Using this LA-ICP-MS technique Becker et al[39] were able to do 50 line scans of a section of tissue in 6 hours. Chemical imaging done using LA-ICP-MS by Becker et al.[39] of a human brain sample can be seen in Figure 2. Quantitative analysis on the amount of element in interest was performed only on the elements for which a suitable standard solution could be created. This therefore creates a limitation on the ions that can be quantified in a mapping scan. The LA-ICP-MS is therefore rather slow compared to other biological surface mapping techniques like MALDI and DESI. As a tool for analytical application to biology the

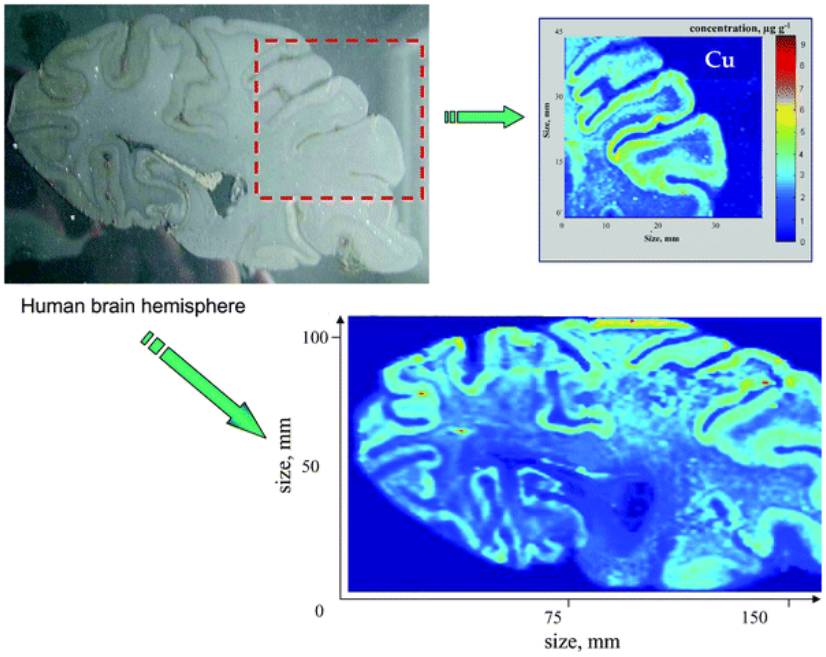

Figure 2. Cu images in part of (top, right) and the whole (bottom, right) human hemisphere measured by LA-ICP-MS compared with the light photograph of the thin tissue section. Used with permission from reference 39.

LA-ICP-MS has been used for a variety of applications such as tissue imaging as discussed earlier as well as for proteomics with protein quantification by the detection of trace elements in proteins by means of polyacrylamide gels.[42, 43]

Laser Desorption Atmospheric Pressure Chemical Ionization (LD-APCI) is another technique that uses laser desorption to produce a plume of neutrals that then undergoes secondary ionization. Atmospheric pressure chemical ionization uses an IR-laser to desorb neutral molecules from a surface and then uses a corona discharge to carry out the secondary ionization. The corona discharge is used as an electron emitter to ionize neutral molecules in the gas phase. The neutral molecules are created by laser desorption from a target that is near to the discharge. The ionized molecules are then sucked into a heated capillary into a mass spectrometer. The LD-APCI apparatus schematic can be seen in Figure 3. Currently Harrison et al[44,45] are developing LD-APCI as tool for detection small organic molecules. Harrison et al used a focused IR 10.6 μm pulsed CO_2 laser to desorb neutral molecules at atmospheric pressure followed by ionization in the gas phase with a corona discharge[46]. By separating out the laser desorption signal from the ionization by corona discharge Harrison et al were able to increase their ion signal 150-fold[46].

To demonstrate an increase in the signal by carrying out secondary ionization of the laser desorbed molecules, Harrison et al toggled the corona discharge on and off while the laser desorption was continuously running.[46] Using this method they were able to show that the 150-fold reduction of sepirerone still yielded a signal using the LD-APCI method and no signal where only direct laser desorption was used. Also, despite the

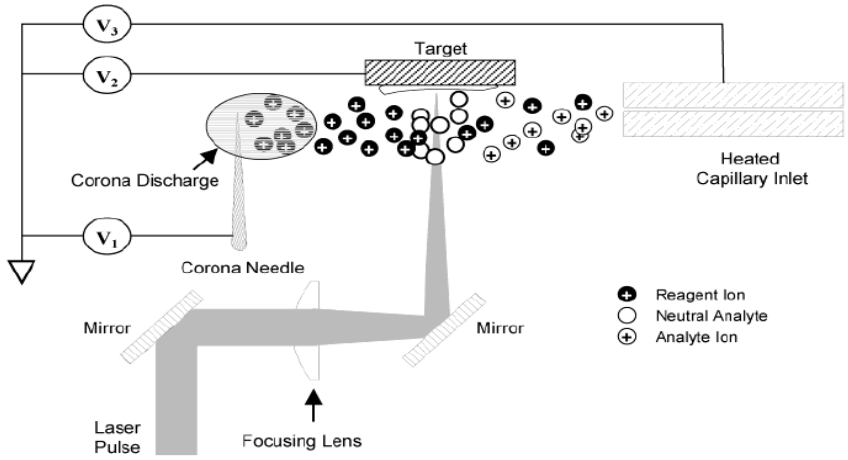

Figure 3. Schematic representation of LD-APCI source. Used with permission from reference 44.

150-fold decrease in the amount of seiperone present in the sample the ion signal only dropped by one quarter of the original signal in the LD-APCI. In later work Harrison et al[45] were able to use the LD-APCI to detect desorbed gas-phase neutral peptide molecules at AP. Using the LD-APCI technique provides benefits over using direct AP-MALDI for detecting peptides because in LD-APCI the matrix containing analyte does not need to assist in the ionization, this allows for the opportunity for examining analyte matrixes that include, biological solutions, tissue, polyacrylamide gels[44,47], and thin layer chromatography plates.

Work has also been done with UV laser sources for the LD-APCI[48], in these experiments a 337 nm nitrogen laser was used to desorb the molecules from a sample. Using a nitrogen laser for desorption rather that an IR laser produced a larger number of neutral molecules, and therefore gave a better signal in the mass spectrometer.

Laser Desorption Electrospray Ionization (LD-ESI) was introduced by Shiea et al[49] under the acronym ***ELDI***, electrospray-assisted laser desorption/ionization. The LD-ESI technique works on the principle that a solid substrate is first desorbed by a pulsed nitrogen laser at atmospheric pressure, followed by secondary ionization of the desorbed material with an electrospray ionization source (ESI)[50], Figure 4. Combining laser desorption with the ESI technique allowed Shiea et al to demonstrate the possibility of detecting intact protein spectra without the use of a matrix compound. The ELDI technique is able to overcome the low mass limit imposed by direct laser desorption by using an ESI source to post-ionize neutral molecules generated by laser desorption[49]. The ELDI set-up consists of a 337 nm nitrogen laser operating at 20 μJ per pulse and a focused laser spot size of 100 μm x 150 μm. The incident angle of the laser beam in

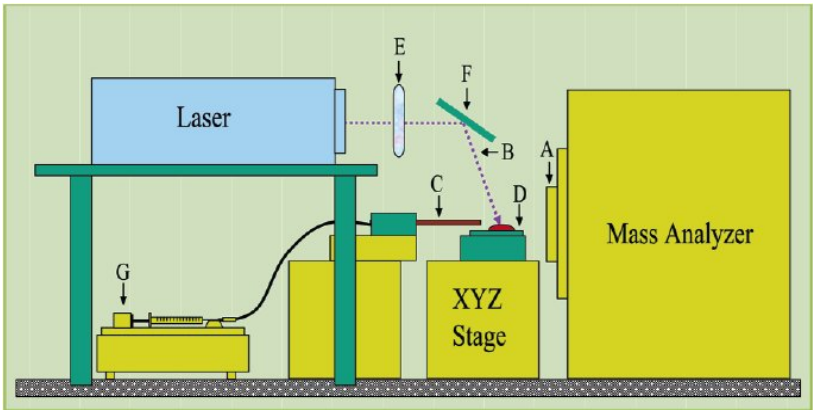

Figure 4. Detailed schematic of ELDI setup, (A) sampling skimmer, (B) laser beam, (C) electrospray capillary, (D) sample plate, (E) focusing lens, (F) reflecting lens, (G) syringe pump. Used with permission from reference 49.

Shiea's work is fixed at 45°.[49] The sample is placed on a translation stage so to produce a continuous ion signal. The laser ablated material is then ionized by electrospraying. Using this technique Shiea et al were able to perform direct characterization of chemical compounds like amines on thin layer chromatographic plates and detect intact proteins in dried biological fluids such as blood, tears, saliva and serum. They were also able to estimate their detection limit using cytochrome c to be from 10^{-4} M to 10^{-9} M. With their laser desorption area ranging between 100 μm - 200 μm they were able to detect 50 amol of protein molecules per each ELDI spectrum.

Very similar to the ELDI technique that uses a UV laser source, Vertes et al[29,30]have developed the ***LAESI*** technique, laser ablation with electrospray ionization, which uses an infrared laser source instead of a UV source. Using a mid-infrared laser source instead of a UV laser source Vertes et al[30] were able to look at biological samples that have resonant frequencies in the infrared versus the near-UV. Vertes et al used an infrared laser source because of the water that is intrinsic to biological samples has a resonance frequency in the infrared. Vertes' approach allows for direct analysis of biological samples without any prior sample preparation such as drying. The LAESI technique depends on the samples high water content and therefore it works very well in water-rich tissue but is limited in analysis of tissue like bone, nail or dry skin which has a low water concentration.

Atmospheric Pressure Matrix Assisted Laser Desorption Ionization (AP-MALDI) was introduced by Dorshenko et al in 2002 as an alternative to vacuum MALDI for carrying out MALDI experiments *in situ.*[51] AP-MALDI operates on the same principles as vacuum MALDI, where a low melting point substrate, the matrix, which is

doped with the analyte is desorbed by laser irradiation. In most cases this is accomplished with a UV-laser source; however, IR lasers have also been used due to the strong absorption of water molecules in the IR region. In the AP-MALDI system ions are transferred from the atmospheric pressure into vacuum via a heated capillary into a differential pressure region, Figure 5.

While ion loss is inevitable during the transfer, the total ion yield in the AP-MALDI is usually higher than in vacuum MALDI due to fast thermal stabilization at atmospheric conditions. The AP-MALDI introduces the possibility of direct coupling separation techniques like liquid chromatography (HPLC) with MS, which is not possible with vacuum MALDI where the samples have to be dried prior to being analyzed. The AP-MALDI has also demonstrated large tolerances to laser fluence variations and minimal fragmentation of molecular ions.[51]

There are different AP-MALDI systems that use different laser sources, the most common laser is the 337 nm UV nitrogen laser. The nitrogen laser is used in the AP-MALDI setup because of the strong interaction of the matrix compounds in the UV regions. Doroshenko et al[51] found the AP-MALDI source to be extremely practical for studies of small molecules because the AP-MALDI allows for low detection limits, and the limitation of mass range was mostly affected by the limits imposed by the mass spectrometer in question and not the AP-MALDI. Doroshenko et al also reported that the AP-MALDI system allowed for softer ionization than vacuum MALDI because the analyte could also become thermally stabalized in the air, subsequently requiring lower laser power for ionization and allowing more fragile samples to be examined.

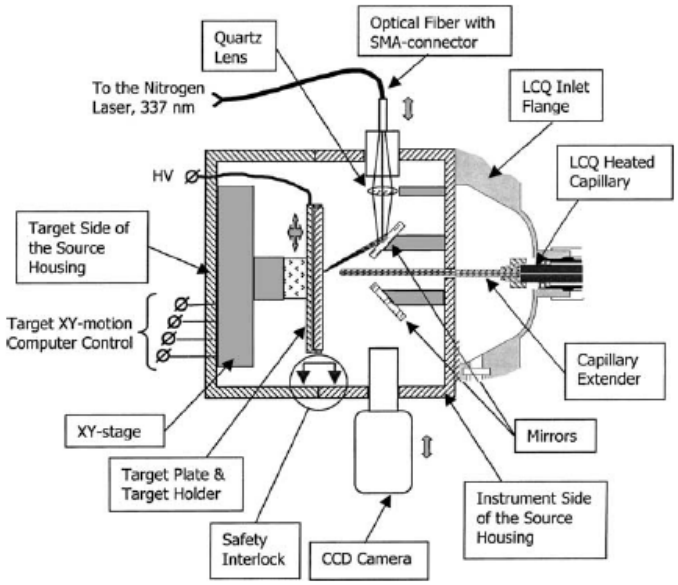

Figure 5. Schematic of AP-MALDI set-up. Used with permission from reference 53.

Recent work by Vertes et al[29], have shown that a 2940 nm IR laser can also be used for carrying out AP-MALDI experiments. Using a wavelength that is in the IR region allows for sampling tissue *in situ* and using the water in the sample as an inherent matrix. Vertes et al have demonstrated this technique on tissue samples of different fruit such as bananas and strawberries.[29] In Vertes' experiments the sample plate sits on an x and y stage controller allowing for rapid analysis of sequential spots as well as opening the door for *in situ* surface sampling of tissue. The AP-MALDI has been successfully used by Vertes et al to image sections of fruit[29] and plants[52] as well as for detecting peptides29.

When it comes to imaging mass spectrometry spatial resolution plays a significant role in the ability to precisely map chemical distributions, therefore, the ability to lower the spatial resolution of in chemical imaging will provide more accurate determination of compounds such as plant tissue, human and animal tissues as well in materials. Currently for laser desorption experiments the spatial resolution is determined by first the laser spot size and the scanning step size. Vertes et al used a 250 μm laser spot size which they used to image an electron microscope grid with bar spacing of 92 μm.[29] Moving their stage in 40 μm increments they were able to generate a chemical image through over sampling where the resolution was determined step size of the stage. This required total ablation in each step movement. The obtained chemical image can be seen in Figure 6. Vertes' work demonstrates the ability to create chemical images at micron resolutions, but at the same time leaves considerable room for improvement and generation of competing techniques.

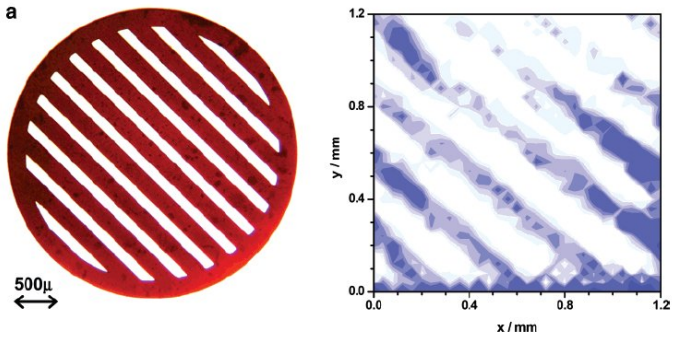

Figure 6. (a) Electron microscope grid. (b) Chemical image of toluidine blue O obtained through over sampling. Used with permission from reference 29.

Thermal Desorption with a Secondary Ionization Mass Spectrometry

Atmospheric pressure thermal desorption (AP-TD) is a well established surface sampling technique in mass spectrometry. In this approach to surface sampling, heat is used to liberate the sample intact from the condensed phase into the vapor phase. Typically, this heating is accomplished through the use of a heated gas passing over the sample and/or a resistively-heated sample surface. Given the nature of the desorption process, this approach is limited to relatively low mass species (ca. 2000 Da or less) that can be liberated intact into the gas phase by heat; thermally labile, highly polar and high molecular-mass species are typically not amenable to vaporization by heating. Once in the gas phase, the sample can be ionized by any number of ion/molecule chemistries.

An example of an emerging AP-TD/MS technique is desorption atmospheric pressure chemical ionization (DAPCI)[53]. As defined and used by Cooks' group,[54] DAPCI consists of a capillary with a taper-tip stainless-steel electrode aimed at the surface. An inert sheath gas, into which a solvent vapor is in some cases introduced, is supplied to the capillary and flows through the emitter at high velocity. A high-voltage power supply is used to apply a voltage (typically ±3-6 kV) to the electrode; this induces a corona discharge at the tip of the electrode, ionizing the introduced solvent vapor. The sheath gas in some cases may be heated. Ionization mechanisms in DAPCI are similar to other APCI ionization sources. As in all APCI systems, the reagent ion species formed can be influenced by the means of initiating the reagent ion plasma, and by the particular solvent vapor and sheath gas used[55]. The desorption mechanisms in DAPCI are in some cases unclear. When the sheath gas is heated, TD is certainly a dominant process. In other cases, the high velocity gas might actually liberate minute particles from the surface that

then can be ionized in the gas phase. Desorption atmospheric pressure photoionization (DAPPI)[56] is similar to DAPCI except that the reagent ion population is initiated by a photoionization process utilizing a UV lamp rather than a corona discharge.

Currently, there are several commercially available AP-TD with secondary ionization sources for mass spectrometry (AP-TD/SI-MS).[19] Direct analysis in real time (DART)[57] is one of the best known. In DART, He gas flowing through a probe is subjected to a discharge at a needle electrode, producing ions, electrons and metastable species. Perforated electrodes downstream act to remove ions from the gas stream, while neutral metastable species are carried by the gas through a heated chamber, passing though a grid electrode before entering the ambient atmosphere. The grid electrode prevents ion-ion and ion-electron recombination, and also acts as a source of electrons, either through Penning ionization of a neutral species or through surface Penning ionization.[58] The exiting gas flow is directed at the entrance of the mass spectrometer and the sample surface to be analyzed is placed between the two. The ionization process in DART is a variation of APCI in which the reagent ion population originates from the gas phase reactions of the metastable He atoms (He^* ($1s2s^3S_1$)) produced in the discharge. Another commercially available device is atmospheric-pressure solids analysis probe (ASAP)[59,60]. Here analyte deposited on the glass melting point capillary is thermally desorbed by a hot gas, ionized by APCI, and analyzed by mass spectrometry (Figure 7). This technique has similar merit to DART, allowing for analysis of individual samples.

None of the above mentioned AP-TD/SI-MS techniques have shown to be pariculary useful for chemical imaging of surfaces. Moreover, they are fundamentally limited in their

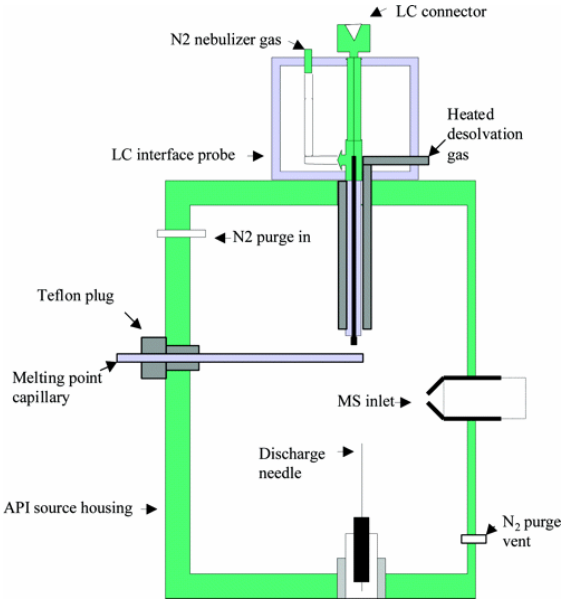

Figure 7. Cross-sectional drawing of an atmospheric pressure LC/MS ion source modified for ASAP analysis. Used with permission from reference 59.

ability to carry out chemical imaging because they sample from a relatively large area (many mm to cm scale).

In order to overcome the limitation of available thermal desorption techniques for chemical imaging Reading et al. used a Wollaston wire AFM tip to carry out local thermal desorption in order to analyze the desorbed material using gas-chromatography mass spectrometry (GC/MS)[67]. With their set-up they were able to desorb material from a PMMA surface by heating to 600 °C the Wollaston probe in contact with the surface. The heated probe created craters that were on the order of 6 μm wide by 1.7 μm deep. Using a syringe co-located with the Wollaston probe they were able to suction out the desorbed vapor and analyze it with GC/MS. The sample was imaged afterwards in an AFM to confirm the presence of ablation craters. Reading et al[137] applied this technique for examination of polymers as well as small molecules found in pharmaceuticals[138]. Reading's work demonstrates the potential for a nanometer spatially resolved TD-based mass spectrometry chemical imaging technique.

Combined Chemical and Surface Microscopy Imaging Using Mass Spectrometry and Atomic Force Microscopy

Combining atomic force microscopy (AFM) and mass spectrometry has been approached from two directions: using laser desorption/ablation as the means to sample the surface[61] and using AFM heated probes to thermally desorb the sample[5]. In recent years Zenobi et al have attempted to couple mass spectrometry with near field scanning optical microscopy (NSOM) in order provide chemical information at the nanometer spatial resolution.[61] Zenobi's technique relied on using tip-enhanced laser ablation to

create submicron sized ablation craters in a material and then sample the chemical composition of the material using mass spectrometry. Aperture based near field optical microscopy works by overcoming the diffraction limit also known as the Abbe criterion

$$\Delta x = 0.61\lambda / NA \ . \qquad (1)$$

Where Δx is the spatial resolution, λ is the wavelength of the interacting radiation, and $NA=n\ sin\ \alpha$ is the numerical aperture of the objective lens. In near-field optical microscopy, the resolution Δx no longer depends on λ but on a characteristic length *d*, the aperture diameter or tip diameter, of a local probe.[61] NSOM relies on a confined photon flux between a local probe and a sample surface. The probe is scanned over a surface and an x-y detector acquires the position and optical information. This idea for overcoming the diffraction limit by confining light to an aperture smaller than the wavelength of light to was first proposed by Edward Synge in his paper in 1928.[61] However, because of a lack of a coherent light source like a laser that would produce a sufficient photon flux as well as necessary electronic and detection equipment Synge's idea was not realized until the 1980 when researchers at the IBM Research Laboratory in Switzerland where able to produce the first near-field optical measurements. In the most common NSOM light is sent down a tapered optical fiber which is uniformly coated in a metal such as aluminum. The fiber is chemically etched to an aperture diameter of around 50 nm. Companies like Nanonics use this technique to create hybrid SNOM/AFM scanning probe equipment to image at the nanometer resolution.

Zenobi's technique relied on using tip-enchanced laser ablation to create submicron sized ablation craters in a material and sampling the ablated material into an

electron ionization (EI) source of a mass spectrometer for ionization and detection. Zenobi's experiments demonstrated proof of principle, but were limited in the types of systems they could study because the experiments were carried out under vacuum and because EI only creates singly charged positive ions as well as fragments of the original molecules.

The initial laser desorption/ablation work developed by Zenobi et al in 2001 using a 355 nm Nd:YAG laser with up to 250 μJ of energy per pulse coupled into the back of a NSOM fiber with a 170 nm diameter aperture to create laser ablation craters with a size of 200 nm diameter by 20 nm deep [61] on an anthracene crystal surface. The volume of material ablated corresponds to a quantity of 1.7 attomol of material desorbed from each individual crater. Using a heated stainless steel capillary, the ablated material was then directed into an (EI) source of a quadruple mass spectrometer. An ion-trap mass spectrometer was used in the experiment because it allows for material from several laser shots to be accumulated in the trap to allow for better signal to noise. It should also be noted that EI requires a vacuum environment to operate and is only capable of producing singly charged positive ions, thereby drastically limiting the samples that can be studied. After ablation of the surface, the NSOM tip was used in a force feedback arrangement to scan the surface to acquire a topographic image.

More recently in 2008 Zenobi et al modified their experiment to operate using a combined ion-trap/time-of-flight (TOF) mass spectrometer to increase the detection sensitivity[62] as well increased the NSOM tip size to be in the range of 500-800 nm in order to produce a larger ablation area, Figure 8. Using the ability of a quadruple to accumulate ions with the sensitivity afforded by a time-of-flight mass spectrometer

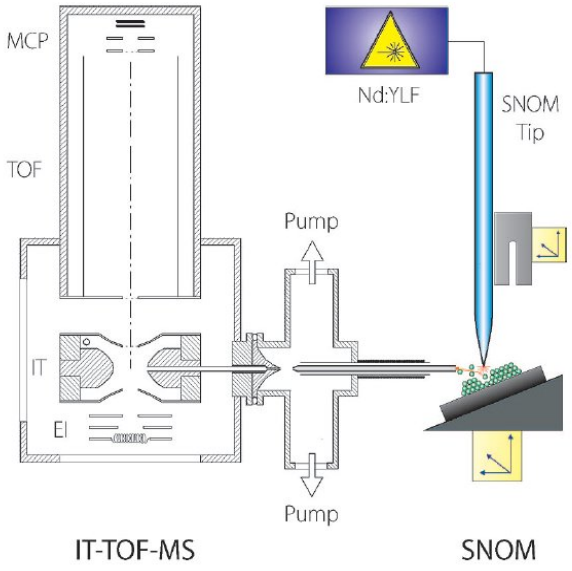

Figure 8. Instrument setup for SNOM-MS. Used with permission from reference 62.

Zenobi et al were able to acquire mass spectra from ~1.7 μm wide x 0.8 μm deep craters in anthracene and 2,5-Dihydrobenoic Acid (DHB).[62] This set-up allowed them to acquire multiple laser shots in the quadruple trap prior to analysis with the time-of-flight. This experiment demonstrated the feasibility of extracting chemically specific information as well as topographic information in tandem using an AFM/MS set-up.

Research has also been performed by Goeringer et al. towards atmospheric pressure apertureless near-field laser ablation mass spectrometry.[63] In the apparatureless approach to near-field laser desorption a laser is focused onto a metallic AFM probe which by way of surface plasmons enhances the electromagnetic field of the laser bean at the very tip of the sharp AFM probe creating an enhancement on the order of several magnitudes. This localized enhancement allows for the desorption craters to be in size on the order of the AFM tip, which is tens of nanometers for standard gold coated AFM probes. In their experiment Goeringer et al used a frequency doubled 532 nm Nd:YAG laser focused at the tip of a gold coated AFM probe that was positioned ~ 10 nm from the surface to create ~ 50 nm craters in a rhodamine 6G thin film. However, they were not able to detect the rhodamine 6G molecules in the mass spectrometer from the 50 nm craters and therefore, more recently Goeringer et al used a quadruple trap mass spectrometer and a focused laser beam to create 1 μm spatially resolved chemical images with corresponding AFM topographic images.[33] These studies demonstrated a clear application of combined AFM/MS technique for chemical imaging.

Another laser desorption technique that shows promise for its application to the set of techniques already incorporating AFM and MS is laser ablation inductively coupled plasma mass spectrometry (LA-ICP-MS). Becker et al have shown the

possibility of using LA-ICP-MS to perform elemental analysis of Cu, Zn, Au, Si and U from ~200 nm craters using what they claimed was near-field enhancement from a frequency doubled 532 nm Nd:YAG laser focused on the end of a sharp silver needle that is position 200 nm above the surface.[64,65] However, since near-field enhancement only produces substantial enhancement effects when a probe is ~ 10-30 nm above the surface their interpretation of the tip-enhancement phenomena remains questionable. Their experiment demonstrated the possibility of nano-local analysis by near-field (NF) laser ablation ICP-MS, and opens the door for coupling NF-ICP-MS with current AFM techniques for an appertureless NF-ICP-MS experiment using AFM probes as the source for the near-field enhancement. The details and applicability of the ICP-MS technique are described in more detail earlier in this chapter.

The other successful avenue for coupling AFM imaging with MS identification was developed using thermal desorption via miro-thermal (micro-TA) AFM probes coupled to an electron impact (EI) gas chromatogram mass spectrometer (GC-MS).[66] In this work Wollaston wire micro-TA AFM probes were used to desorb craters ~ 7 μm wide x 1.7 μm deep. The evolved gas was extracted via a heated capillary and sent to an EI GC-MS for analysis. The same micro-TA/GC-MS analysis technique has also been applied to the study of pharmaceuticals[67] were the precise distribution of chemicals can be correlated to an AFM topographic image. Recently, the use of thermal desorption combined with AFM as a means for studying samples at the nanoscale has become possible with the invention of silicon based heated AFM probes, that have a 50 nm radius of curvature and are able to rapidly heat and cool up to 400 C. Using these new nano-TA AFM probes for thermal desorption combined with mass spectrometry opens up a new

avenue for analyzing samples. This technique alleviates tedious experimental set-up that is associated with near-field laser desorption/AFM experiments. Using thermal desorption also minimizes the tip to tip fluctuation in enhancement that is found when using near-field tip enhancement technique.

The goal of true nanoscale chemical imaging is now becoming a reality due to recent advances in both mass spectrometry and scanning probe microscopy. The availability of commercial mass spectrometers that are able to efficiently detect attomole of material transferred from atmospheric pressure as well as the development of online atmospheric pressure secondary ionization techniques have increased sensitivity to the point needed for nanoscale sampling. Closed loop stages that reduce drift making long dwell times needed for spectroscopy possible, and the development of new AFM probe technology that makes thermal desorption possible on the nanoscale have brought about the successfully marrying of AFM and MS for nanoscale chemical imaging.

The work discussed in this dissertation is aimed at creating novel approaches to chemical imaging that ultimately allow for submicron resolution. This goal has been approached from two direction using laser based desorption and coupling it with an AFM using apertureless tip enhanced laser ablation/ionization. This work on the scaling down spatial resolution of laser desorption/ionization experiments through the use of an AFM/MS platform is the basis for discussion in the subsequent chapter. The second direction was through the development a new approach to thermal desorption based mass spectrometry experiments by using a proximal probe to spatially desorb the surface and ionizing the plume of neutrals using a secondary ionization source at atmospheric pressure. The thermal desorption approach allows for the easy scaling of the technique all

the way from the millimeter to the nanometer regime. In the nanometer regime an AFM platform with silicon based heating AFM probes is used to locally desorb material from nanometer sized craters. The development and the application of the technique in both the millimeter, micrometer and nanometer regime are discussed in detail in a later chapter.

The final work in this thesis focused on trying to improve laser based desorption through a secondary ionization of the neutrals plume by capturing the laser desorption plume into a liquid and then electrospaying the solution into a MS. The added benefit of being able to capture the desorption plume into a liquid is the ability to carry out post sampling processing of the captured analyte via high performance liquid chromatography. The ability to clean up a sample via HPLC also allow for the detection of isobaric compounds as well as trace level materials which otherwise would be obscured by matrix effects in complicated sample matrixes like tissues. This application of laser desorption with a secondary ionization by capture into a liquid could be envisioned to be applied to AFM based laser desorption techniques where boosting the ionization efficiency is crucial for signal detection.

CHAPTER II
DEVELOPED ADVANCES IN LASER DESORPTION/IONIZATION CHEMICAL IMAGING

Combined Chemical and Topographic Imaging Using Mass Spectrometry and Atomic Force Microscopy

Scanning probe microscopy (SPM) techniques such as scanning tunneling microscopy (STM), atomic force microscopy (AFM), and near-field scanning optical microscopy (NSOM) are versatile methods for topographical imaging of surfaces. However, the images intrinsically provide little or no information about the fundamental chemical composition of regions within the images. Because optical spectroscopic methods can provide such information, it is highly desirable to combine them with NSOM, thereby enabling spectral analysis of spatially resolved features. In such nanoscale analytical techniques, laser radiation is typically focused onto a sharp metal tip resulting in enhancement of the electric field at its apex. Because the tip-enhanced field is confined to a region (i.e., the optical near-field) that is comparable in radius to the tip (< 30 nm), it can be used as a light source for spectroscopic imaging at the nanoscale. Although the currently achievable spatial resolution of tip-enhanced, near-field scanning optical spectroscopy (< 20 nm) does not compare with SPM methods (sub-nanometer), its combination of resolution and chemical information are remarkable. On the other hand, mass spectrometry can yield substantially more molecular information than optical spectroscopy. Consequently, chemical (molecular) imaging[68,69,70,71,72] based on desorption/ionization processes coupled with mass spectrometric analysis, broadly termed mass spectrometry imaging (MSI), is a rapidly developing area. Laser desorption methods (including laser desorption/ionization[73,74,75,76] (LDI) and matrix-assisted laser

desorption/ionization[77,78,79] (MALDI)) and ion beam sputtering[80,81,82] (secondary ion mass spectrometry (SIMS)) are the most widely used sampling probes in MSI. While the latter process is restricted to high vacuum systems, it is possible to perform LDI and MALDI under ambient atmospheric pressure conditions[83]; indeed, the use of mid-IR lasers even makes possible matrix-free, atmospheric pressure MSI[29,30]. Microprobe-mode MSI determines the spatial distribution of analytes by moving the target in an *x*-*y* raster under a focused probe while simultaneously collecting and mass analyzing representative sample ions. Recently, Spengler and co-workers[84] have developed a scanning microprobe MALDI ion source, suitable for either atmospheric or mid-pressure operation, and demonstrated high spatial resolution MSI at high mass accuracy and resolution with the device interfaced to an ion trap/Fourier transform ion cyclotron resonance MS. In contrast, spatial resolution in microscope-mode MSI[85] is achieved using two-dimensional detection of analyte ions generated by large area sample illumination with an unfocused probe; the mass analyzer is designed to project the sample spatial distribution of chemical species through the instrument onto the detector. The continued growth in importance of MSI as an analytical and research tool is due in large degree to the intrinsic capabilities of MS for acquiring chemical information, in the form of molecular mass and detailed structural characterization, from a wide array of molecular species present in a variety of complex matrices. It is, however, the high detection sensitivity of MS that makes it possible to bring that inherent ability for characterization to bear in micron-scale chemical imaging (a 1 μm diameter region from a monolayer of sample contains on the order of 106 molecules). Despite the advances in instrument development for MSI, however, relatively little consideration has been given to the sample topography[86]. For

example, although height mapping is possible using MALDI[87], the height resolution is dependent on spatial resolution (minor changes in sample topography become averaged out with degradation in the lateral resolution). Topography-induced ionization biases, which are due to variations in laser fluence with sample topography, also can result in imaging artifacts in MALDIMSI. In addition, if the sample area corresponding to the rastered array of sampled locations is not flat, projection distortion (i.e., projection of the actual analyte spatial distribution onto the raster) can occur. Using a different approach to surface mapping via MSI, Kossakovski et al.[88] employed a fiber optic-based NSOM apparatus to effect MALDI. MS spectra obtained during a topographical line scan were subsequently used to determine the distribution of an acetyl choline/dihydroxybenzoic acid matrix sample deposited on a calibration grid in the vacuum chamber. Based on the slope in a part of the line scan image corresponding to a grid edge, they estimated a spatial resolution of ~ 1 μm. More recently, Zenobi et al.[62] demonstrated 5 μm lateral resolution MSI of solid anthracene using near-field ablation, the molecular ions being generated via EI and mass analyzed with an ion trap/time-of-flight MS. In addition, topographical images of the sample were obtained by scanning the fiber optic tip over the surface in shear-force feedback mode.

We have previously described the development of a scanning apparatus for nanoscale surface sampling that utilizes the interaction of laser radiation at a sharp atomic force microscopy (AFM) probe tip to effect tip-enhanced desorption/ablation on opaque substrates[63]. Because its digitally controlled scanning stage operates in closed-loop mode, nanometer-scale array-based sampling protocols could be performed over relatively long time periods with little drift and hysteresis. Discussed in this section it the, adaptation of

the instrument for both topographic mapping and chemical imaging of surfaces via atmospheric pressure LDI-MS. With the AFM tip in its retracted position, far-field LDI is used to generate gas-phase ions which are then mass analyzed with a quadrupole ion trap MS. We demonstrate mass analysis of desorbed ions over a wide *m/z* range and production of associated chemical images having a spatial resolution of ~ 2 μm; topographical images (with nanometer-scale spatial and height resolution) of the same surface features, produced using the same instrumentation, are also shown.

Experimental

Instrumentation.

The mechanical subsystem is comprised of a Veeco Metrology (Santa Barbara, CA) MultiMode AFM head and nPoint (Madison, WI) sample stage (model iCXYZ100-DM), which could be scanned over a 100 x 100 μm region with sub-nanometer resolution. Base-level AFM functions for stage movement and topographic imaging were executed using standard Nanonis (Zurich, Switzerland) components (RC4 real time controller, OC4 oscillation controller, SC4 signal conditioner, and AKVM Veeco interface unit) and associated control software. An nPoint (Madison, WI) digital closed-loop controller (C-300) powered the nPoint stage and provided the interface between it, the MultiMode, and the Nanonis controller. Laser pulses from a frequency-doubled Minilite (Continuum, Santa Clara, CA) Nd:YAG laser (532 nm, ~5 ns pulse width) were transmitted via a single-mode optical fiber to the previously described optical subsystem33 (with the linear polarizer removed). Because the transverse intensity distribution at the output of a single-mode fiber is largely independent of the input beam

profile, the optical beam profile entering the optical subsystem was assumed to be near Gaussian. Focused light from the output objective of the system was projected onto the sample surface at an angle of ~35° above horizontal and approximately orthogonal to the long axis of the AFM cantilever. The resulting elliptical spot size (~ 5 x 3 mm axes) was determined by AFM topography of single-shot laser ablation sites. The geometrical constraints of the AFM head and protrusion of the cantilever edge into the optical path prevented any steeper approach for the laser beam. In addition to steering and focusing of the laser beam, the optical subsystem provided the ability to view the position of the laser spot coaxially using a CCD camera. A second 12X zoom lens/CCD camera setup located directly over a window in the top of the MultiMode head allowed fine positioning of the sample stage relative to the laser spot.

A rendered drawing of the modified instrument is shown in Figure 9. In that apparatus, desorbed ions produced at atmospheric pressure were collected using a sampling capillary (1.27 mm o.d., 0.838 mm i.d.), which was interfaced to a Thermo Scientific (San Jose, CA) LTQ quadrupole ion trap mass spectrometer. The ion-sampling capillary (4.5 cm long, 316-RW 18 gauge stainless steel) was press-fitted into a shallow hole that was counter-bored into the LTQ inlet capillary; a tight fit was further ensured by thermal expansion of both capillaries during normal LTQ operation. Measurements showed that the sampling capillary typically had a temperature ~50K lower than at the junction to the mass spectrometer inlet, which was held at 500K during these studies. Because the location of the ion-sampling capillary was fixed in space due to its rigid interface with the LTQ, the complete MultiMode unit was moved via translation stages to

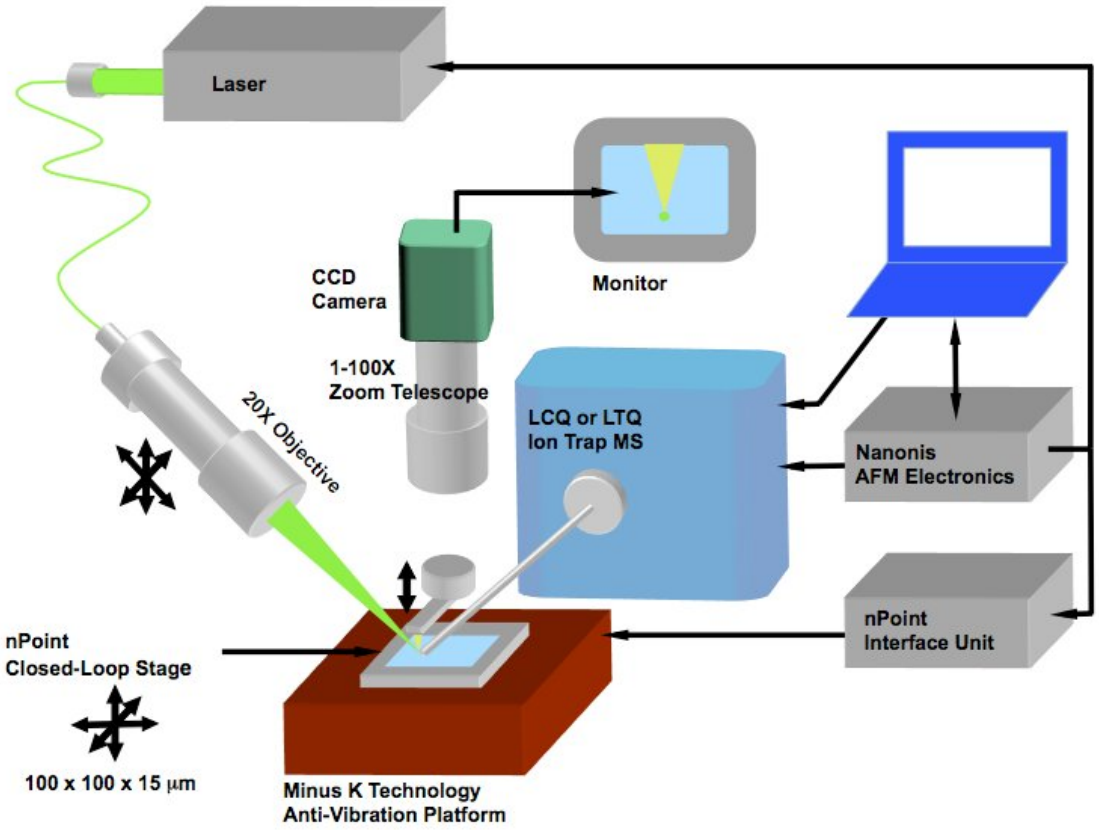

Figure 9. Overview of instrumentation for combined AFM and LDI-MS imaging.

position the capillary inlet with respect to the AFM tip/sample surface. During the imaging experiments, the capillary inlet was ~ 0.5 mm above the surface and ~ 1 mm from a surface normal originating at the desorption location. An adjustable potential, variable over a ±100V range, could be applied to the sample substrate. The modified apparatus also had a TTL-controllable mechanical shutter located between the laser output and the input to the fiber optic cable.

Custom code, which accessed various Nanonis controls via the LabVIEW programming interface, was used for array-based positioning of the sample surface relative to the fixed tip, shutter control, and mass spectral data acquisition. The Nanonis RC4 unit controlled the timing for shutter activation and LTQ scan triggering via the SC4 signal conditioner. A TTL output pulse from the SC4 module entered a digital delay generator (DG535, Stanford Research Systems, Sunnyvale, CA) that then generated two separate TTL pulses. The pulses, with independent, adjustable delay intervals, were used to activate the laser shutter and trigger LTQ mass scans (via a relay contact closure).

Data Acquisition.

Two different modes were available to collect mass spectra for compiling into chemical images. In the stepped mode the stage was sequentially positioned at each pixel in a pre-assigned *x*-*y* surface sampling array, pausing at each location and opening the shutter while the desired number of spectra were collected. The raster mode, having a significantly faster throughput albeit inducing a slight image aberration (see below), scanned the sample using a series of vertically stacked, horizontal lines with mass spectra only being collected while scanning in one direction. Each row of pixels (i.e., horizontal

line) was scanned continuously with the shutter open while mass spectra were collected as LTQ ion mass chromatograms (i.e., as a series of mass spectra vs. time). In either mode, the laser and LTQ were operated asynchronously, with the laser free running (10 Hz) at all times to minimize pulse-to-pulse variation in its output intensity. Laser output measurements indicated that whereas single-shot energies could vary by more than ±50%, the typical pulse-to-pulse energy variation at 10 Hz was less than ±2.3%. Image pixels were assigned *x*-*y* coordinates according to row numbers and specific time windows therein. Data were compiled into images using custom software.[27]

Sample Preparation.

Samples were prepared using a fine point Sharpie marker (Sanford Corporation, Oak Brook, IL) that contained rhodamine 6G dye. A smooth single coat of rhodamine ink was applied to standard copper-foil-coated AFM pucks then allowed to dry and partially anneal at an elevated temperature (~343K) for at least one hour. AFM topography scans indicated that a typical 100 x 100 μm area made with this simple procedure had a surface thickness fluctuation of d = 200 nm. Patterns to be imaged were created by complete removal of the dye layer using laser ablation, thereby providing a controlled contrast for evaluation of the spatial resolution in chemical images. Repeated ablation of pattern traces with slow scanning ensured the removal of as much material as possible. Custom LabVIEW code was used to import various patterns.

Results and Discussion

AFM Imaging. AFM images of laser-ablated patterns were acquired at 128 pixels-line^{-1} (0.78 μm *x*-*y* resolution) and a scan rate of 10 seconds-line^{-1} using the standard AFM tapping mode of the apparatus. MikroMasch (Tallinn, Estonia) NSC15/AIBS aluminum backside silicon tips were used at a typical resonant frequency of 300 kHz. A false-color image for two ablated channels intersecting at 90° is presented in Figure 10a; the superimposed blue line indicates the position of the corresponding cross-section graph shown in Figure 10b. Immediately apparent is the exceptional sharpness of the separation between chemically contrasting areas. Significantly, the channel walls are sufficiently steep to allow estimation of resolutions down to ~1 μm with only a single chemical standard. The somewhat elevated (i.e., lighter-colored) regions in the image exceed the normal variations in height of the surrounding surface topography (≤200 nm). Such regions were present in most sample images, and can be attributed to the sample preparation protocol described above.

Ion Signal Optimization.

Prior to acquiring chemical images, protonated rhodamine 6G (*m/z* 443) signal was optimized while in raster scan mode, both by adjusting experimental parameters as the mass spectrum (Figure 11) was monitored in real-time and by using the proprietary LTQ auto-tune function. The laser pulse energy, which was varied using the laser's integrated energy attenuator, was set to ~ 30 μJpulse^{-1} as measured at the input to the fiber optic cable (1.5% typical transmission efficiency). The indicated pulse energy was a compromise between producing sufficient desorbed ion signal and inducing fiber damage

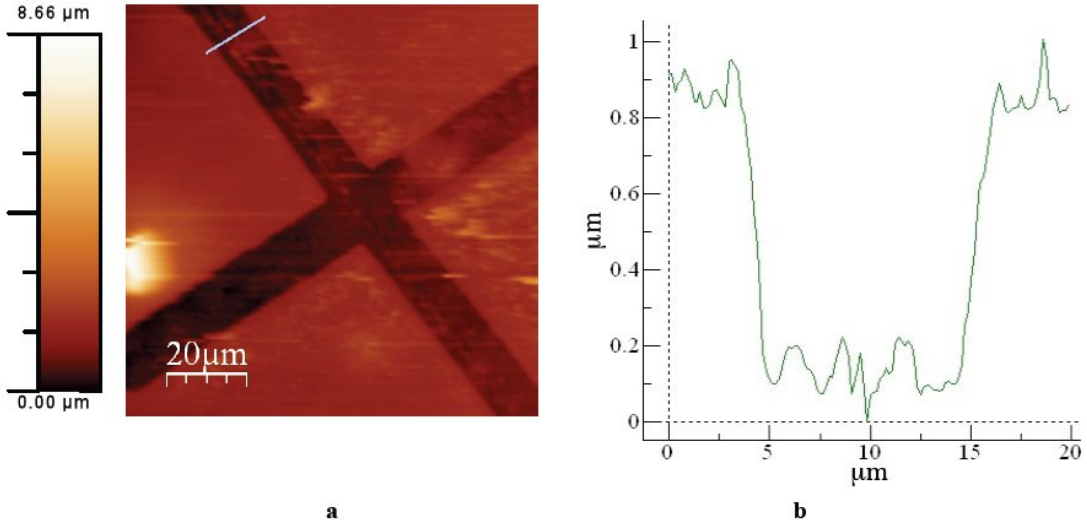

Figure 10. (a) False-color AFM image of a rhodamine 6G layer after laser ablation of a target pattern. The color scale indicates the relative range in the z-axis. (b) Cross-section of the ablated channel indicated by the blue line superimposed in 10(a).

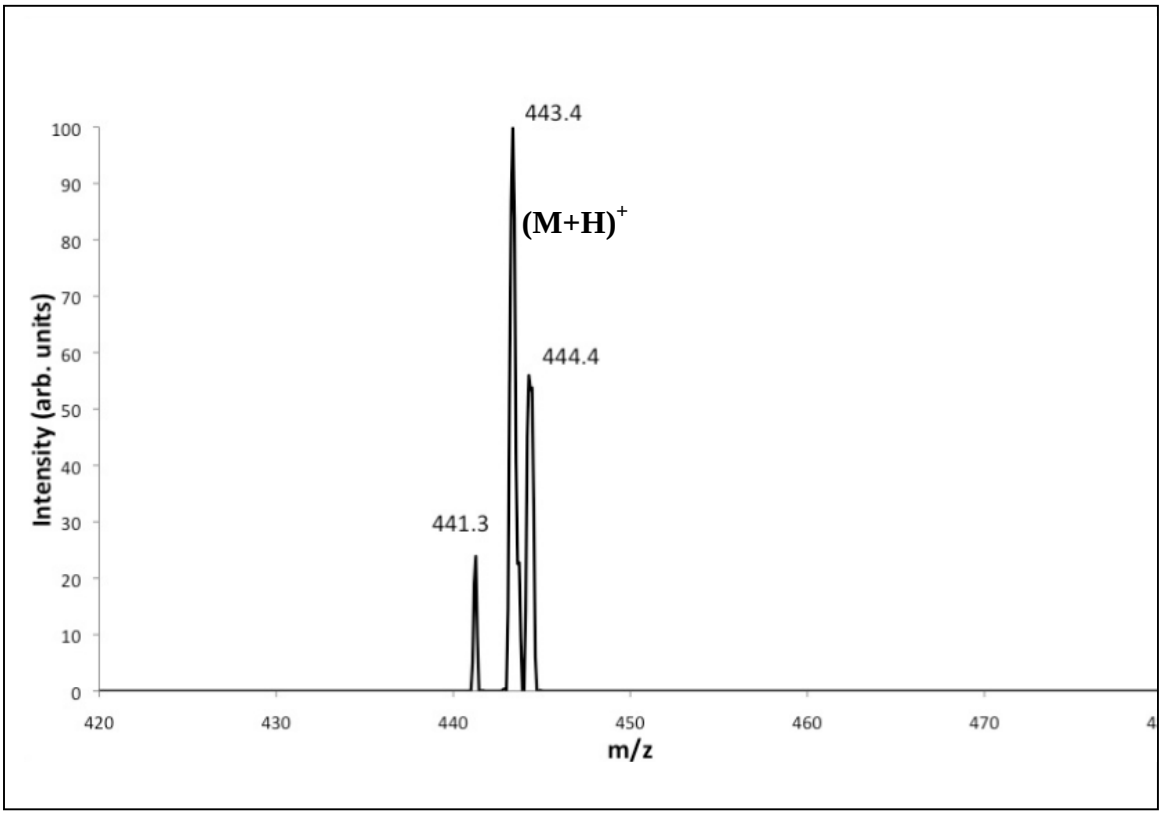

Figure 11. LTQ mass spectrum of the ions collected following LDI of a rhodamine 6G (*m/z* 443) sample layer.

(maximum usable input energies were observed to be ~ 60 μJ-pulse^{-1}). The indicated pulse energy also far exceeded the observed ablation threshold value of ~ 25 mJ-cm^{-2}. The viscous gas flow[89] in the ion sampling capillary was assumed to aid ion transport from its entrance to the atmospheric pressure interface of the LTQ. Application of a +100 VDC potential to the sample substrate, the maximum possible voltage with the current instrument configuration, increased the ion signal by nearly two orders of magnitude. The desorbed ion signal might be further enhanced by applying a pulsed voltage to the substrate, as is done in the pulsed dynamic focusing (PDF) method.[90] However, it was not possible to implement PDF in the current apparatus due to difficulties in high voltage isolation of the sample from the AFM piezo stage.

Mass Spectral Chemical Imaging.

Chemical images normally comprised 100 x 100 evenly spaced pixels acquired in raster mode. Each mass spectral data acquisition cycle (i.e., microscan) included an ion injection time of 350 ms, thereby allowing the signal from three laser shots to be summed per microscan. Three such microscans were averaged to produce each mass spectrum (i.e., pixel), giving an overall data acquisition rate of (3 x 350 ms)-pixel^{-1} = 1.05 s-pixel^{-1}; thus, the total time for image acquisition was ~5.8 hrs. To optimize the mass spectrometric performance of ion trap mass spectrometers, it is often advantageous to store a constant number of ions prior to mass analysis (with that number being below the space charge limit). For the LTQ this can be accomplished by varying the ion injection time as a function of the incoming ion current, a method termed automatic gain control (AGC). However, AGC was not used here because the imaging experiments operated in a regime for which 1) the number of ions produced per laser shot was far below the space

charge limit, and 2) that number was subject to variations that became increasingly greater as the limit of spatial resolution (and signal-to-noise, see below) was approached. At the final effective spatial resolution of 2 μm and typical ablation depth of 1 μm, as seen in Figure 10b, the minimum sampled volume per assigned pixel was estimated to contain approximately 6 x 10^9 molecules. The use of diffractive focusing optics imposes a minimum barrier for the focused laser spot size that is equal to the Abbé diffraction limit, ~ λ/2. If, however, the analyte is essentially depleted prior to moving the laser microprobe to each new spatial location, it is possible to obtain images at resolutions smaller than the laser spot size. With this oversampling technique[91], the image pixels partially overlap since the stage is advanced a distance less than the spot size between successive laser pulses. Therefore, the lateral resolution becomes a function of the incremental movement for the sample stage. Nevertheless, a reduction in image quality ultimately occurs due to a loss in signal associated with the reduction in amount of analyte removed, jitter in stage positioning, or non-uniformity in the laser beam intensity profile.[92,93]

For a stage scan rate of 5 μm-s^{-1}, the lateral resolution for our apparatus was approximately equal to the laser spot size (i.e., 1.05 s-$pixel^{-1}$ x 5 μm-s^{-1} = 5.25 μm-$pixel^{-1}$). Thus, use of the oversampling technique required stage scan rates less than ~ 5 mm-s^{-1}. The spatial resolution at which mass spectra were collected was gradually reduced (i.e., improved) by successively decreasing the stage scan rate, with the ion signal optimized (see above) for each rate. The desorbed ion signal at *m/z* 443 also decreased with the scan rate, since the amount of material sampled at each pixel decreased as well. The laser was

additionally used to provide a spatial reference point for each line during image acquisition. A variable delay of up to a few hundred milliseconds followed the contact closure trigger for the LTQ mass scans; the stage was programmed to remain stationary during that time, so that a few laser pulses would then ablate a small crater at the sample edge. Therefore, a rastered image would include an ablated reference channel at its edge, thereby ensuring that any image aberrations resulting from time-lag issues could be corrected. The only sources of aberration not corrected for by the measurement protocol were minute variations in alignment of the laser objective due to thermal fluctuations, which resulted in spot diameter changes and deterioration in overall quality of ablation patterns over time. However, shifts in the position of the focused laser spot due to minor variations in the temperature of the optical assembly were not observed. Figure 12a shows a false-color AFM image of an ablated pattern similar to that in Figure 10a; the corresponding mass spectral chemical image in Figure 12b has an intensity scale indicative of the signal level for the *m/z* 443 ion of rhodamine 6G. The imaging data were acquired using a stage scan rate of 2 $\mu m\text{-}s^{-1}$, which was the lowest rate that produced images having acceptable signal-to-noise ratios (i.e., without signal "dropout" in any pixels). At the same time hand, the sharp image demarcations seen at the channel walls in Figure 12b indicate the absence of significant analyte carryover between pixels. Inspection of the spatial reference along the right edge (not shown) revealed that no aberration corrections to the initial image were necessary (see above). The speckle pattern seen in sample-containing regions of the chemical image was caused by variations in ion signal. Because the ion yield in LDI is a nonlinear function of the optical power density at the surface, pulse-to-pulse fluctuations in laser power can be

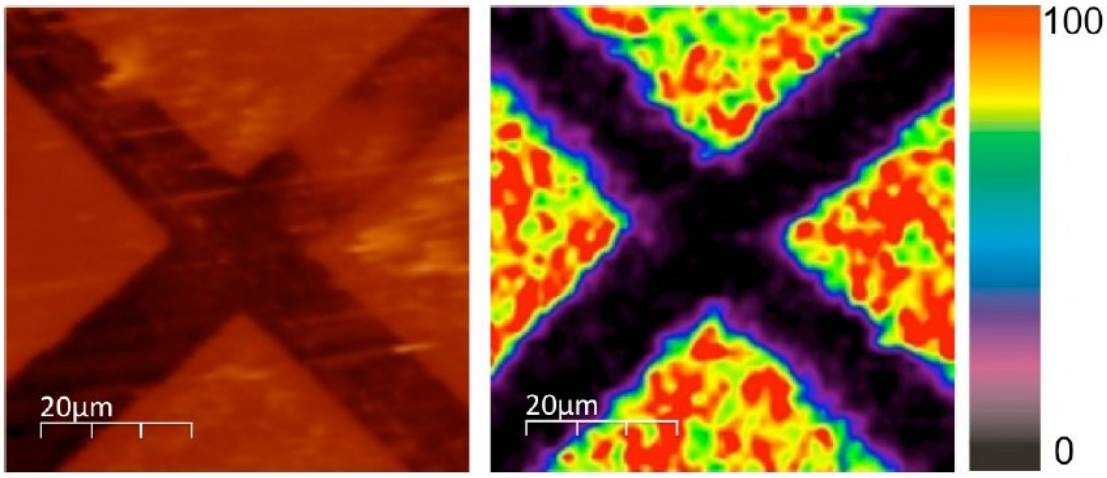

Figure 12. (a) False-color AFM image, similar to that shown in Figure 10a, of a pattern ablated in a rhodamine 6G sample layer. (b) Corresponding mass spectral chemical image of 12(a); the distance scales have 1 µm divisions. The color scale indicates the relative signal level for the molecular ion of rhodamine 6G at *m/z* 443, normalized to a maximum of 5 x 10^4 counts.

manifested as even greater variations in the desorbed ion signal. Furthermore, the low signal-to-noise ratios noted above indicate that the instrument was near its ion detection limit. Thus, the oversampled resolution (i.e., 1.05 s-pixel^{-1} x 2 μm-s^{-1} = 2.1 μm-pixel^{-1}) for the image is taken as the lower limit for spatial resolution.

Conclusions

This section has focused on the operational characteristics and preliminary figures-of-merit for a new MSI instrument comprising an AFM coupled with a pulsed laser and a linear quadrupole ion trap mass spectrometer. Although instrument performance data were acquired using only a single chemical compound, the capability of MS for multi-component analysis makes more complex MSI applications possible. The initial results indicate that the effective spatial resolution for chemical images is a function of the limit of detection. Thus, it is clear that high quality chemical imaging is dependent on efficient generation and collection of analyte ions from desorbed surface moieties. Because desorption and ionization are intrinsically coupled in LDI-MS, therefore, direct ion yields are sensitive to the experimental factors that affect the individual processes. Consequently, since the number density of desorbed neutral species is known to be orders-of-magnitude greater than that of ions, post-ionization methods will be investigated as a means for reducing variations in ion yields and improving detection limits. Furthermore, because ion-ion repulsion and gas-phase ion-neutral collisions subsequent to AP-LDI result in ion cloud expansion and scattering, thereby degrading ultimate sensitivity, changes to parameters expected to be of crucial importance in such processes will be explored; these include ion collection geometry and

associated potential distributions, time dependence and magnitude of applied voltages, and gas flow dynamics. Additionally, a more dimensionally stable optical subsystem is under development to further minimize aberrations as improved ion sensitivity allows for enhanced spatial resolution.

Towards Chemical Imaging Using Apperatureless Tip-Enhanced Plasmon Resonance Laser Desorption Mass Spectrometry

Scanning probe microscopy (SPM) techniques[94,95], are versatile surface imaging methods that provide the capability for ascertaining the structural framework of matter on the atomic scale. Such instruments use various interaction forces between a sharp, nanometer-scale probe tip to monitor and control the tip-to-sample distance. Correlating the control signal with the tip location as it is scanned across a surface then enables nanoscale topographic images to be acquired for groups of individual atoms and molecules. Moreover, when properly polarized laser light is focused onto the probe[96,97], its acts as an optical antenna producing strong enhancement of the radiation intensity in a localized region at the apex and comparable with the radius of curvature of the probe tip (i.e., near-field enhancement). Metal tips can locally enhance electric fields up to 10^3 if the wavelength of light is in resonance with surface plasmons[98]. Thus, the probe can function as a confined, intense, near-field source, the resolution essentially being defined by the tip diameter. By subsequently collecting the scattered light in the far-field, it is possible to image features below the diffraction limit; the final instrumental configuration can take a number of forms, but is known collectively as apertureless or tip-enhanced near-field scanning optical microscopy (NSOM). Furthermore, because this effect results

in orders-of-magnitude signal gain, metal-probe imaging has been combined with fluorescence[99], Raman[100], and infrared[101] spectroscopies to yield additional chemical information.

The enhanced radiation intensity responsible for NSOM optical spectroscopy also can produce nanoscale surface effects, so that the tip can serve as a near-field desorption/ionization source for mass spectrometry (MS) as well. Since MS can yield substantial molecular information in the form of molecular mass and detailed structural characterization and can be combined with atmospheric pressure ionization sources, tip-enhanced desorption/ablation MS surface imaging has enormous potential as an alternate spectroscopic method for investigating nanoscale structures. Although nanoscale MS imaging is itself over 10 years old, only a few methods have been reported and optimal instrumental designs for it are still under investigation. For example, micrometer to sub-micrometer lateral resolution MS analysis has been achieved in a couple of instances by using a near-field source and extracting the desorbed species into a TOF-MS[61,88]. However, in these experiments the ionization performed in vacuum, using an aperture based approach, which yielded no chemical imaging of the surface. Other novel designs have nanoscale sensitivity but have not been reported to form a full image with nanometer-sized pixels[102].

Consequently, we are pursuing development of an instrument for atmospheric pressure, nanoscale topographic and chemical imaging of surfaces via MS. Below we describe the initial task in the overall development process, construction and operation of a versatile scanning surface probe for nanoscale tip-enhanced, near-field laser desorption/ablation. In addition, we relate its use for experimental investigation of

absorption of near-field radiation as the mechanism for the desorption/ablation process, since other effects such as tip heating, deformation (nano-indentation) due to tip expansion, secondary particle bombardment, etc. also could be responsible.

Instrumentation

A rendered drawing of the near-field nanoscale instrument used in our investigations is shown in Figure 13. A Veeco Metrology (Santa Barbara, CA) MultiMode atomic force microscope (AFM) head and nPoint (Madison, WI) sample stage (model iCXYZ100-DM: 15 μm *z* ; 100 μm *x,y* ranges) comprise the tip/sample mechanical subsystem. Cantilever-mounted AFM probes are placed in a holder that, when inserted into the AFM head, positions the cantilever at ~12° with respect to the sample surface. A low-power cw diode laser beam, reflecting off the back face of the cantilever, provides topographical information through its deflection as the tip moves across the surface. The nPoint stage is powered by a digital closed-loop controller (C-300) that enables nanometer-scale *x,y* positioning/scanning of the sample with little drift and hysteresis over the course of an experiment, thereby allowing for array-based sampling protocols over relatively long time periods. The probes used here are standard cantilever-mounted silicon AFM tips with conical tapers, having ultimately nanometer-sized tip curvature and different compositions, such as metal coatings or dopant changes.

A telescope-based optical subsystem, situated approximately orthogonal to the long axis of the cantilever, transfers laser radiation to the tip and underlying sample

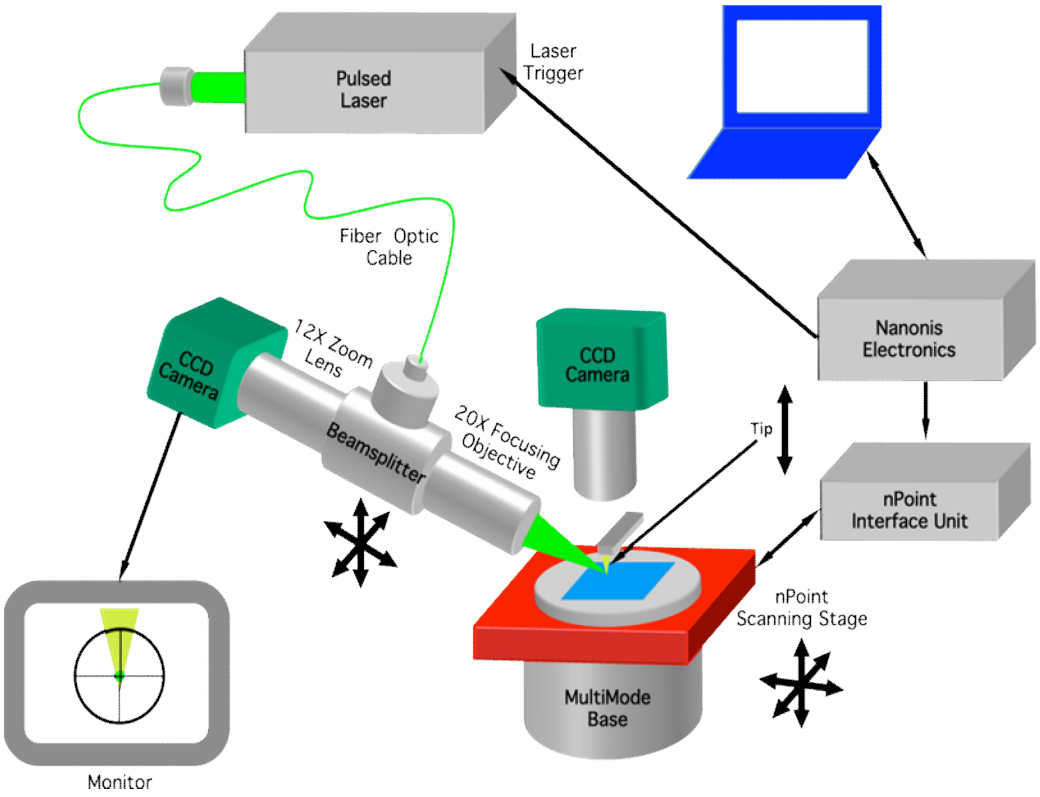

Figure 13. Sketch of tip-enhanced nanoscale laser desorption apparatus designed and used in these studies.

surface. Geometrical constraints imposed by protrusion of the cantilever edge into the optical path between the tip apex and laser beam restrict the associated minimum polar angle to ~60°, which is used here. Laser pulses from a frequency-doubled Minilite (Continuum, Santa Clara, CA) Nd:YAG laser (532 nm, ~5 ns pulse width), running in single-shot mode, enter a mechanically stabilized multimode fiber and become collimated via an AR-coated FiberPort (OFR, Caldwell, NJ) on exiting into the side arm of the alignment system. After the pulses pass through an adjustable linear polarizer and reflect towards the sample via a non-polarizing cube beamsplitter, they are focused using a Mitutoyo M Plan Apo SL 20X microscope objective; the result is a far-field elliptical spot (~ 50 x 100 μm axes) at the surface. The linear polarizer enables the polarization of the laser radiation to being adjusted either parallel or perpendicular to the tip cone center axis.

The same optical subsystem used for laser beam steering and focusing is also employed for laser focus/tip alignment and sample observation. The image of the tip/sample region is sent back into the objective, from which it then transits the cube beamsplitter before passing through a 12X zoom lens, a second adjustable linear polarizer, a 650-nm cut-off optical filter, a reticle, and finally focusing on a CCD continuous imaging camera. The second polarizer prevents secondary laser reflections off the cube beamsplitter from swamping and/or damaging the CCD camera, and the filter blocks the AFM laser diode light. The reticle acts a convenient sight for subsequent positioning of the tip and laser focus once they are initially aligned via remote-controlled Picomotor™ (New Focus, San Jose, CA) actuators. The tip/sample region can also be viewed from another perspective (i.e., normal to the sample surface) via a second 12X

zoom lens/CCD camera setup located directly over a window in the top of the MultiMode head. White light illumination of the tip/sample region is performed using incandescent/fluorescent lighting.

AFM control and data acquisition are performed using the Nanonis (Zurich, Switzerland) SPM software and controller, which is interfaced to the MultiMode via the nPoint C-300. The Nanonis programming interface is employed to create custom LabVIEW codes that control the *x,y,z* positioning of the tip relative to the surface as well as the triggering of laser pulses.

Results and Discussion

Tip-enhanced, near-field laser desorption/ablation experiments were carried out via the following sequence of events: the tip, after being brought into contact with the surface, is moved lightly across the sample to a given location, and is then raised off the surface by a specified amount; a single laser pulse focused at the tip/surface region is triggered immediately thereafter; finally, the tip is withdrawn to a relatively high distance. Topographical imaging of the region in the vicinity of the affected area was subsequently performed using the AFM's standard tapping mode. Blank measurements, which are performed using the above procedure without laser triggering, were often used to initially determine if mechanical damage was possible with the given conditions.

For a model analyte, Sharpie® Red marker, known to contain the dye Rhodamine 6G, was swiped onto glass cover slips. A deep red surface deposit, believed to be mostly a dye layer tens of nanometers or greater thick, remained after vacuum drying over

several hours. Blank AFM scans revealed 25-100 μm^2 regions of relative smoothness (12 ± 1 nm) in which the experiments described below were carried out.

Figure 14 shows an AFM image of the affected sample region following near-field ablation using an uncoated NSC15 tip (MikroMasch, San Jose, CA) and a single 15 nJ laser pulse, with other conditions indicated. The crater profile indicates a FWHM of ~50 nm with a depth of ~4 nm. Far-field damage was not observed for 15 nJ laser pulses when the tip was retracted. By gradually increasing the laser energy with the same far-field focusing conditions, the corresponding damage threshold was estimated to be ~1 μJ/pulse, suggesting that the near-field tip enhancement for desorption is ~100x or greater. For reproducibility assessment of tip-enhanced near-field ablation, large-scale arrays of > 200 similar ablation craters, each resulting from a single ~15 nJ laser pulse, were also analyzed via AFM imaging. Craters were observed throughout the entire array, allowing us to conclude high reproducibility and enabling us to perform statistical analyses of hole depths that were independent of tip degradation. Examination of a later series of craters created under similar conditions showed a variation of ~50% in depth. It is yet unclear as to whether shot-to-shot laser fluctuations, the surface and/or environment, precision in tip placement above the surface, or other factors are responsible for the variability.

According to temperature profile simulations performed by Downes et al.[103], no substantial temperature-jump should be induced in an unmodified Si tip when using laser peak powers similar to those in our experiments. Nevertheless, to eliminate the possibility of sample nano-indentation produced by tip expansion due to laser heating as well as the possibility of transient downward forces caused by light interaction, we tested for

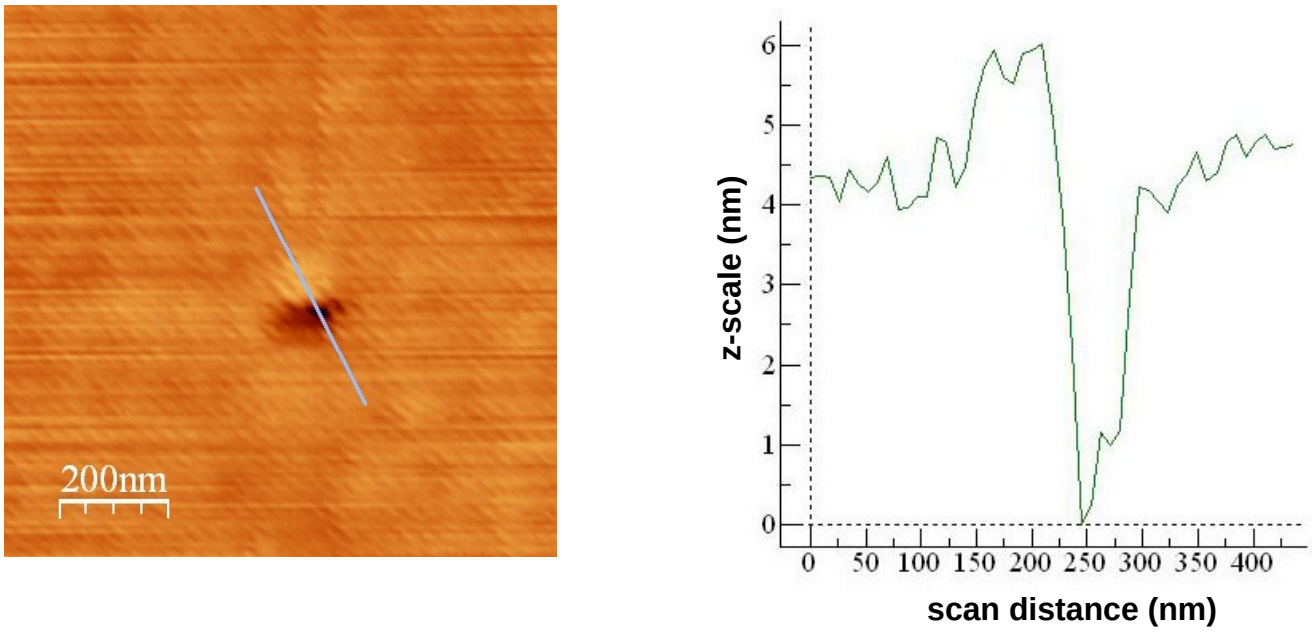

Figure 14. AFM image of a laser desorbed nanohole on Sharpie® Red surface using a bare doped silicon tip. Tip was located 3 nm above the surface before laser pulse was applied. The laser pulse was polarized linearly along the axis of the tip and was applied in a direction from bottom to top in the image. The blue line indicates the line at which a profile at right was made. The raised feature in the image was not present in the blank and possibly indicates where ablated material condensed under these conditions. Images created by WSxM 4.0 software (Horcas, I. et al. *Rev. Sci. Instrum.* 78 013705 (2007)).

tip-enhanced laser ablation at 15 nJ, but with the laser polarization aligned perpendicular to the tip. Simulations for metallized tips, indicate that *p*-polarized light (i.e., polarized nearly parallel to the tip central axis) is capable of much more significant enhancement than *s*-polarized light (i.e., light polarized nearly perpendicular to the tip axis). Resulting AFM images did not show evidence of crater formation under the tip. Further, the possibility of mechanical deformation due to inadvertently forcing the tip against the test surface during experiments was also scrupulously tested for. While it is unclear what effect a laser pulse itself might induce mechanically, we believe that at least these simplest of deformation models cannot explain our observations. These findings lead us to conclude that the dominant mechanism for nano-crater formation during our tip-enhanced ablation investigations is field enhancement of the laser at the tip.

We have also been able to generate nano-craters using gold-coated Si tips for near-field enhancement. However, because we were limited to energies much closer to the far-field ablation threshold in those situations, thermal effects may have been more prominent. In addition, not all gold-coated tips produced evidence of nano-ablation. More studies are required to resolve these problems.

Conclusions

As part of this work we developed a versatile scanning apparatus for surface sampling that uses near-field enhancement of laser radiation at a sharp probe tip to effect nanoscale desorption/ablation on opaque substrates. Experimental data and observations suggest that the dominant mechanism for the process is absorption of radiation produced

via near-field enhancement and not other possibilities, such as mechanical deformation due to thermal expansion of the tip. Our experimental results also show that the tip field enhancement factor results in near-field ablation at laser intensities far below the corresponding far-field ablation threshold. Consequently, we believe that the latter process should not degrade the spatial resolution attainable for proposed chemical imaging methods based on the scanning surface probe. Furthermore, because electric fields can be highly concentrated at the laser-illuminated tip, the potential capability to isolate associated higher-order interactions there may enable the observation and understanding of effects not seen or distinguished in far-field experiments.

CHAPTER III
THERMAL DESORPTION WITH A SECONDARY IONIZATION MASS SPECTROMETRY

Proximal Probe Thermal Desorption with a Secondary Ionization Mass Spectrometry (TD/SI-MS)

The coupling of thin-layer chromatography (TLC) and mass spectrometry (MS) has been an ongoing, steadily advancing research area for nearly three decades.[104,105,106,107,108,109,110,111] Direct mass spectrometric analysis of the analytes separated on a TLC plate provides a simple means to achieve sensitive and compound specific detection as well as achieve molecular identification of unknowns. A variety of *in vacuo* surface sampling/ionization techniques with mass spectrometry have been used to analyze TLC plates over this time period. Fast atom bombardment (FAB),[112] secondary ion mass spectrometry (SIMS)[113] and matrix assisted laser desorption-ionization (MALDI)[108,110] were among the first techniques used. Of these, MALDI is currently the most widely employed. A variety of atmospheric pressure (AP), or ambient, surface sampling/ionization techniques are now also available for use with mass spectrometry. [19,20,21] A number of these techniques have already been used for TLC-MS as detailed in a recent review.[114] In general, these ambient methods all circumvent the need to place the sample into the vacuum chamber of the mass spectrometer, easing restrictions on the size, shape and general nature of the developed plates (e.g., wet versus dry) that can be analyzed. These ambient techniques include a variety of desorption/extraction processes to sample analytes from surfaces including thermal desorption, laser desorption (ablation), liquid and gas jet desorption, and direct liquid

extraction.[19,20,21] These various desorption/extraction methods are typically coupled with an AP ionization method like atmospheric pressure chemical ionization (APCI)[11] or electrospray ionization (ESI) [12]. The best desorption/ionization combination to use for a particular analysis will be dictated in part by the nature of the analyte (e.g., thermal stability, molecular mass, polarity) and the ions desired for the analysis (e.g., singly or multiply charged).

Discussed here is ambient thermal desorption/ionization (TD/I) as a means to couple TLC and MS. Thermal desorption/ionization methods are expected to be limited in application to relatively low mass species ($\leq$ 2000 Da) amenable to vaporization by heating. This suite of compounds might be expected to be similar to those that can be directly analyzed by gas chromatography (GC) or TD with GC.[115] High-mass, thermally labile or highly polar species typically are not suitable for analysis using TD. Of the existing ambient thermal desorption/ionization methods,[19,20,21] only direct analysis in real time (DART) [57] has appeared in the peer-reviewed literature as a means to couple TLC and MS.[116,117,118,119] In DART a stream of heated He or N_2 carrier gas, which has been subjected to a discharge at a needle electrode, is directed at the entrance of the mass spectrometer. Neutral metastable species produced in the discharge react with molecules present in air to produce a reagent ion population that can ionize the gas phase analytes. DART has been successfully used for readout of isopropyl-9H-thioxanthen-9-one (ITX)[116,117] caffeine,[117,119] cinnamaldehyde,[119] phenolphthalein,[119] and acetaminophen[119] on developed TLC or high performance (HP) TLC plates.

Presented here is a simple robust proximal probe, TD technique for sampling of analytes from a HPTLC plate with secondary ionization by APCI or ESI. This approach

does not require an external heated gas or a specialized ionization source. Thermal desorption is accomplished by placing a heated metal probe close to or in contact with the surface to be sampled. Desorbed species from the surface are drawn into the ionization region of the existing ESI/APCI source of the mass spectrometer and ionized. The particular instrument used in this work allows either ESI or APCI to be used exclusively, or to be used alternatively during an experiment (so called ESCi source)[120] to increase the ability to ionize compounds of disparate properties simultaneously. In addition, various solvents and dopants are easily added to the ionization region through the ESI probe to promote the formation of selected ionic forms of the analytes of interest. The effect of proximal probe temperature, surface scan speed, gas flow rate into the ion source, and surface type on read-out resolution, detection level, and linearity of response was investigated and reported for selected compounds. The general applicability of this TD approach to coupling TLC and MS is demonstrated by the automated lane scan analysis of a range of analyte types including explosives, dyes, herbicides and pharmaceuticals separated on various types of HPTLC plates.

Experimental Methods

Chemicals

HPLC grade acetonitrile was purchased from Burdick and Jackson (Muskegon, MI). HPLC grade methanol, ACS grade chloroform, toluene and methylene chloride were obtained from J.T. Baker, Inc. (Phillipsburg, NJ). ACS grade acetone and ethyl acetate were acquired from EM Sciences (Gibbstown, NJ). Glacial acetic acid, 99% ethanol, Sudan Red 7B (CAS No, 6368-72-5), 2-acetoxybenzoic acid (aspirin, CAS No, 50-78-2)

and N-(4-hydroxyphenyl)ethanamide (acetaminophen or paracetamol, CAS No, 103-90-2) were purchased from Sigma Aldrich (Milwaukee, WI). Test Dye Mixture V containing Sudan Red 7B, solvent green 3 (CAS No, 128-20-3), and solvent blue 35 (CAS No, 17354-14-2) in toluene was obtained from Analtech, Inc. (P/N 30-05, Newark, DE). Standard solutions (1000 μg/mL in acetonitrile) of 1,3,5,7-tetranitro-1,3,5,7-tetrazocane (HMX, CAS No, 2691-41-0), 1,3,5-Trinitroperhydro-1,3,5-triazine (RDX, CAS No, 121-82-4) and 2,4,6-trinitrotoluene (TNT, CAS No, 121-14-2) were obtained from Supelco (Bellefonte, PA). Stock solutions (1000 μg/mL) of 1,3,5-triazine-2,4,6-triamine (melamine, CAS No 108-78-1) in diethylamine/water 80/20 (v/v)) were purchased from Restek (Restek Corp., Bellefonte, PA). 2,4-Dichlorophenoxyacetic acid (2,4-D, CAS No, 94-75-7), 4-(2,4-dichlorophenoxy)butyric acid (4-(2,4-DB)), CAS No 94-82-6) and 2,4,5-trichlorophenoxyacetic acid (2,4,5-T, CAS No 93-76-5) were obtained from PolySciences Corp. (Niles, IL). 1,3,7-Trimethyl-1H-purine-2,6(3H,7H)-dione (caffeine, CAS No, 58-08-2) was purchased from J.T. Baker. Extra Strength Excedrin (Bristol-Meyers Squibb, New York, NY) containing 250 mg aspirin, 250 mg acetaminophen, and 65 mg caffeine per tablet was purchased over the counter locally. Structures of all compounds investigated are shown in Figure 15 as the free acid forms to simplify the mass spectrometry nomenclature for the gas-phase ions observed.

A solution of Sudan Red 7B was prepared in methanol (2.4 μM) for TLC and ESI/APCI-MS detection optimization. Standard solutions from 0.1-10000 μg/mL of this dye for TLC were prepared by serial dilution of a methanolic stock solution with methanol. Solutions of HMX, RDX, and TNT for ESI/APCI-MS detection optimization

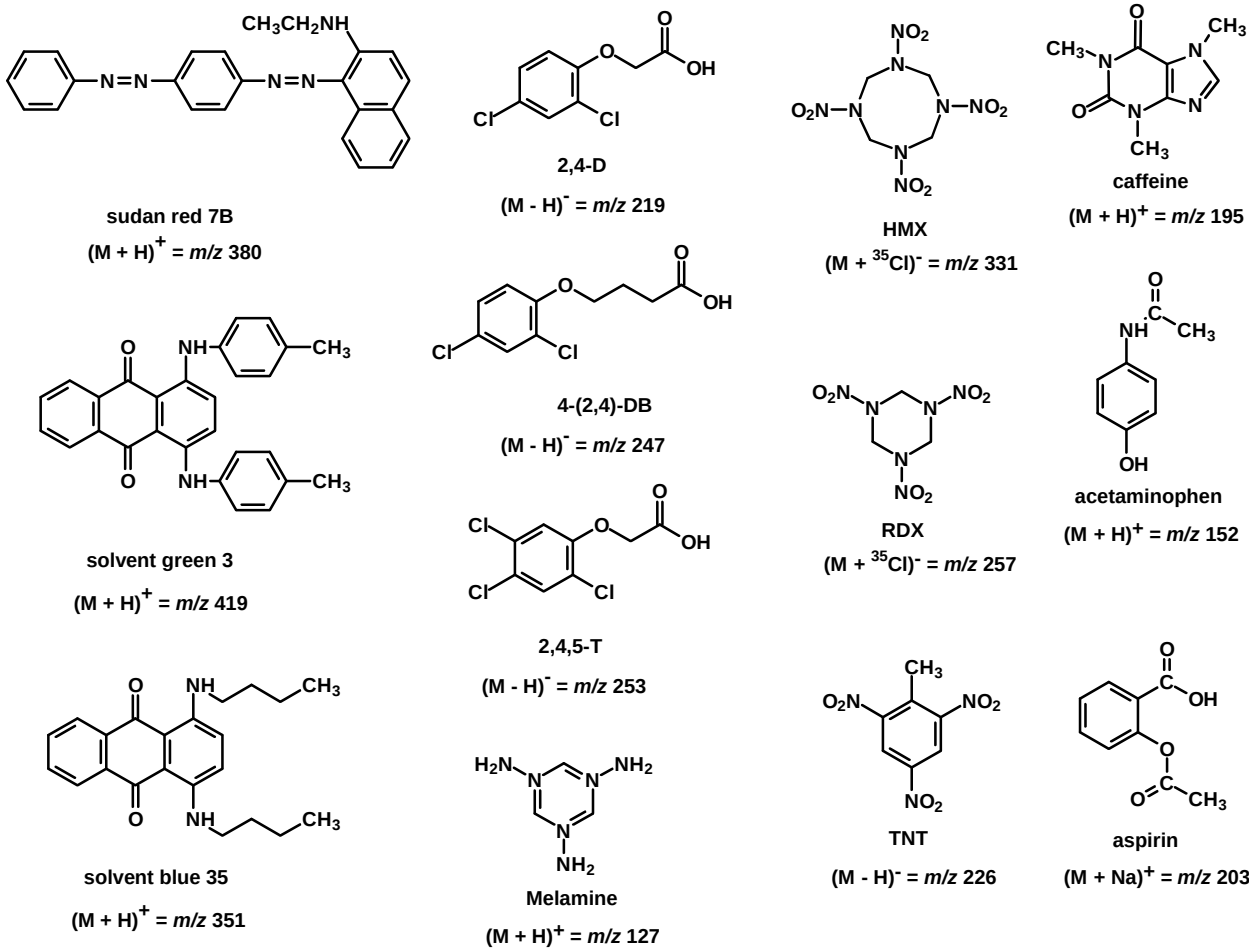

Figure 15. Structure and mass-to-charge ratio for specific molecular ionic species observed for the compounds investigated.

(4.4 μM) were prepared by dilution of 1000 μg/mL stock solutions in acetonitrile. The analytical standards for TLC were prepared by diluting this standard stock solution in acetonitrile. Solutions of acetaminophen (1 μM), aspirin (1 μM), caffeine (1 μM), 4-(2,4-DB) (1.5 μM), 2,4-D (1.2 μM), and 2,4,5-T (1.5 μM) were prepared for ESI/APCI-MS detection optimization by dissolving the compounds in methanol.

TLC

In all cases, application of sample solutions to the TLC plates was performed manually using a 10 μL syringe. Vertical development of all the plates was carried out in a covered flat-bottom chamber.

The components, Sudan Red 7B, solvent green 3, and solvent blue 35, of Test Dye Mixture V (about 1000 μg/mL of each dye) were separated on glass backed normal-phase silica gel plates with organic binder and UV 254 indicator (HPTLC-HLF, 150 μm phase, P/N 59077, AnalTech Inc., Newark, DE). The dye mix was spotted as a band (a closely spaced series of 1 μL aliquots) and the plate was developed in toluene. Developed plates were dried in an oven at (110 ˚C) for 5 min just prior to analysis. Photographs of the developed plates prior to analysis were taken with an Olympus SP-500UZ digital camera (Olympus Imaging Corp., Tokyo, Japan) using white light illumination. Serial dilutions of Sudan Red 7B, (0.01 - 10,000 μg/mL) in methanol were prepared and 1 μL aliquots with 5 mm spacing were applied to same type of HPTLC plate. The plates were developed in toluene then dried in an oven (110 ◦C) for 5 min prior to analysis.

The explosives TNT, RDX and HMX were separated on glass backed normal-phase HPTLC plates (ProteoChrom HPTLC silica gel 60 $F_{254,}$ 150 - 200 μm phase, P/N 1.05650.001, Merck KGaA, Darmstadt, Germany) using a procedure adapted from Douse.[121] The explosives mix (1000 μg/mL of each explosive) was spotted as a band (a closely spaced series of 1 μL aliquots). Serial dilutions of TNT (0.001 - 1000 μg/mL) were prepared in acetonitrile and 1 μL aliquots with 5 mm spacing were applied to same type of HPTLC plate. A 1000 μg/mL solution of TNT was prepared in acetonitrile and 1 μL aliquots with 5 mm spacing were applied to the ProteoChrom HPTLC silica gel 60 plates, a glass backed RP-18 HPTLC plates (HPTLC Silica gel 60 RP-18 F_{254}S, 150 - 200 μm phase, P/N 13724/5, Merck KGaA, Darmstadt, Germany) and plain glass slides (Gold Seal Products, Portsmouth, NH). The HPTLC plates were developed in 2/1 (v/v) chloroform/acetone and dried in an oven (110 ◦C) for 5 min prior to analysis. Photographs of the developed plates prior to analysis were taken with an Olympus SP-500UZ digital camera using short-wavelength UV illumination.

The TLC separation of herbicides, 4-(2,4-DB), 2,4-D, and 2,4,5-T was adapted from Guardigli et al.[122] using glass backed normal-phase silica gel plates with organic binder and UV-254 indicator (HPTLC-HLF, 150 μm phase, P/N 59077, AnalTech, Inc.). The herbicide mix (10000 μg/mL of each herbicide) was spotted as a band (a closely spaced series of 1 μL aliquots) and the plate developed in 85/15 (v/v) toluene/glacial acetic acid. Developed plates were dried in an oven (110 ◦C) for 5 min prior to analysis. Photographs of the developed plates prior to analysis were taken with an Olympus SP-500UZ digital camera using short-wavelength UV illumination.

The separation of aspirin, acetaminophen, and caffeine extracted from Excedrin tablets was carried out using a procedure adapted from Williamson[123] on glass backed normal-phase silica gel plates with organic binder and UV 254 indicator (HPTLC-HLF, 150 μm phase, P/N 59077, AnalTech Inc.). The pharmaceutical components were extracted from a ground-up fraction of an Excedrin tablet using 50/50 (v/v) ethanol/ethyl acetate (1.4 mg of tablet/mL of solution). The extract was centrifuged and filtered. Plates were pre-developed with a 99/1 (v/v) ethyl acetate/glacial acetic acid and then dried in an oven at (110 ◦C) for 30 min. The filtered solution containing aspirin, acetaminophen, and caffeine was spotted as a band (a closely spaced series of 1 μL aliquots) and the plate was developed in 99/1 (v/v) ethyl acetate/glacial acetic acid. Developed plates were dried in an oven (110 ◦C) for 5 min. Serial dilutions of acetaminophen (0.001 - 1000 μg/mL) were prepared in methanol and 1 μL aliquots with 5 mm spacing were applied to same type of HPTLC plate. The plates were developed in 99/1 (v/v) ethyl acetate/glacial acetic acid and then dried in an oven (110 ˚C) for 5 min prior to analysis. Photographs of the developed plates prior to analysis were taken with an Olympus SP-500UZ digital camera using short-wavelength UV illumination.

Aliquots (1 μL) of a 1000 μg/mL solution of melamine in diethylamine/water (20/80) (v/v) were applied with 5 mm spacing to glass backed normal-phase HPTLC plates (ProteoChrom HPTLC silica gel 60 F_{254}), glass backed RP-18 HPTLC plates (HPTLC Silica gel 60 RP-18 F_{254}s, 150 - 200 μm phase, P/N 13724/5, Merck KGaA), and plain glass slides (Gold Seal Products). Both types of plates were developed in 6/2/2 (v/v/v) acetonitrile/water/ethyl acetate then dried in an oven (110 ˚C) for 5 min prior to analysis.

TLC/Proximal Probe TD-MS System.

Figure 16 shows a schematic and a photograph of the TLC/TD/I-MS experimental setup. The mass spectrometer used was a Waters TQD triple quadrupole with ESCi capability (Waters Corp., Milford, MA). Analyte detection was performed using full scan mode, single ion monitoring (SIM), or selected reaction monitoring (SRM) with Ar as a collision gas (0.20 mL/min). The SRM transitions monitored were: TNT (*m/z* 227 → *m/z* 210, CE = 10 eV*),* Sudan Red 7B (*m/z* 380 → *m/z* 183, CE = 16 eV), solvent blue 35 (*m/z* 351 → *m/z* 251, CE = 30 eV*)*, solvent green 3 (*m/z* 419 → *m/z* 327, CE = 33 eV), acetaminophen (*m/z* 152 → *m/z* 110, CE = 16 eV) and melamine (*m/z* 127 → *m/z* 85, CE = 19 eV).

A special cone electrode in the TQD ionization source can was fabricated by removing the normal curved gas inlet connection and attaching a straight 1.5 in. long stainless steel tube (1/8 in. o.d., 1/16 in. i.d.). This tube was connected to a modified Cajon connector secured into the window of the ion source can. The normal glass window in the door into the source can was replaced with plexiglass. An opening for the Cajon connector was constructed from two plexiglass pieces secured to one another with an o-ring and six screws. Either a 12 V, 1.5 amp KNF Neuberger Inc N815KTE mini vacuum pump (KNF Neuberger Inc., Freiburg, Germany), powered with a variable DC supply, or a Vacuubrand GMBH + Co vacuum pump MZ 2D (Vacuubrand GMBH + Co, Werhteim, Germany) with a Parker F200S bleed valve (Parker Inc, Elyria, Ohio) was put

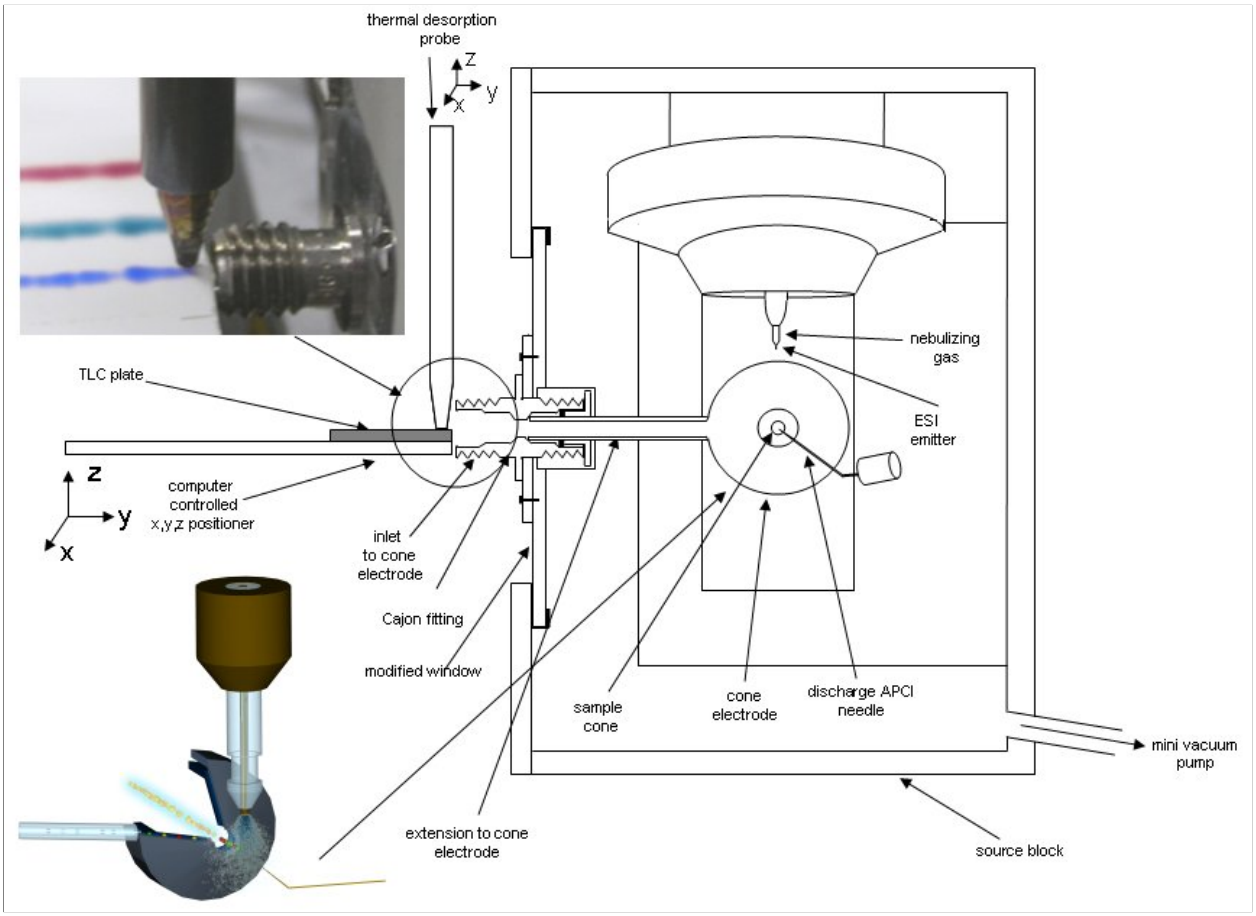

Figure 16. Schematic illustration of the TLC/TD/I-MS experimental setup.

in the ion source exhaust line. Pumping on the source exhaust pulled air from the sampling region external to the source block through the modified source can window and modified cone electrode and into the ionization source. An Aalborg Instruments GFM 37 gas flow meter (Orangeburg, NY) was connected to this gas inlet to calibrate gas flow rate into the source through the cone connection.

An MD 80 wand from a Weller WD 1 soldering station (Weller, Germany) was used as the heated proximal probe. The exchangeable heated probe tip used had a width of 1.6 mm and a thickness of 0.7 mm. A digital controller was used to adjust the temperature at the probe tip from about 25 to 350 °C. The heated probe used was mounted directly in front of the intake orifice into the ionization region though the modified source can window and gas cone electrode. The TLC plate was mounted so that the edge of the plate was as close as possible to the sampling inlet used to draw gas and vapors into the cone electrode region of the ionization source block. The glass backed TLC plates were cut along the length of or perpendicular to the development lanes using a CAMAG *Smart*Cut device (Wilmington, NC) to enable close positioning of the heated probe and bands on the plate to the inlet region into the ionization source. The plates were affixed to a platform on top of the stage using double sided tape.

The MS2000 *x-y-z* robotic platform (Applied Scientific Instrumentation Inc., Eugene, OR), and control software used to manipulate the TLC plate relative to the stationary heated probe has been described in previous work.[124] The stage could be moved in all directions by manual or computer control to allow for scanning the developed TLC lanes. The initial positioning of the stage and the sample to be investigated was done manually. The development lane along the TLC plate was scanned

in the x-y plane under computer control. The exact position of the heated probe relative to the surface during an experiment was monitored using a CCD camera and a monitor.

Results and Discussion

Optimization and General Performance Metrics

The schematic in Figure 16 shows the optimized setup of the TLC/TD/I-MS experiments. This TD/I system used a heated metal probe placed close enough to just touch the surface of interest, but yet not physically disrupt the surface during a scan of the surface versus the stationary probe. Components desorbed from the surface were drawn into the ionization region of the existing ESI/APCI source, through the cone electrode, where they merged with reagent ions and/or charged droplets from a corona discharge or an electrospray emitter and were ionized. The ionized components were then drawn through the atmospheric sampling orifice into the vacuum region of the mass spectrometer and analyzed, (Figure 16). Others have already demonstrated this same type of counter flow sample vapor introduction for ambient ionization to be highly effective.[125]

Determining the best position of the heated probe relative to the inlet of the mass spectrometer was important for optimum performance of the TLC/TD/I-MS system. This was accomplished by mounting the probe on an x-y-z translation stage and adjusting the vertical and horizontal position of the probe relative to the inlet into the cone electrode while monitoring the signal intensity of the analyte with the mass spectrometer. The region of the surface to be analyzed was positioned as near to the sampling tube as possible, within the constraints of the current instrument interface design, and at the

vertical mid point of the inlet tube. For the analysis of the TLC plates, this required the development lanes to be near the edge of the plate. Therefore, the developed plates were scored and cut parallel or perpendicular to the development direction to provide access to the bands of interest for analysis. Alternate probe/inlet arrangements that might include an extension on the inlet tube could be implemented in the future to allow analysis of uncut plates.

Beyond positioning of the heated probe and sample, optimal performance of the TLC/TD/I-MS system was also dependent upon the temperature of the heated probe, gas flow rate into the ionization region, and surface scan speed relative to the stationary heated probe. Optimal settings for the temperature of the heated probe were investigated using the relatively volatile compound TNT (Table 1). TNT was applied to HPTLC plates as 1 μg spots (1 μL of a 1 mg/mL standard) with 5 mm spacing between the spots and then the plate was developed. The TLC plate was scanned relative to the stationary heated probe at a rate of 200 μm/s while monitoring the signal for the SRM transition of TNT. Multiple experiments were performed using probe temperatures ranging from 100 ^{o}C to 350 ^{o}C and a gas flow rate into the ion source region of 30 mL/min (Figure 17a). A probe temperature of 350 ^{o}C, the highest temperature possible with the current apparatus, produced the maximum signal levels and was used for all subsequent studies. However, an even higher probe temperature might further improve the signal levels for this or other analytes, especially those less volatile than TNT. However, thermal degradation of the surface or the compounds of interest may become a factor at even higher temperatures.

Using this same TNT HPTLC separation, surface scanning, and mass spectrometry detection protocol, the effect of gas flow rate into the ion source region on

Table 1. List of compounds used and their respective vapor pressures, boiling points, and melting points.

Compound	Vapor Pressure (Pa)	Boiling Point (^{o}C)	Melting Point (^{o}C)
caffeine[1]	4.7×10^{-6} @ 25 C	178	238
acetaminophen[1,2]	8.4×10^{-3} @ 25 C	387.8	169-170
aspirin[1,3]	4.0×10^{-3} @ 25 C	135	140
TNT[1,3]	2.7×10^{-2} @ 25C	240	80.1
RDX[1,3,3]	3.5×10^{-19} @ 25 C	234	205.5
HMX[1,3,3]	2.8×10^{-30} @ 25 C	234 (auto-ignition temperature)	275
2,4,5-T[1,3,3]	1.33×10^{-5} @ 25 C	376.3	158
2,4-D[1,3,3]	3.1×10^{-3} @ 25 C	160	140
2,4,-DB[1,2,3]	4.0×10^{-6} @ 25 C	150	118
melamine[1]	4.7×10^{-8} @ 20 C	280	350
Sudan Red 7B[1,2]	1.5×10^{-12} @ 25 C	606.6	130
solvent blue 35[1,2]	8.0×10^{-11} @ 25 C	568.7	180
solvent green 3[4]	9.4×10^{-11} @ 25 C	633.8	220-221

[1] International Programme of Chemical Safety (IPCS), https://www.inchemchem.org

[2] Royal Society of Chemistry, ChemSpider Database, http://www.chemspider.com/About.aspx

[3] CAMEO Chemicals, Database of Hazardous Materials, http://cameochemicals.noaa.gov/

[4] United States Environmental Protection Agency, http://www.epa.gov/opprd001/inerts/foodcolors.pdf

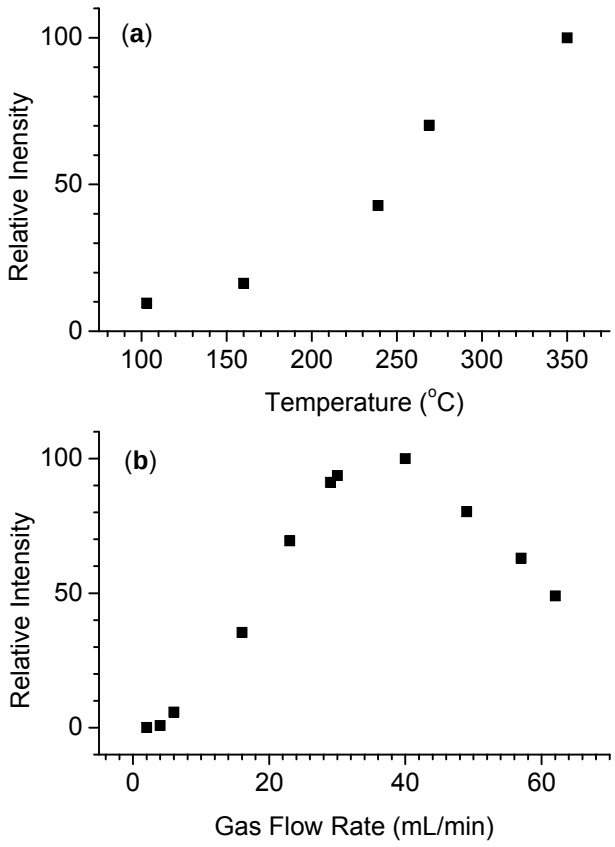

Figure 17. Normalized SRM intensity for TNT (*m/z* 227 → *m/z* 210, CE = 10 eV) in APCI negative ion mode versus (a) proximal probe temperature, and (b) gas flow rate into the ion source can of the mass spectrometer. TNT was applied to the HPTLC plates as 1 μg spots (1 μL of 1 mg/mL standard) with 5 mm spacing between the spots and then the plate was developed. The TLC plate was scanned relative to the stationary heated probe at a rate of 200 μm/s while monitoring the SRM transition of TNT. Gas flow rate into the ion source region was 30 mL/min for (a) and probe temperature was 350 °C in (b). Glass backed NP HPTLC plates (ProteoChrom HPTLC silica gel 60 $F_{254,}$ 150 - 200 μm phase, P/N 1.05650.001, Merck KGaA, Darmstadt, Germany) were used for both experiments. SRM dwell time was 500 ms.

signal intensity was also investigated. By varying the voltage applied to the KNF pump on the ion source block, the gas flow rate into this region was varied from 5.5 mL/min up to 30 mL/min. The gas flow rate from 40 mL/min up to 62 mL/min was achieved using the Vacuubrand pump, by varying a Parker bleed valve (Figure 17b). The maximum signal levels were achieved in the flow rate range of 30-40 mL/min. Note that this flow rate was well within the recommended cone gas flow setting for the mass spectrometer (i.e., 0 – 833 mL/min). For simplicity of operation, the KNF pump providing a flow rate of 30 mL/min into the source region was used for all subsequent studies.

Effects of surface scan speed on analyte signal intensity were also investigated using the Test Dye Mixture V. The mixture was spotted (~1 μg spots with 5 mm spacing) and developed on an HPTLC plate. The peak height and area, and baseline peak width measured for surface surface scan speeds from 50 μm/s to 800 μm/s, with specific reference to the data obtained for the separated spots of Sudan Red 7B, is shown in Figure 18. The largest integrated peak area (SRM mode) was observed at the slowest scan speed (50 μm/s), with peak area decreasing as the scan rate increased (Figure 18b). The observed peak height reached a maximum plateau in the surface scan range from about 200 - 400 μm/s (Figure 18c). Importantly, the observed mass spectral chronographic band widths (i.e., the time it takes to scan over a band) decreased with scan speed and correlated well with the predicted mass spectral band width values up to about 700 μm/s (Figure 18a). The predicted mass spectral peak width, W, was calculated using eq. 1 where d_B is the diameter of the analyte band determined visually, d_P is the diameter of the probe, and r was the scan speed. The diameter of the probe was included

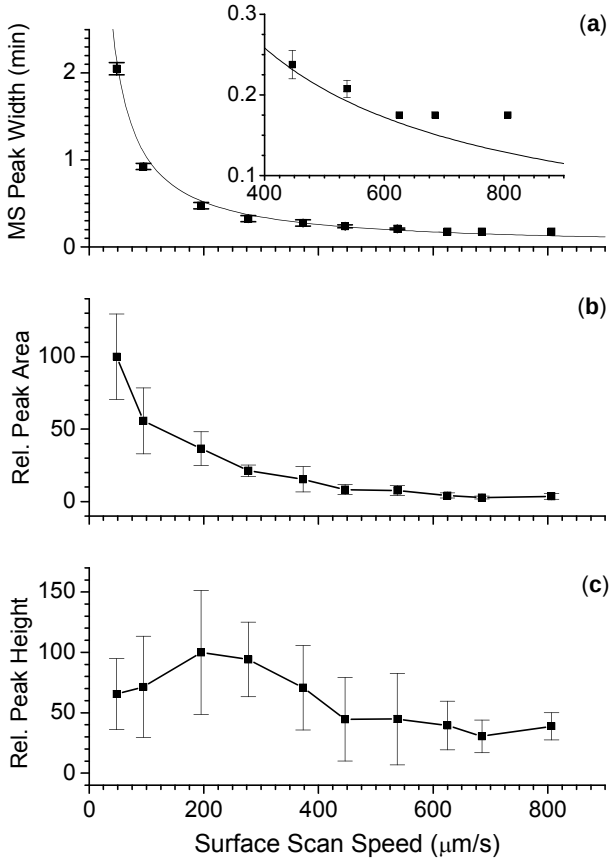

Figure 18. (a) Measured (■) and calculated (*solid line*) mass spectral peak width, (b) normalized measured peak area and (c) normalized peak height versus surface scan speed for Sudan Red 7B using SRM detection (*m/z* 380 → *m/z* 183, CE = 16 eV) in positive ion mode APCI. Experiments were carried out using the Analtech Test Dye mixture V which was spotted (~1 μg spots with 5 mm spacing) and developed on a glass backed NP silica gel plates with organic binder and UV 254 indicator (HPTLC-HLF, 150 μm phase, P/N 59077, AnalTech Inc., Newark, DE). SRM dwell time was 500 ms. Error bars represent $\pm$1 standard deviation calculated from three replicate experiments.

in eq. 1 to account for TD of analyte from the time the near side of the probe first probe approaches the band until the far side of the probe passes completely through the band.

$$W = \frac{(d_B + d_P)}{r} \tag{2}$$

At the fastest scan speeds (~700 μm/s to 800 μm/s) the measured peak width reached a plateau level and began to diverge from the predicted peaks widths. This trend was attributed to the finite time necessary for the vapors from the desorbed species to pass into and through the interface and be detected by the instrument. The same set of experiments was carried out with the other two dyes from the mixture, viz., solvent green 3, solvent blue 35, as well as with TNT. The same basic trends in peak height and peak width were observed for these compounds as well (data not shown).

The detection levels for this TLC/TD/I-MS technique were examined for three different compounds of greatly differing volatility, viz., TNT, acetaminophen and Sudan Red 7B, listed in order of decreasing volatility (see Table 1). Aliquots (1 μL) of serial dilutions of TNT (0.001 - 1000 μg/mL), acetaminophen (0.001 - 1000 μg/mL), and Sudan Red 7B (0.01 - 10000 μg/mL) were spotted on the appropriate HPTLC plates with 5 mm spacing and the plates developed as described in the experimental section. The SRM transitions for these compounds were monitored in positive ion mode APCI while scanning the development lanes at 200 μm/s. The normalized peak areas measured versus plate loading are shown in Figure 19.

These calibration data were evaluated using a least-squares regression and fit the model $A = bx + a$, where A is the integrated peak area for a compound with mass x spotted on the TLC plate. The values b and a are the slope and intercept, respectively, of the

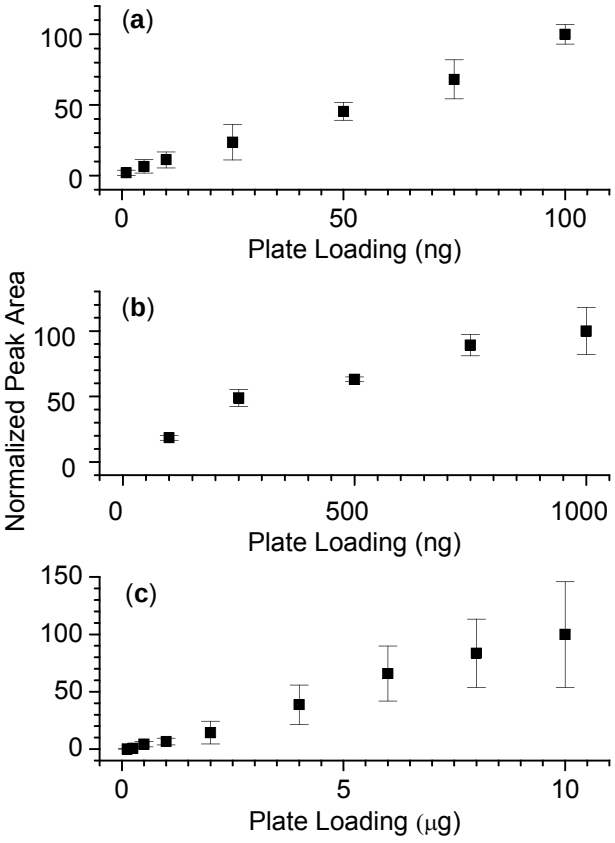

Figure 19. Normalized SRM peak areas versus amount spotted on the HPTLC plate for (a) TNT (*m/z* 227 → *m/z* 210, CE = 10 eV) in APCI negative ion mode, (b) acetaminophen (*m/z* 152 → *m/z* 110, CE = 16 eV) in APCI positive ion mode, and (c) Sudan Red 7B (*m/z* 380 → *m/z* 183, CE = 16 eV) in APCI positive ion mode. Aliquots (1 μL) of serial dilutions of TNT (0.001 - 100 μg/mL), acetaminophen (0.001 - 1000 μg/mL), and Sudan Red 7B (0.01 - 10000 μg/mL) were spotted on the appropriate HPTLC plates with 5 mm spacing and the plates developed as described in the experimental section. The SRM transitions were monitored while scanning the development lanes (200 μm/s - TNT, acetaminophen, and Sudan Red 7B) relative to the heated probe (350 ^{o}C). SRM dwell time was 500 ms for each *m/z* monitored. Error bars represent $\pm$1 standard deviation calculated from three replicate experiments for TNT and acetaminophen and five for Sudan Red 7B.

calibration curve, and are presented for each compound in Table 2. From the linear calibration curves the detection limit was estimated (3 $s_{x/y}$/slope, where $s_{x/y}$, the standard error of the y value estimates, is assumed to approximate the standard deviation of the blank, s_B)[126] This translates to detection levels of 24 ng (0.11 nmol), 370 ng (2.4 nmol), and 5700 ng (15 nmol) for TNT, acetaminophen and Sudan Red 7B, respectively (Table 2). Thus the best detection level was obtained for the more volatile compound. This might be expected to be a general trend for a TD-based process, but other factors such as varying ionization efficiency among compound types will also affect detection levels. While these detection levels are not exceptional from a mass spectrometric point of view, they are within typical plate loadings for HPTLC (i.e., low μg levels), especially for the more volatile compounds.

It is worth comparing how the signal levels vary for any one analyte when desorbed from different stationary phases and simply a plain glass surface. This surface effect was illustrated for both melamine and TNT from glass backed ProteoChrom HPTLC plates and glass backed RP-18 HPTLC plates as well as plain glass slides. Solutions of TNT (1000 μg/mL) and melamine (1000 μg/mL) were spotted in 1 μL aliquots with 5 mm spacing on the respective plates and the HPTLC plates developed. The SRM transition of TNT and melamine were monitored in positive ion mode APCI while scanning the development lanes (100 μm/s for TNT, and 300 μm/s for melamine) relative to the heated probe. The largest integrated peak area for both melamine and TNT was observed when scanning across the analyte spots on plain glass slides and lowest when analyzing the developed spots on the NP plates (Figure 20). The different surfaces had a similar effect on the signal levels for both TNT and melamine.

Table 2. Figures of Merit for the Calibration Curves and Calculation of the Detection Limit for TLC/TD/I-MS

Compound	TNT	Acetaminophen	Sudan Red 7B
Calibration range, ng	1-100	100-1000	125-10000
Slope (b) ± Std dev	2.17 ± 0.11	0.027 ± 0.003	1065 ± 87
Intercept (a) ± Std dev	1.0 ± 5.7	5.8 ± 1.6	-212 ± 430
r^2	0.95	0.89	0.78
Standard error of the y value estimates, $s_{x/y}$ or s_B	17	3.3	2015
Detection limit, ng ($3 * s_B/b$)	24	370	5700
Molecular weight, ng/nmol	227	152	379
Detection limit, nmol	0.11	2.4	15

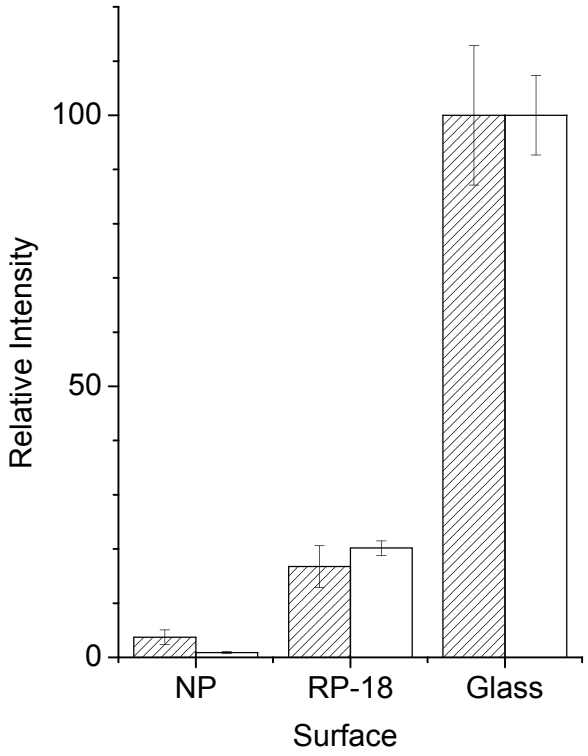

Figure 20. Normalized SRM signal for TNT (*m/z* 227 → *m/z* 210, CE = 10 eV) (*hatched*) in APCI negative ion mode and melamine (*m/z* 127 → *m/z* 85, CE = 19 eV) (*solid white*) in APCI positive ion mode from glass backed normal-phase HPTLC plates (ProteoChrom HPTLC silica gel 60 $F_{254,}$ 150 - 200 μm phase, P/N 1.05650.001, Merck KGaA, Darmstadt, Germany), glass-backed RP-18 HPTLC plates (HPTLC Silica gel 60 RP-18 F_{254}s, 150 - 200 μm phase, P/N 13724/5, Merck KGaA, Darmstadt, Germany) and plain glass microscope slides (Gold Seal Products, Portsmouth, NH). Solutions of TNT (1000 μg/mL) and melamine (1000 μg/mL) were spotted in 1 μL aliquots with 5 mm spacing on the respective plates and the plates developed according to the protocols in the experimental section. The SRM transitions were monitored while scanning the development lanes (100 μm/s - TNT, and 300 μm/s melamine) relative to the heated probe (350 ^{o}C). SRM dwell time was 500 ms. Error bars represent $\pm$1 standard deviation calculated from four replicate experiments.

With both of these relatively polar compounds, the signal from the plain glass surface was ~10 times greater than that from the NP plate and ~5 times greater than the signal level from the RP-18 plate. Obviously the nature of the surface and particular analyte/surface interactions will influence the signal levels and limits of detection.

Selected Applications

Beyond the investigation of variable parameters and performance metrics discussed above, also examined are four mixtures of significantly different analyte types, viz., pharmaceuticals, solvents dyes, herbicides and explosives to illustrate the prospective applicability of this proximal probe TD/I approach for coupling TLC and MS. The pharmaceutical applications will be discussed here in some detail. The results from the studies using solvents dyes, herbicides and explosives can be found in the Appendix (Figures S1-S3).

An Extra Strength Excedrin tablet containing 65 mg of caffeine, 250 mg of acetaminophen, and 250 mg of aspirin was ground-up and the extract containing these three compounds was spotted as a series of tightly spaced spots containing 1.4 μg of material per spot and separated on a glass backed NP HPTLC-HLF silica gel plate. Panel (a) in Figure 21 shows a picture of the development lane and the three separated bands. To acquire the mass spectral data shown in panels (b) – (e), the HPTLC plate was scanned (200 μm/s) from low to high R_F (left to right in the picture) relative to the heated probe (350 ^oC) while full scan mass spectral data was acquired. In this case, two of the compounds, caffeine and acetaminophen, were found to best ionize and be detected as the respective protonated molecules using positive ion mode APCI. Detection of aspirin was

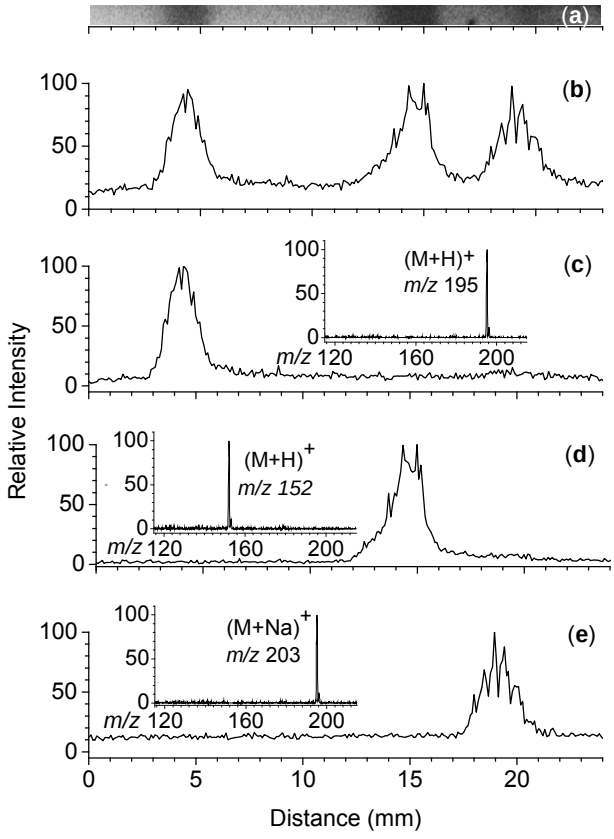

Figure 21. (a) Black and white photograph of glass backed normal-phase silica gel plate (HPTLC-HLF) development lane showing the separated bands of a three component Excedrin mixture containing caffeine, acetaminophen and aspirin. (b) The total ion current from full scan ESCi mode and the individual extracted ion current chromatograms for (c) caffeine (*m/z* 195) using APCI, (d) acetaminophen (*m/z* 152) using APCI, and (e) aspirin (*m/z* 203) using ESI. Also shown in panels (c) – (e) are the averaged, background subtracted full scan mass spectra (*m/z* 115 – 215) for the respective compounds. The development lane was scanned at 200 μm/s relative to the heated probe (350 ^{o}C). The solution containing caffeine, acetaminophen and aspirin was spotted as a band (a closely spaced series of 1.4 μg loadings) on the HPTLC plate.

optimized using ESI to form the sodiated adduct $(M + Na)^+$. That being the case, positive ion mode ESCi was used for this experiment with the ion source switching scan to scan between APCI and ESI mode. To promote ESI, methanol was sprayed through the ESI probe at a flow rate of 60 μL/min. The averaged, background subtracted mass spectra obtained while scanning the respective bands are shown as insets in Figure 6 (c) – (e) for caffeine ($(M + H)^+$ = *m/z* 195), acetaminophen ($(M + H)^+$ = *m/z* 152), and aspirin ($(M + Na)^+$ = *m/z* 203), respectively. This group of compounds in particular highlights the versatility of the technique by utilizing both APCI and ESI ionization sources in tandem for the detection of analytes with varying ionization requirements.

Using this set of data, it was possible to compare the chromatographic resolutions obtained by HPTLC and MS. Chromatographic resolution, *R*, of two chromatographic bands was calculated using eq. 2, where *d* is the distance between the centers of the bands and W_1 and W_2 are the widths of the two bands.[127]

$$R = \frac{d}{(W_1 + W_2)/2} \tag{3}$$

From the optical data obtained using the photograph of the plate in Figure 6a, the chromatographic resolution for the TLC separation of caffeine (C) and acetaminophen (A) was calculated as ($R_{C/A}$) = 3.64 and for acetaminophen (A) and aspirin (S) as ($R_{A/S}$) = 1.54. From the mass spectral data we calculated ($R_{C/A}$) = 3.42 and ($R_{A/S}$) = 1.38, or about 6- 10% lower than the apparent chromatographic resolution. This was considered to be good agreement between the two datasets (optical and MS) given the difficulty in accurately determining the extent of the bands on the plate by simple visual observation.

Conclusions

This work demonstrates a simple proximal probe thermal desorption/ionization approach for coupling TLC and MS. The experimental setup was optimized for probe and plate positioning relative to the inlet into the ionization region of the mass spectrometer as well for the variable parameters of probe temperature, gas flow into the mass spectrometer and surface scan speed using single lane scans for selected analytes developed on various HPTLC plates. Experiments showed that the mass spectrometric determined compound band widths matched the chromatographic band width up to surface scan speeds of about 700 μm/s. Limits of detection varied with the analyte studied, but there was a direct correlation with compound volatility. With all else equal, higher volatility compounds were found to give higher signal levels, as expected for a TD based technique. Surface/analyte interactions and analyte ionization efficiency however, will also contribute to the effective detection limits for any particular compound. In general, plate loadings ranging of a few micrograms or less, which are typical for HPTLC, produced high quality mass spectral signals by this approach. Improved detection levels might be achieved by one or more simple modifications to the present setup including the use of a wider chisel tip probe to desorb a larger fraction of the total analyte band width, while preserving spatial resolution in the surface scan direction along a development lane. A probe that can be heated to higher temperatures might also improve results, especially in the case of less volatile analytes. A different interface design that might include a tube extension could be envisioned as one way to accommodate the analysis of development lanes on intact plates.

The wide ranging applicability of this TLC/TD/I-MS technique was demonstrated using compounds with very disparate volatilities and ionization behavior, including dyes, herbicides, explosives and pharmaceuticals. The use of a commercial ionization source capable of operation in ESI, APCI or ESCi mode added to the usefulness of the present approach. When scanning a HPTLC lane the optimal ionization mode (ESI or APCI) could be selected for the particular compounds in question including fast switching between the two during the lane scans. The ESCi approach might be expected to be particularly useful in a discovery mode where the nature of the analytes and the best ionization method to utilize may not be known.

Micrometer Scale Chemical Imaging of Surfaces at Atmospheric Pressure with TD/SI-MS

In the previous section proximal probe thermal desorption with a secondary ionization (TD/SI)[128] was introduced as a member of the family of rapidly expanding atmospheric pressure (AP) surface sampling and ionization techniques for use with mass spectrometry (MS).[19,20,21,129,130,131,132] In proximal probe TD/SI-MS, a heated probe tip is used to locally desorb from a surface intact molecular species that are subsequently ionized at AP using electrospray ionization (ESI), atmospheric pressure chemical ionization (APCI), or another ionization method, then mass analyzed. The technique offers a simple, robust way to sample molecular species amenable to thermal desorption from surfaces without the use of lasers, gases, or solvents that are often requisite in a number of the other AP surface sampling/ionization techniques.

The proximal probe TD/SI-MS technique was originally demonstrated for use in coupling thin layer chromatography (TLC) with MS. Thermal desorption from the developed TLC plates was accomplished by placing a millimeter size, chisel-shaped heated metal probe close to or just in contact with the TLC surface to be sampled. The surface was then scanned in the direction of the development lane relative to the stationary probe. Species thermal desorbed from the surface (e.g., explosives, dyes, herbicides and pharmaceuticals) were drawn into the ionization region of the existing ESI/APCI source of the mass spectrometer and ionized. Using the millimeter size probe, these lane scans provided millimeter scale spatial resolution in the read out of the TLC plate development lanes.

On the basis of the successful TLC lane scanning experiments, it should be possible that by simply using a smaller probe and optimizing other scan parameters, the proximal probe TD/SI-MS approach could be used as a means to image the spatial distribution of analytes on a surface at the micrometer scale. A number of other more intricate AP surface sampling/ionization techniques have been applied to molecular chemical imaging on this size scale.[25,26,27,28,29,30,31,32,33,34] For example, the best achievable spatial resolution of methods employing a liquid/gas desorption process is related to the size of the liquid/gas jet cross section impacting the surface and has been found to be around 50 μm for desorption electrospray ionization (DESI)[27] and about 250 μm with a low temperature plasma probe (LTP).[28] Techniques employing a laser beam for analyte desorption have demonstrated spatial imaging resolutions between 2 μm and 400 μm depending on the laser spot size, wavelength and repetition rate.[29,30,31,32,33] In addition,

the use of a solid needle surface sampling probe for imaging, when combined with ESI, has accomplished a spatial resolution of about 60 μm.[34]

Herein, we report on an investigation of various aspects of the proximal probe TD/SI-MS technique for molecular surface sampling and chemical imaging with the aim of maximizing the spatial resolution and image quality. Employing a probe with a fixed diameter, probe-to-surface distance, lane spacing and surface scan speed are shown to be important factors in achieving the best spatial read-out resolution possible. Using printed patterns on photo paper as test substrates and a circular proximal probe with a tip diameter of about 50 μm, chemical imaging with a spatial resolution of about 50 μm is demonstrated.

EXPERIMENTAL METHODS

Sample Surface. 2 x 2 grids, in sizes of 1 mm x 1 mm and 0.5 mm x 0.5 mm, and a 2 x 4 grid, in size of 0.5 x 0.5 mm were printed with one-pixel wide lines (ca. 50 μm line width) on ultra premium photo paper (Epson America Inc, Long Beach, CA) using Epson yellow T0884 ink and an Epson Stylus NX110 inkjet printer (Epson Inc., Tokyo, Japan) controlled with an in house developed software. Optical images of the printed patterns were obtained using an Olympus SZX16 optical microscope (Olympus Corp., Tokyo, Japan) equipped with an Olympus DP71 digital camera and associated computer software. Surface profile scans of printed patterns were acquired at a scan rate of 100 μm/s using a Tencor P-10 Surface Profilometer (KLA-Tencor, Milpitas, CA).

Proximal Probe TD/SI-MS Setup. The proximal probe TD/SI-MS experimental setup is shown in Figure 22 and has been described in detail elsewhere.[128] Briefly, the glass window of the ion source can of a Waters TQD triple quadrupole mass spectrometer (Waters Corp., Milford, MA) was replaced with a plexiglass window fitted with a Cajon connector. This connector led to a straight 1.5 in. long stainless steel tube (1/8 in. o.d., 1/16 in. i.d.) leading to a TQD ionization source chamber and a modified cone electrode. Pumping on the source exhaust pulled air from the sampling region outside the source can into the ionization source at a rate of 30 mL/min. A KNF Neuberger Inc N815KTE mini vacuum pump (12 V/1.5 A, KNF Neuberger Inc., Freiburg, Germany), powered with a variable DC supply was used for pumping. The heated proximal probe was mounted directly in front of the sampling orifice. An MD 80 wand and digital controller from a Weller WD 1 soldering station (Weller, Germany) were used to heat the proximal probe tips. Probe tips were fabricated by machining standard Weller LT1 soldering iron tips (250 μm diameter) down to a diameter of 50 μm as measured using an Olympus SZX16 optical microscope equipped with an Olympus DP71 digital camera.

Data Collection. The MS2000 *x-y-z* robotic platform (Applied Scientific Instrumentation Inc., Eugene, OR), and control software used to manipulate the sample surface relative to the stationary heated probe has been described in previous work.[133] The position of the heated probe relative to the surface during an experiment was monitored visually using a Navitar 90 degree telescope with a 12X objective (Navitar Inc., Rochester, NY) connected to a Costar SI-C400N CCD camera (Costar Inc., Anaheim, CA) and a Marshall V-ASL8080 LCD monitor with a 4:3 aspect ratio (Marshall Electronics Inc., El Segundo, CA). This setup provided a 500 μm horizontal

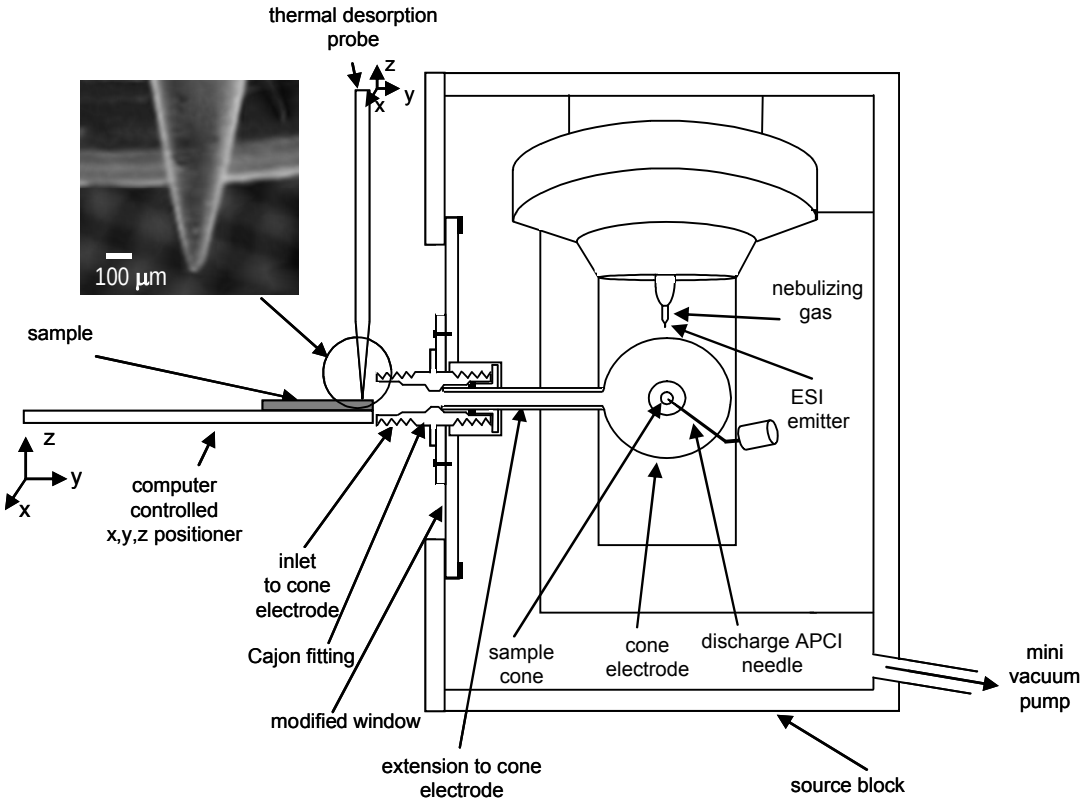

Figure 22. Schematic illustration of the TD/I-MS chemical imaging experimental setup. Top left inset shows an SEM image of the 50 μm diameter probe tip.

field of view at the highest, 12X magnification, allowing for accurate monitoring of the position of the probe relative to the surface.

The data collection procedure for the TD/SI-MS imaging is similar to the DESI imaging set-up we reported earlier.[27] Briefly, at the beginning of an imaging experiment the heated proximal probe was positioned manually at one corner of the area of interest at given distance above the surface. After that, stage movements were conducted under computer control. The first lane was scanned by moving the surface parallel to the *x* axis at a forward surface scan rate. At the end of the first lane, the surface was lowered by 0.5 mm followed by moving the surface at a return speed back to the beginning of the first lane. With the surface lowered there was a 0.5 mm gap between the heated proximal probe and the surface such that the probe did disturb the sample integrity of the yet unanalyzed surface. When the beginning of the first lane was reached, the surface was moved parallel to the *y* axis to achieve the required lane spacing distance followed by raising the surface 0.5 mm so the heated proximal probe was again the desired distance from the surface for analysis. The subsequent lanes were scanned in a similar fashion.

Data for each lane scan was collected into individual data files. Movement of the stage was synchronized with the corresponding mass spectral data by triggering the start of the data collection at the beginning of a lane scan using the stage control software (HandsFree Surface Analysis©).[133]

Image Creation. The most intense ion signal in the mass spectrum of the yellow ink using positive ion mode APCI was observed at *m/z* 387 (unidentified ink component) and was chosen to create the chemical images. The intensity of the *m/z* 387 species was monitored using single ion monitoring (SIM) with a dwell time of 50 ms for surface scan

speeds of 200 μm/s, 100 μm/s and 50 μm/s, while 15 ms and 7 ms dwell times were used for 400 μm/s and 800 μm/s scan speeds, respectively. Spatial distribution of the analyte of interest was visualized as a chemical image using the image visualization module of the HandsFree Surface Analysis© software package.[133]

RESULTS AND DISCUSSION

Effect of Probe-to-Surface Distance on Analyte Signal Amplitude and Reproducibility. For a given proximal probe temperature, the distance between the probe tip and the surface was expected to determine the heat transferred to the surface and thus the amount of material desorbed from the surface and subsequently ionized and ultimately detected in the mass spectrometer. We found in fact that this probe-to-surface spacing not only affected signal levels but also signal reproducibility. The effect of probe-to-surface distance on the magnitude and reproducibility of the analyte signal was investigated by scanning across three 50 μm-wide printed lines spaced 100 μm center-to-center using a 50 μm wide probe. For the separate experiments the probe was positioned to just touch the paper surface (0 μm above surface), or positioned at 5, 10, 15, 20 and 25 μm above the paper surface. These distances were selected so that the degree of interaction of the probe with the approximately 12 μm thick ink layers printed on top of the paper surface would vary. Profilometer scans were used to determine 12 μm as the mean thickness of the ink layers on top of the paper surface (data not shown).

Figure 23a shows the schematic representation of the interaction of the proximal probe with the inked lines at the different probe-to-surface distances. Because the inked

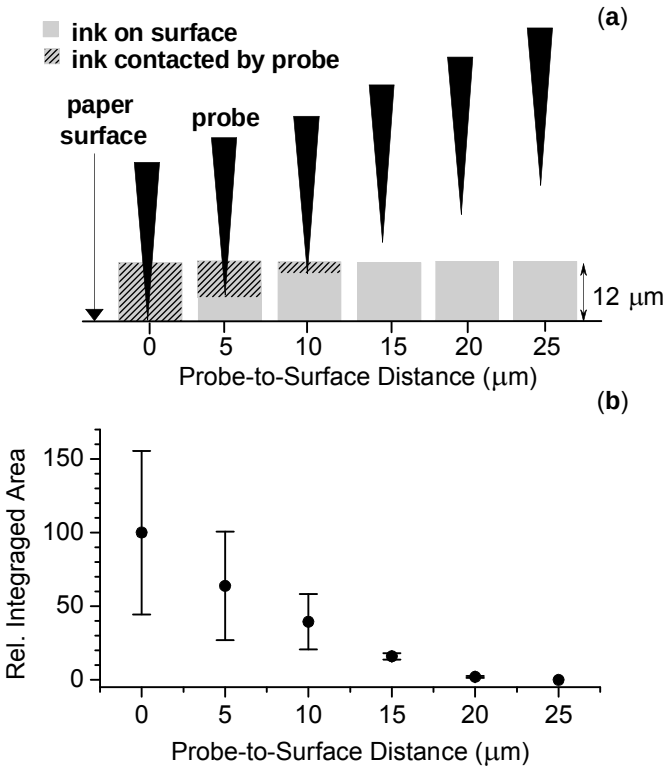

Figure 23. (a) Illustration of the positional relationship of the heated probe to the 12 μm high printed line of ink and the amount of ink that is directly contacted by the probe for probe-to-surface distances of 0, 5, 10, 15, 20, and 25 μm. (b) Normalized peak area for *m/z* 387 as a function of probe-to-surface distance. The data was collected in positive ion mode APCI using SIM mode with dwell time of 30 ms. Probe tip temperature was 350 °C. Error bars represent ±1 standard deviation calculated from three replicate experiments.

layer was 12 μm thick, a direct contact between the ink and the heated probe could be expected when the probe was initially positioned to just touch the paper surface and at a spacing of 5 and 10 μm above the surface. In contrast, the probe could not directly contact the ink during the lane scans performed with 15, 20 and 25 μm probe-to-surface distances. In these latter three cases, thermal desorption would be due solely to radiative heat transfer from the probe through the air gap between the probe and the ink.

Figure 23b shows the average and relative standard deviation (RSD) of the integrated SIM signal from the ink component monitored for these lane scans as a function of the probe-to-surface distance. As might be expected, the highest signal levels were observed with the probe positioned to just touch the paper surface. Under this condition the probe could interact with the entire thickness of the printed ink layer. However, this positioning also resulted in the largest RSD of the signal (55%). With the probe spaced away from the surface during the lane scans, there was a decrease in the average integrated peak area in direct correlation to the separation distance. Importantly, the RSD values of the signal improved with increasing probe-to-surface spacing. For example, when scanned with the probe 15 μm above the surface, the average integrated peak area from the printed lines was only 16% of the integrated peak area measured when the probe was positioned to just touch the surface, but the RSD of the signal was only 14%. The larger fluctuations in peak area when the probe was positioned closer than 15 μm to the surface can be attributed to the uneven topography of the paper surface on which the approximately 12-μm-thick ink lines were printed. This surface topography led to physical damage to the paper by direct contact between the probe and the paper and

caused varying amounts of ink to be in direct contact with the probe during the lane scans over consecutive printed lines.

The results of these experiments evaluating the effect of probe-to-surface positioning on analyte signal amplitude and reproducibility suggested the use of 15 μm or a larger probe-to-surface spacing for chemical imaging. Unfortunately, when imaging was attempted at those spacings, quality chemical images could not be produced due to low signal-to-noise ratios (data not shown). Thus, a probe-to-surface distance of 5 μm was chosen for all subsequent experiments as a compromise between mass spectrometric signal amplitude and signal reproducibility. Importantly, these results suggested that incorporating a means to maintain a fixed optimal probe-to-surface distance real-time, continuously adapting to the changing topography of the surface during a lane scan, could provide a means to improve signal reproducibility leading to better quality chemical images.

Spatial Resolution Dependence on Surface Scan Speed. The effect of surface scan speed on spatial resolution was evaluated by scanning printed lines on paper at different rates with a fixed probe-to-surface distance (5 μm). Four 50 μm wide lines were printed with a 250 μm center-to-center distance creating spaces between the lines that were about 200 μm wide. This line spacing was chosen so that the 50 μm wide probe tip would comfortably fit into the space between the printed lines, theoretically allowing the signal from the desorbed ink components to return to baseline before the next line was encountered by the probe. Figure 24a shows the ratio of the signal recorded from the printed lines to the signal observed in the spaces between the lines ("printed line/blank

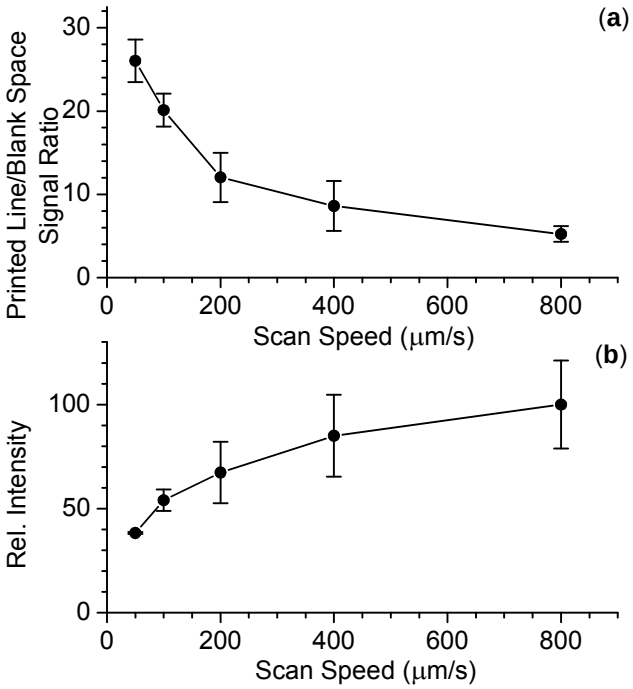

Figure 24. (a) Averaged ratio of the signal recorded from the printed lines to the signal observed in the spaces between the lines ("printed line/blank space signal ratio") and (b) average signal intensity when scanned across four printed lines as the function of scan speed. The four 50 μm wide lines were printed with a 250 μm center-to-center distance creating spaces between the lines that were about 200 μm wide. The data was acquired using SIM of *m/z* 387 in positive ion mode APCI with a probe tip temperature of 350 °C and a probe-to-surface distance of about 5 μm. Error bars represent ±1 standard deviation calculated from three replicates.

space signal ratio") for scan speeds of 50, 100, 200, 400, and 800 μm/s. The highest value for the printed line/blank space signal ratio (i.e., the best apparent separation between the printed lines and blank spaces) was observed at the lowest scan speed. This printed line/blank space signal ratio decreased and RSD of this ratio increased with increasing scan speed. Also, as the surface scan speed was increased both the absolute signal intensity when scanning over the lines (Figure 24b) and the signal level in the blank space increased (data not shown). The signal increase at the higher scan speeds was caused by more material being removed from the surface in a shorter period of time. Higher signal for the black areas with increasing scan speed was due to the finite, but not completely sufficient, amount of time required for the analyte vapor from a scanned printed line to fully clear the space from the probe tip through the ionization region.

To balance the effects of scan speed on signal intensity and printed line/blank spacing signal ratio to obtain the best quality chemical image in the shortest time available, a scan speed of 100 μm/s was used to collect all subsequent lane scan data and chemical images.

Spatial Resolution Dependence on Surface Scan Lane Spacing. Surface scan speed affects the spatial resolution in the dimension parallel to the scanning direction, whereas the spacing of the lane scans affects the spatial resolution in the dimension orthogonal to scan direction (e.g., the vertical versus horizontal directions on the surface). It would seem apparent that regardless of the probe size, the smaller the lane spacing the better the possible spatial resolution in the direction of the spacing steps. This type of smaller than probe size lane stepping is called "oversampling".[30] However, if the spacing between lane scans is less than the probe diameter, not only is a new area of the surface

interrogated during each lane scan, but also a previously analyzed area. Obviously, if all the material of interest is removed from the surface in the previous lane scan, the signal observed is only from the newly interrogated area. However, all material may not be removed in a lane scan particularly with a continuously moving probe. For example, in the present case, we found that 9, 4, 3.5, and 2% of the initial lane scan signal could be observed in the second, third, forth and fifth subsequent lane scans over the same printed lines (Figure 25). Thus, the signal observed in sequential lane scans then originates partly from freshly interrogated areas and partly from areas interrogated in previous scans (Figure 26).[27] Using this data, we were able to estimate the effect of this "carryover" from previously scanned lanes on image quality to be negligible when using a 50 μm probe and 10 μm lane scan spacing. Details of this estimation can be seen in Figure 27, and are briefly described here**.**

Contribution to the total signal from new and already interrogated surface areas can be simply calculated using the experimentally determined weights and width of the areas interrogated in the different number of previous scans. As indicated in Figure 25, 100, 9, 4, 3.5, and 2% of the initial lane scan signal could be observed in the first, second, third, forth and fifth subsequent lane scans over the same printed lines. Using these "carryover" percentages, the chemical image of a vertically 50 μm wide printed line (schematically depicted in Figure 27a) was modeled as if scanning over the line using a 50-μm-diameter probe at a lane spacing of 10 μm as shown in Figure 26. Figure 27b shows the theoretical optical image of the modeled surface and Figure S3c the simulated chemical image. Figure 27d shows the theoretical and calculated relative signal

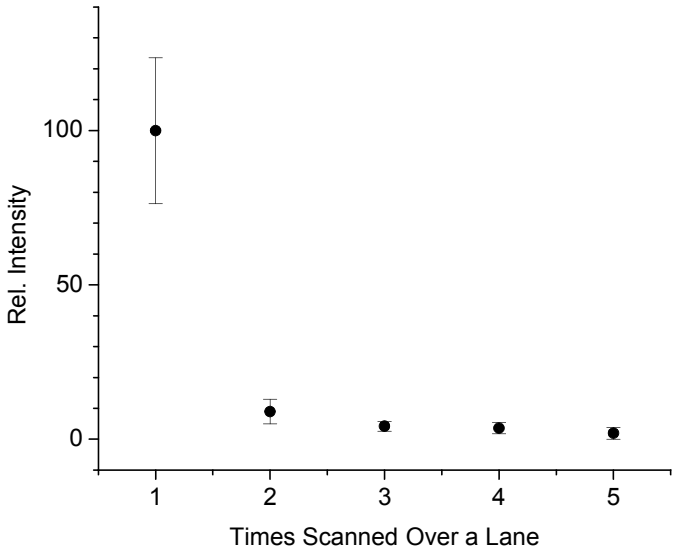

Figure 25. Average ink SIM signal intensity when proximal probe was scanned across the same lane of four printed lines as the function of the number of times the lane was interrogated. The five 50 μm wide lines were printed with a 250 μm center-to-center distance creating spaces between the lines that were about 200 μm wide. The data was acquired using SIM of *m/z* 387 in positive ion mode APCI with a probe tip temperature of 350 ˚C and a probe-to-surface distance of about 5 μm at a surface scan speed of 100 μm/s. Error bars represent ±1 standard deviation calculated from the five replicate experiments.

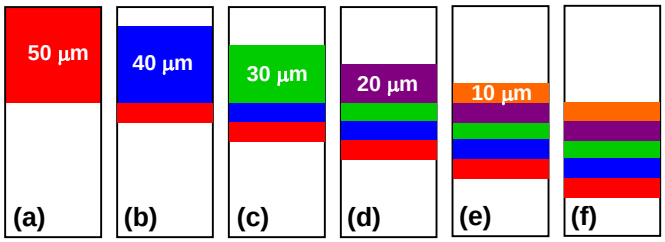

Figure 26. Schematic illustration of interrogated areas in lane scan number (a) one, (b) two, (c) three, (d) four, (e) five and (f) six using a 50 µm diameter probe and 10 µm lane scan spacing. Bands in red, blue, green, purple and orange represent areas interrogated in the current scan, areas that were interrogated in the current and previous lane scans, areas interrogated in the current and previous two lane scans, areas interrogated in the current and previous three lane scans and areas interrogated in the current and previous four lane scans, respectively. In the fifth and later lane scans a 10 µm wide fresh surface band is analyzed together with four 10 µm wide surface bands that were interrogated in the previous lane scan, in the previous two lane scans, in the previous three lane scans and in the previous four lane scans, respectively.

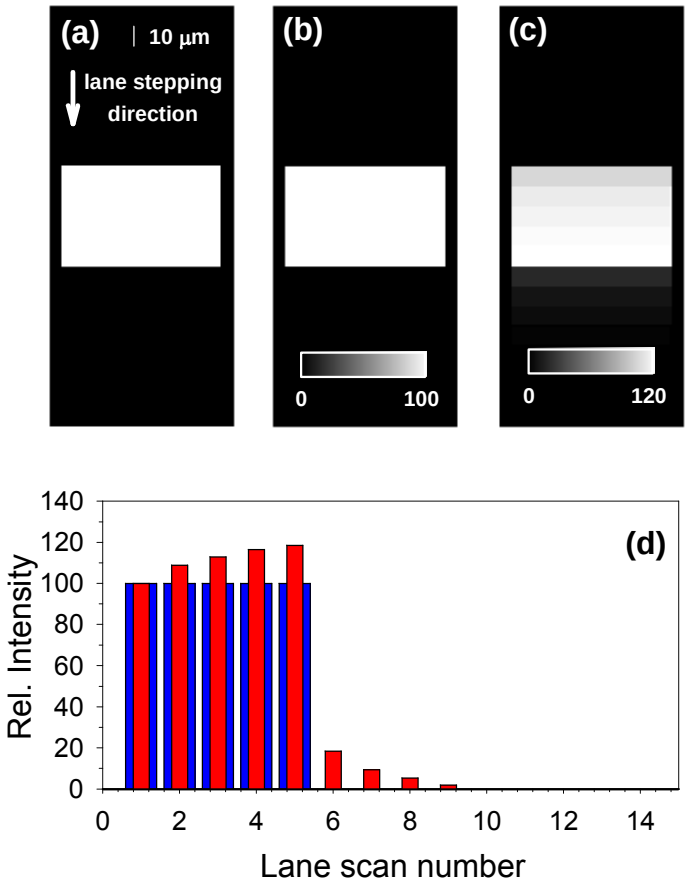

Figure 27. (a) Schematic representation of a section of a 50-μm-wide printed line. (b) Theoretical and (c) simulated chemical images of (a) using "carryover" percentages from the data in Figure S1 when scanning over the line using a 50-μm-diameter probe at a lane spacing of 10 μm as shown in Figure S2. Lane stepping direction and intensity scale as shown in (a). (d) Theoretical (blue bars) and calculated (red bars) show relative signal intensities that were used to make the images in (b) and (c), respectively.

intensities as the function of lane number that were used to make the images in (b) and (c), respectively. Comparing Figures 27b and 27c it can be concluded that "carryover" percentages in Figure 25 do not significantly affect the quality of the chemical image and therefore using 10 μm lane spacing in the experiments is justified.

The best lane spacing value for the current proximal probe setup and surface was determined using five 50 μm wide printed lines spaced 200 μm apart. These lines were scanned across multiple times with spacings between the lane scans of 50 μm, 20 μm, 10 μm and 5 μm. The latter three tested lane spacings were smaller than the size of the probe that resulted each successive lane scan to partially overlap the area interrogated by the probe in the previous lane scan(s). Figure 28a shows the printed line/blank space signal ratio and Figure 28b shows the relative signal intensity when scanning over the lines. As expected, the highest printed line/blank space signal ratio and signal when scanning over the lines were observed using 50 μm lane spacings resulting in the most fresh, previously uninterrogated area to be scanned across in a lane scan. Both of these performance metrics decreased with decreasing lane spacings. Importantly, the printed line/blank space signal ratio fell below a value of 3 when the lane spacing was decreased to 5 μm. The printed line/blank space signal ratio can be viewed as a kind of signal-to-noise measure, and a value of 3 is normally defined as the limit of detection. For this reason, a lane spacing of 10 μm was used in subsequent imaging experiments as a compromise between detectable signal and the best spatial resolution in the direction parallel to the lane scans steps.

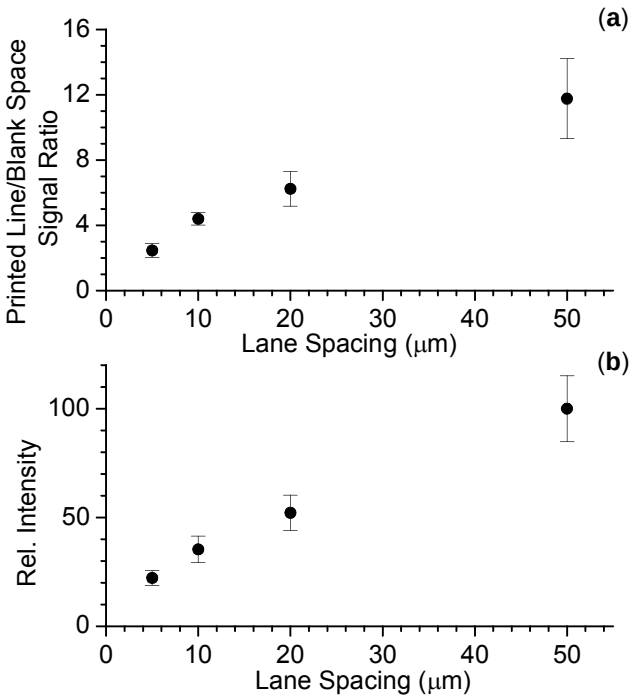

Figure 28. (a) Averaged ratio of the signal recorded from the printed lines to the signal observed in the spaces between the lines ("printed line/blank space signal ratio") and (b) average signal intensity when scanned across five printed lines as the function of lane spacing. The five 50 μm wide lines were printed with a 250 μm center-to-center distance creating spaces between the lines that were about 200 μm wide. The data was acquired using SIM of *m/z* 387 in positive ion mode APCI with a probe tip temperature of 350 °C and a probe-to-surface distance of about 5 μm at a scan speed of 100 μm/s. The results shown was calculated from the data obtained for the last five lane scans out of 10 or 20 lane scans recorded using 50 μm and 20 μm, or 10 μm and 5 μm lane spacing, respectively. Error bars represent ±1 standard deviation calculated from the five replicates.

Chemical Imaging of Printed Patterns. The quality of the chemical images and achievable imaging resolution possible with the current proximal probe TD/SI-MS system was evaluated using printed grids on paper as test substrates. The grid sizes were selected comparable to previously reported imaging resolutions of other ambient mass spectrometry based imaging.[25,27,28,29] Figures 29a and 29b show the optical and chemical images of a 2 x 2 grid, 1 x 1 mm in size, respectively. The printed vertical and horizontal lines measured from the optical image had a line width of about 50 μm. Correlation between the optical and chemical images were in good agreement with both printed lines and blank spaces clearly distinguishable. This result triggered the imaging of a similar grid with half the size to further evaluate the achievable highest spatial resolution. Figures 29c and 29d show the optical and chemical images of a 2 x 2 grid, 500 μm x 500 μm in size, respectively. Clearly, the optical and chemical images again showed good correlation, and the grid openings of about 200 μm in size are clearly distinguishable from the printed ink lines.

The quality of these two chemical images suggested that even smaller grids could be successfully resolved. However, with the printer used, when attempting to print a 2 x 2 grid, 250 μm x 250 μm in size with 125 μm center-to-center line spacing, the hole openings between vertical lines were inconsistent. Therefore, 2 x 4 grids, 500 μm x 500 μm in size were printed that exhibited smaller hole openings in one direction than the grid in Figure 29c. The three vertical lines were equally spaced in the grid 250 μm center-to-center resulting in about 190 μm wide hole openings, while the five horizontal

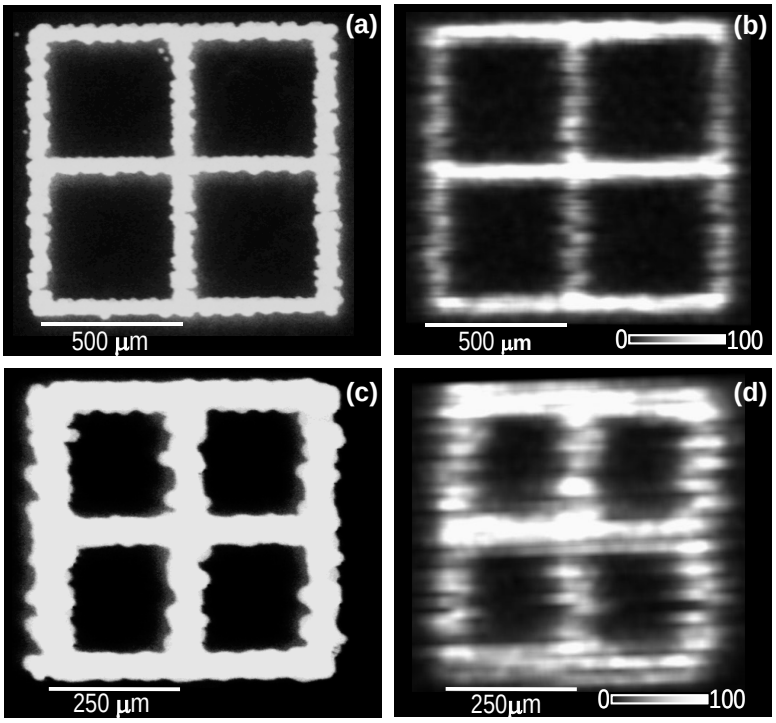

Figure 29. Optical images of (a) a 2 x 2, 1 x 1 mm grid and (c) a 2 x 2, 0.5 x 0.5 mm grid. Interpolated TD/SI-MS chemical images of grids in (a) and (c) are shown in (b) and (d), respectively. The imaging data was acquired using SIM of *m/z* 387 in positive ion mode APCI with a dwell time of 50 ms, surface scan rate of 100 μm/s, lane spacing of 10 μm and probe tip temperature of 350 ˚C. Probe-to-surface distance was ~5 μm.

lines were spaced at about 105, 145, 105 and 145 μm center-to-center resulting in about 45, 85, 45 and 85 μm wide grid spaces (see Figures 30a and 30c), respectively.

Figures 30a and 30b show the optical and chemical images of the printed 2 x 4 grid when scanning parallel to the five horizontal lines of the grid. Obviously, the images showed good correlation with grid spaces clearly resolved. This result suggests that the imaging resolution was at least 190 μm in the direction parallel to and about 45 μm in the direction perpendicular to the surface scanning direction. To further evaluate imaging resolution parallel to the scanning direction, the same pattern that was used in Figure 30a was printed again, rotated 90o clockwise and scanned parallel to the three horizontal lines in the grid. Figures 30c and 30d show the optical and chemical images of the printed grid. Here both the 45 and 85 μm wide grid spaces parallel to the scan direction were resolved, resulting in good correlation between the optical and chemical images. The chemical images in Figures 30b and 30d demonstrate that 45 μm wide grid spaces and 50 μm wide lines can be clearly resolved when scanning either parallel or perpendicular to openings and lines of these sizes, providing spatial resolution of about 50 μm in both scan orientations.

CONCLUSIONS

This work demonstrates the use the proximal probe TD/SI-MS technique, using a circular cross section probe 50 μm in diameter and an optimized probe-to-surface distance, surface scan speed and lane scan spacing, was capable of chemical imaging with approximately 50 μm spatial resolution as demonstrated using printed patterns on

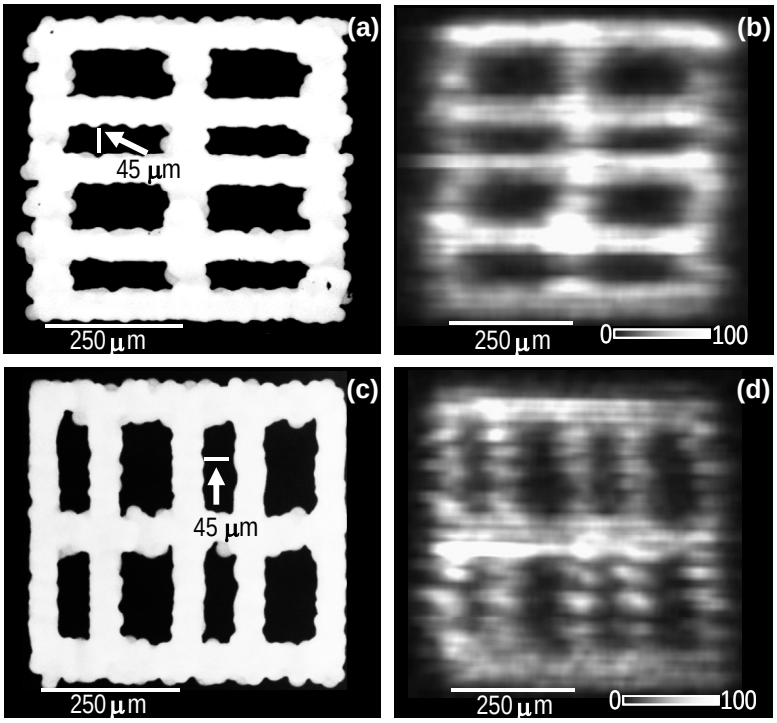

Figure 30. Optical images of (a) a 2 x 4, 0.5 x 0.5 mm grid and (c) an identical 2 x 4, 0.5 x 0.5 mm grid rotated 90^{o} clockwise. Interpolated TD/SI-MS chemical images of grids in (a) and (c) are shown in (b) and (d), respectively. The imaging data was acquired using SIM of *m/z* 387 in positive ion mode APCI with dwell time of 50 ms, surface scan rate of 100 μm/s, lane spacing of 10 μm and probe tip temperature of 350 ˚C. Probe-to-surface distance was ~5 μm.

paper as test substrates. This spatial resolution compares well with the best resolution demonstrated with other atmospheric pressure surface sampling and ionization techniques that have been used for imaging. The results presented suggest the use of a smaller heated proximal probe, combined with a means to maintain a fixed optimal probe-to-surface distance real-time during a surface lane scan (to optimize signal level and reproducibility) may enable the spatial imaging resolution of this technique to extend into the sub-micrometer range. At that size scale, the limit to imaging resolution may ultimately be limited as much by the ability to detect the minute quantities of material liberated from the surface as by the sampling process itself.

Combined Chemical and Topographic Imaging at Submicron Resolution Using Proximal Probe Thermal Desorption with a Secondary Ionization Mass Spectrometry and Atomic Force Microscopy

Proximal probe thermal desorption/secondary ionization-mass spectrometry (TD/SI-MS)[128,134] is a recently introduced approach, among the many other existing approaches, for atmospheric pressure (AP) surface sampling and ionization with mass spectrometric detection.[135,136,19,20,21,129,130,131,132] The TD/SI-MS approach uses a heated probe tip placed in close proximity to, or actually contacting, a surface to locally desorb intact molecular species from that surface that are then ionized by an AP secondary ionization source like electrospray ionization (ESI) or atmospheric pressure chemical ionization (APCI) and analyzed using MS. This approach offers a very simple and fast way to sample and analyze intact molecular species from a surface that are suited to thermal desorption. Though not demonstrated, the proximal heated probe could as easily

be used for pyrolysis of intractable surface materials rather than for desorption of intact molecular species through the use of suitably elevated probe temperatures.

Initially, this AP-based TD/SI-MS technique was applied to the read out of the development lanes on thin layer chromatography (TLC) plates by performing line scans with a millimeter sized chisel shaped heated probe across compounds separated on the plates (e.g., explosives, dyes, herbicides and pharmaceuticals).**Error! Bookmark not defined.** Using this setup, millimeter scale spatial resolution in the sampling process was accomplished. Subsequent work with a circular cross section, 50 μm diameter, heated probe showed it was possible with optimized surface scan parameters to chemically image printed patterns on photo paper with ~ 50 μm spatial resolution through selected detection of the ink components thermally liberated from the surface.[134] As these reports established, the achievable spatial resolution of the TD process was limited ultimately by the size of the heated probe tip. Thus, it was expected that spatial resolution and chemical image quality could be further improved by using probes of smaller cross section size. In addition, the results showed that reproducible mass spectral signal and imaging quality would be improved by incorporating a means to maintain a fixed optimal probe-to-surface distance real time, particularly in an imaging mode, continuously adapting to the changing topography of the surface during a lane scan.

Low micrometer to sub-micrometer size heated probes and built-in capabilities for real time probe - to - surface positioning are available with appropriated configured atomic force microscope platforms. For example, Reading and coworkers in a series of reports have demonstrated the use Wollaston wire heated AFM probes with a 5 μm tip diameter to perform either point thermal desorption or pyrolysis, capture the desorbed

vapor material, then inject it into a gas-chromatograph mass spectrometer (GC/MS) for separation, electron ionization, and mass analysis. They also have shown the ability to directly sample the vapors generated at AP into the vacuum-based electron ionization source using a heated transfer capillary. They were able to accomplish these experiments through the use of force-feedback on the AFM system that allowed for the precise positing of the Wollaston wire probes on the surface during the heating process as well as for subsequent surface imaging. Using this approach they were able to sample from single points on the surface of polymers, plant tissue, as well as pharmaceuticals.[137,138,15,66,67] With those setups, the smallest desorption craters were conical in shape with approximately 6 μm in diameter and 1.7 μm deep.

Herein, we expand on the prior AP proximal probe TD/SI-MS work using a heated proximal nano-TA probes and an AFM control system in the same genre as that used by Reading, et al. We demonstrate AP thermal desorption of caffeine thin films with 250 nm spatial resolution using 30 nm tip diameter silicon nano-TA AFM probes followed by AP secondary ionization by ESI and subsequent detection via MS. Using our atmospheric pressure continuous air sampling and secondary ionization set-up we are able to detect intact caffeine molecules desorbed from ~1.6×10^6 nm^3 volumes which translates to about 10 attomoles (2 fg) of caffeine. Results presented here show the ability to desorb and then detect material from conical TD craters just 250 nm wide by 100 nm deep. Spatially resolved spot sampling and detection superior to any AP-based surface sampling and ionization technique yet demonstrated with mass spectrometry.

EXPERIMENTAL

Chemicals

Caffeine (99%) and analytical reagent grade methanol (99.9%) were obtained from Fisher Scientific (Fisher Scientific, Pittsburgh, PA), Formic acid (99.9%) was obtained from Sigma-Aldrich (Aldrich, St. Louis, MI). Caffeine solutions were prepared by dissolving the appropriate amount of caffeine in methanol to make 1 μM solutions. The caffeine thin film was formed by freely dispersing 70 μL of 1 μM caffeine solution onto a glass cover slip that was attached to a steel puck using super glue. The ESI spray solvent was 100% methanol with 0.1% formic acid.

Experimental Setup

The experimental setup is shown in Figure 31. A Veeco Multimode AFM (Bruker AXS, Santa Barbara, CA) equipped with a closed loop N-Point stage (N-Point, Madison, WI), a Nanonis (SPECS Zurich GmbH, Zurich, Switzerland) system controller were used to both to obtain the nanometer scale topographical surface images and to control the nanoscale thermal desorption spot sampling. Material was thermally desorbed from a thin film caffeine surface using VITA-MM-NANOTA-300 (Bruker AXS, Camarillo, CA) nano-TA AFM probes. Temperature calibration of the nano-TA AFM probes was carried out using a voltage ramp across a high density polyethylene (HDPE) melting point standard.[139,140] This approach for calibrating the dynamic transfer function was first introduced by Lee et al.[141]

Thermally desorbed material was transferred to the mass spectrometer from the AFM tip area using an extractor with a "Y" geometry intersecting ESI source. This

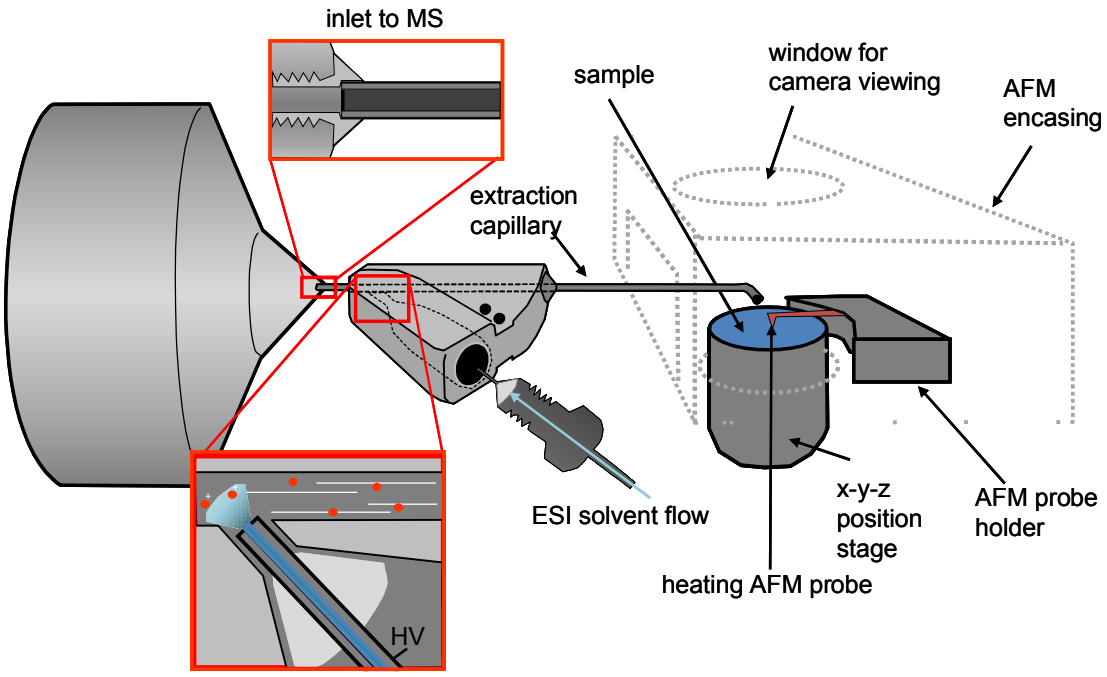

Figure 31. Schematic illustration of the AFM and proximal probe TD/ESI-MS experimental setup.

extractor/ESI source, fabricated from stainless steel and 1.27 mm o.d. x 0.84 mm i.d. stainless steel capillary, was press fit into a counter bored sampling capillary of an LCQ Deca XP interface mated with a LCQ Deca quadrupole ion trap mass spectrometer (Thermo Scientific, San Jose, CA). The vacuum draw from the mass spectrometer (~7 mL/min) pulled the vapors from the AFM region into this interface and on into the mass spectrometer. ESI solvent was delivered into the device through a metal capillary emitter (500 μm o.d. x 127 μm i.d) at a rate of 2 μL/min using a syringe pump (Harvard Apparatus, Holliston, MA). The emitter was held in a PEEK fitting/ferrule assembly that screwed into the extractor unit. The position of the ESI emitter inside the extractor/electrospray device was adjusted to achieve a constant ESI current. The PEEK fitting/ferrule assembly provided electrical isolation between the metal emitter held at high voltage (3.5 kV) and the body of the extractor, which was connected to the interface heated capillary (200 ^{o}C), which was held at 23 V. Ionization of the vaporized materials took place via interaction with the ions and charged droplets produced from the ESI emitter (see inset in Figure 1). The sampling end of the device had a 90° bend to allow for positioning of the capillary within 1 mm of the AFM tip given the AFM mounting configuration. The total length of the extractor/ESI adaptor was 160 mm. The AFM assembly was positioned on a Zaber NA14B60 (Zaber Technologies Inc, Vancouver, Canada) motorized linear actuator and a Newport 9064-X-P motorized translation stage (Newport, Irvine, CA) to allow for the close positioning of the extractor with the AFM tip. The position of the AFM tip relative to the extractor was visualized using a Navitar telescope with a 12X objective (Navitar Inc., Rochester, NY) connected to a Costar SI-C400N CCD camera (Costar Inc., Anaheim, CA) and a Marshall V-ASL8080 LCD

monitor with a 4:3 aspect ratio (Marshall Electronics Inc., El Segundo, CA). This setup provided a 500 μm horizontal field of view at the highest, 12X magnification, allowing for accurate monitoring of the position of the probe relative to the extraction capillary.

Desorbed and ionized species were monitored with full scan mass spectra and MS/MS product ion spectra were acquired (caffeine transition *m/z* 195 → 138). In-house designed grid software were used to control the AFM tip position and temperature as well as the mass spectrometer data acquisition.

RESULTS

In order to effectively couple the ambient AFM-based TD experiment with mass spectrometric detection required the ability to effectively transport the desorbed material to the ionization region, ionize that material, then transport the ions into the mass analyzer. High relative efficiency for each step was important because the expected nanometer scale desorption process will liberate into the gas phase only attomole amounts of material. These levels of materials would be challenging to detect even if 100% of the material sampled could be ionized and transported through the mass analyzer. In this case, desorbed material was transported through a tube from the region of the heated AFM tip into an ESI region via the vacuum draw from the mass analyzer (Figure 31). A 90^{o} curve at the sampling end of this interface allowed very close positioning of the capillary to the TD region. A "Y" intersection of the ESI plume and vapors from the desorption region proved effective as a secondary ionization process for the desorbed species (see inset in Figure 1). Because this extractor/ESI adaptor was fitted into the normal heated capillary of the mass spectrometer interface (200 ^{o}C), it was kept

substantially above ambient temperature minimizing condensation of the desorbed material in the transport region.

The ability to detect mass spectrometric signal from material thermally desorbed with the AFM is demonstrated by the data in Figure 32. In this case, the sample surface was a thin film of caffeine on a glass microscope cover slip. Figure 32a shows the full scan mass spectrum obtained when the nano-TA AFM probe was placed on the surface without turning on the heater (probe temperature ~25°C). Figure 32b show the corresponding full scan mass spectra when the AFM tip was lifted to a position 10 μm above the surface with the tip heated to 350°C. In neither case were ions corresponding to caffeine or any other species apparent in the mass spectra. Figure 32c shows the full scan averaged spectrum that was obtained when the AFM tip was engaged on the caffeine surface and heated to 350°C. In this case, ions corresponding to the protonated molecule of caffeine at were observed at *m/z* 195. Other unidentified ionic species were also observed including those at *m/z* 147, 160 and 168 (anything more to say about these ions). These data clearly demonstrate that caffeine is thermally desorbed from the surface, transported into the ionization region, ionized, and then transported into the mass spectrometer.

A thermal desorption crater created under identical experimental conditions used to acquire the data shown in Figure 32c was imaged with the same AFM tip used for the TD. The topographical image (Figure 33a) and profile cross section across the crater (Figure 33b) show the desorption crater was conical in shape approximate 250 nm across and 100 nm deep. This corresponds to a volume of ~1.6×10^6 nm^3 removed from the thin

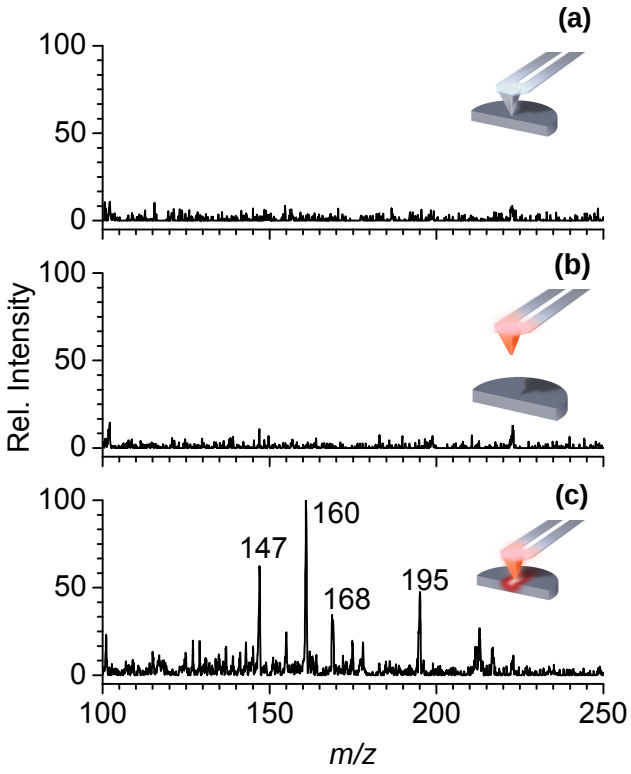

Figure 32. Averaged full scan mass spectrum obtained from a thin film caffeine surface while (a) the AFM tip was engaged on surface and not heated, 25˚C, (b) the AFM tip was removed from surface 10 μm and heated to 350˚C, and (c) the AFM tip was engaged on surface and heated to 350˚C. The relative intensity in panels a and b is normalized to the intensity of the base peak *m/z* 160 in panel c.

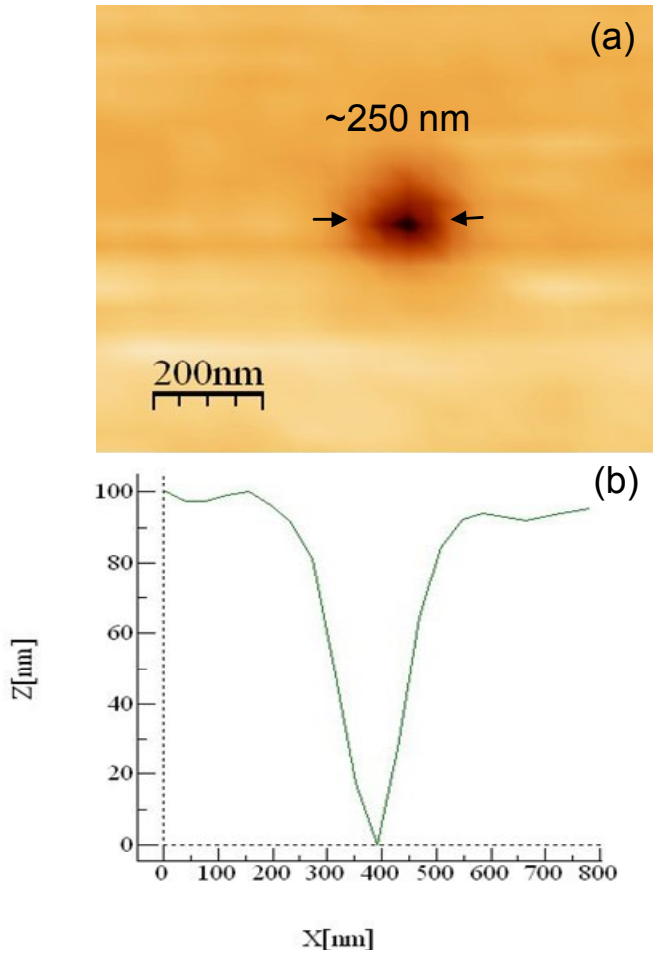

Figure 33. (a) AFM topographical image and (b) line profile of single desorption spot created by heating a thin film caffeine surface with the AFM probe tip engaged to the surface for 30 s at 350°C.

film, which translates to about 10 attomoles (2 fg) of caffeine, Figure 34. To estimate the amount of material desorbed from an individual heating cycle, i.e a single crater, from the experiment shown in Figure 33, we assume that all the material on the surface is caffeine and the volume desorbed is conical. Equation 3 is that for a conical volume V crater

$$V = \frac{1}{3}\pi r^2 h \tag{4}$$

where r is the radius (125 nm) and h is the height (depth, 100 nm) of the crater in this experiment. Assuming the complete surface is caffeine, and the given the density of caffeine $\rho_{caffeine}$= 1.23 g/cm^3 and a molecular weight, $MW_{caffeine}$ =194 g/mol the moles the mass of caffeine (moles) desorbed from the surface can be calculated using the following formula,

$$mole = \frac{\pi r^2 h \rho}{3MW} \tag{5}$$

Using this formula we estimate that we are desorbing about 10 attomoles of material from each crater.

To demonstrate the reproducibility and the potential for automated surface sampling and analysis, a grid experiment was carried out where the nano-TA AFM probe was brought in contact with the same caffeine thin film surface for 30 s while heated to 350 °C then removed from the surface and the heater turned off for 20s in between subsequent grid points. During this sequence the mass spectrometer was continually operating in MS/MS mode, monitoring the *m/z* 195 → 138 transition characteristic for caffeine. Figure 35a shows the topographic image of the caffeine surface acquired prior to carrying out the thermal desorption grid spot sampling experiment and Figure 35b

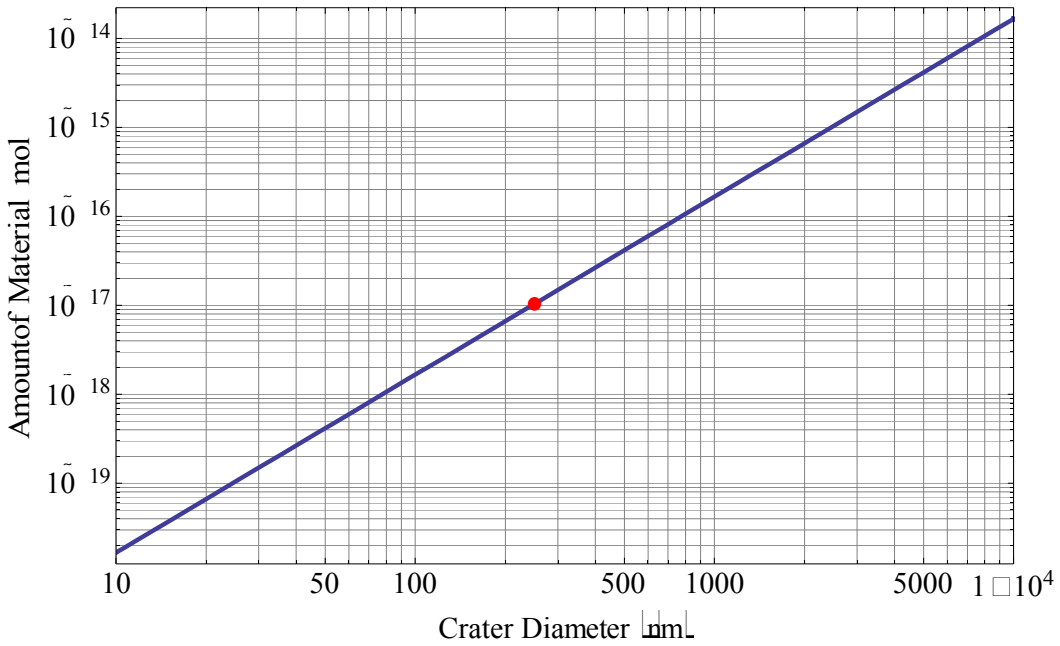

Figure 34. Calculations for the amount of caffeine removed from conical holes (100 nm) depth) of varying diameters assuming the surface is 100 percent caffeine. Red dot indicates our crater diameter of 250 nm.

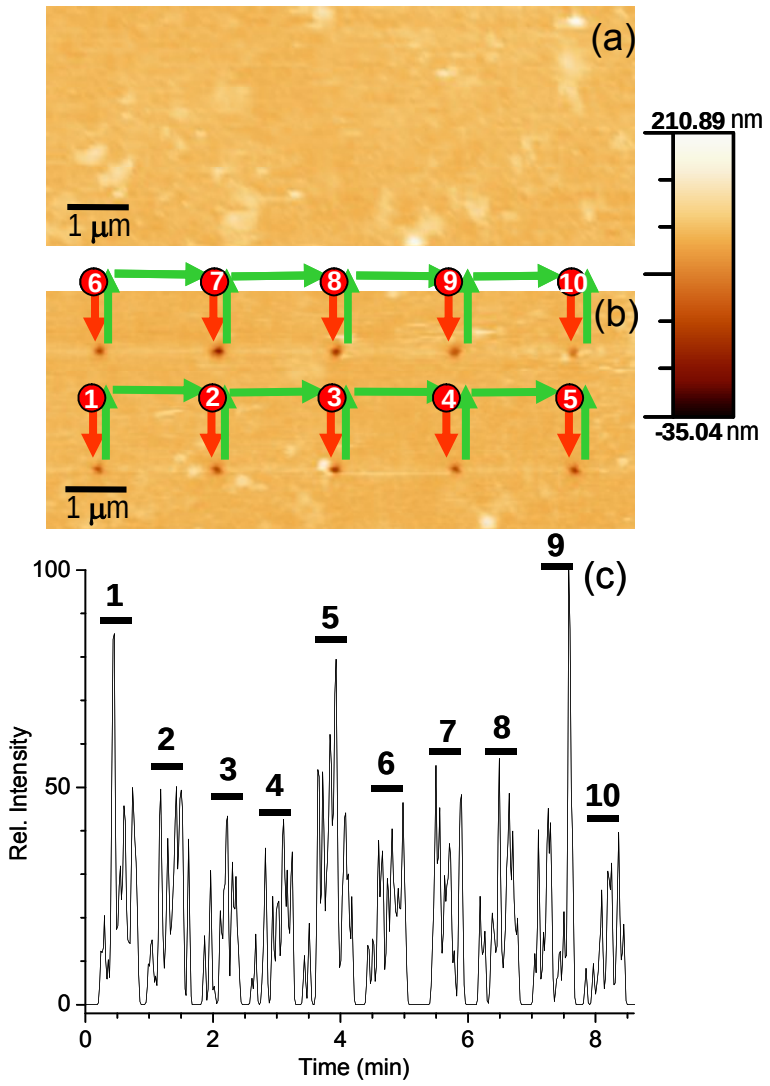

Figure 35. AFM topography of a caffeine thin-film surface (a) pre-heating and (b) post-heating the surface for 30 sec per spot in a 5 x 2 array. (c) MS/MS ion current chronogram (5 pt gaussian smooth) for caffeine (*m/z* 195 → 138, C.E. 35) recorded during the 30 sec per spot sampling of the 5 x 2 array. The red and green arrows in (b) correspond to the movement of the AFM probe while probe is at 350 C, and at ambient temperature 25 C respectively . Crater numberings in (b) correspond to MS chronogram peaks in (c) with line below the numbering in (c) representing the 30 s heating interval while the AFM probe is on the caffeine thin-film surface.

shows the topographic image after the experiment. After this spot sampling experiment the image shows 5 x 2 array of desorption craters each ~ 250 nm across x 100 nm deep spaced 2 μm apart. The corresponding mass spectrometric chronogram shown in Figure 35c reveals the appearance of ten separate increases in the signal for caffeine corresponding to the ten sampling events. The signal observed, though obviously distinct from the signal levels observed when the sample was not on the surface, was relatively low level. Again, only about 10 attomoles of caffeine (~ 2 fg) was desorbed to form each crater. Though the signal levels observed in experiments of this type might be compound dependent, these results illustrate that without improvements in the efficiency of sampling, ionization, transport and mass spectral detection, further improvement in spatial resolution may not be possible. On the basis of the baseline signal separations between sampling events, carry-over contamination sampling spot to spot did not appear to be an issue.

CONCLUSIONS

Using our set-up we have demonstrated for the first time local nanometer scale thermal desorption and characterization of attomoles of caffeine using mass spectrometry as well as simultaneous surface topography by using atomic force microscopy. Potential improvements to the system that would increase the sensitivity of the technique are currently being investigated such as heating the transfer line with higher temperatures as well as modeling the transfer of both neutrals and ions down the extractor line to increase the ion count. We are also currently developing a platform that would allow the coupling of nanoscale thermal desorption with various mass spectrometers and ionization sources

including atmospheric pressure chemical ionization (APCI) for the detection of polar molecules and inductively coupled plasma (ICP) for elemental analysis. We believe that this new analytical tool that allows for multimodal surface sampling and chemical imaging by providing spatially resolved chemical information by using an MS and physical characterization of the sample through AFM analysis will have a broad application for the study of material and material junctions with both chemical and physical characterization at the nanoscale. A combined AFM, nanoscale TD/SI-MS chemical imaging instrument might be used to co-register local nanomechanical measurements and topography using AFM with MS-based chemical imaging to correlate features with spectral signatures. This approach to nanoscale multimodal surface sampling and chemical imaging has the potential to de applied to many other desorption/sampling methods, including but not limited to tip-enhanced laser desorption.

CHAPTER IV
SPATIALLY RESOLVED SURFACE SAMPLING USING LASER DESORPTION FOLLOWED BY LIQUID EXTRACTION

The coupling of atmospheric pressure (AP) surface sampling and ionization with mass spectrometry (MS) dates back to at least the mid-1970's, but there has been a resurgence in interest, research and use of such techniques since the early 2000's. [19,20,21,129,130,131,132,135,136] Numerous applications have been demonstrated or explored including, among others, the direct identification and sometimes quantification of small molecules, like pharmaceuticals, metabolites, and lipids, and larger molecules like peptides and proteins, from various analytically relevant surfaces including planar separation media, [114]biological tissue,[142] and surfaces of forensic interest.[143]

Among these many AP surface/sampling ionization approaches, our group has focused in large part on the use of direct liquid extraction methods that employ variations of what has been termed a liquid microjunction surface sampling probe (LMJ-SSP).[19,131] These probes reconstitute or extract analytes from surfaces into a fluidic junction between the sampling end of the probe and the surface. These probes can be operated either in a continuous sampling mode[144] or in a droplet dispensing/retrieving mode.[145,146,147] A unique advantage of the LMJ-SSP approach to surface sampling is the ability, with some of the implementations, to process the materials extracted into solution post-sampling. Relative to a direct mass spectrometric analysis, this provides the capacity to eliminate matrix effects or add an additional, orthogonal dimension of detection selectivity or specificity. The importance of this capability was recently demonstrated by combining the use of the droplet sampling mode with a subsequent HPLC separation and targeted

detection of a drug and its isomeric glucuronide metabolites from thin tissue sections of drug dosed mice using an autosampler.[148] These isomers were not distinguished from a similar sample using simple MS or MS/MS detection methods.[146]

One limit of the LMJ-SSP approach is the lack of ability to robustly sample from some wettable and absorbent surfaces.[19,149] With such surfaces, the extraction solvent can be drawn out from the probe into the surface and trapped, thus the sampled material cannot be efficiently aspirated back into the probe and analyzed. Another limit of the LMJ-SSP approach is the achievable spatial resolution of the technique, viz., ≥100 μm,[150,151] which is restricted by the size of the probe and the fluidic junction to the surface. One might envision constructing and using smaller probes than employed at present, but such implementations might be expected to limit the robustness of operation because of simple issues like precise probe positioning relative to the surface and probe plugging.

Laser desorption (LD) or ablation (LA) based approaches provide a proven means to sample from a surface at AP with a spatial resolution substantially better than 100 μm and to create in the gas phase intact molecular species for mass analysis.19 Theoretically, laser spot size is limited by the diffraction limit (D) of the light ($D \sim \lambda/2$),[152] or when using near field phenomena, to even smaller dimensions.[14,153] To date, laser-based AP surface and ionization approaches have reported spatial sampling resolutions from about 50-70 micrometers[154] down to as small as a few micrometers.[155,156,33] Like most of the other AP surface sampling/ionization approaches, however, these laser based methods do not provide the opportunity to process for analytical benefit the sampled material prior to ionization and mass analysis.

We report here on an AP surface sampling/ionization combination that provides both the higher spatial resolution surface sampling of LA and the post sampling processing capabilities of liquid extraction-based sampling probe methods. This combination also circumvents the need for direct contact between the surface and the liquid extraction solvent, which is expected to eliminate problems in the analysis of unmodified absorbent surfaces that have previously limited liquid extraction-based sampling probe methods. Specifically, a commercially available autosampler was adapted to produce a liquid droplet at the end of the syringe injection needle while in close proximity to the surface to collect the sample plume produced by a vertically aligned transmission geometry LA system. The sample collection was followed by either flow injection or an HPLC separation of the extracted components. In this case, electrospray was used for ionization, but any liquid introduction ionization source could be used in this combination. Analyses of thin films of a commercial ink sample containing rhodamine 6G (compound 2 in Figure 36) and of mixed isobaric rhodamine B (compound 1 in Figure 36) and rhodamine 6G dyes on glass microscope slides were used to illustrate the analytical utility of this coupling.

EXPERIMENTAL METHODS

Transmission Geometry

Chemicals. HPLC grade acetonitrile (ACN). methanol (MeOH) and water were purchased from Burdick & Jackson (Muskegon, MI). Formic acid (FA) (≥96% purity) was purchased from Sigma-Aldrich (St. Louis, MO). Rhodamines B and 6G were

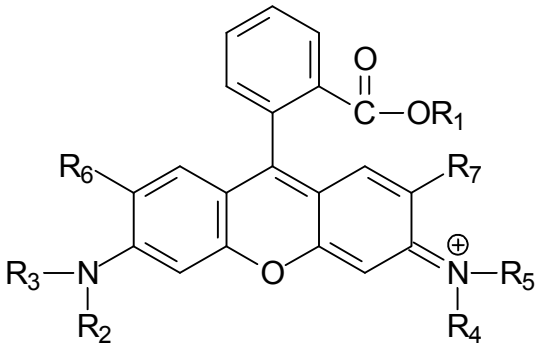

rhodamine B (cpd **1**, *m/z* 443)
R_1, R_6, R_7 = H
R_2, R_3, R_4, R_5 = CH_2CH_3

rhodamine 6G (cpd **2**, *m/z* 443)
R_1, R_2, R_4 = CH_2CH_3;
R_3, R_5 = H; R_6, R_7 = CH_3

Figure 36. Structure and mass-to-charge ratio for rhodamine B (1) and rhodamine 6G (2).

purchased from Kodak (Rochester, NY); their structures are shown in Figure 36 of the main text. A Red Sharpie Fine Point Permanent Marker (Sanford, Oak Brook, IL) and Rain-X (SOPUS Products, Huston, TX) were purchased commercially. The thin-film surfaces of red Sharpie ink containing rhodamine 6G were made by applying a single layer of the ink to a glass microscope slide. Sampling solution for this surface was 80/20/0.1 (v/v/v) ACN/water/FA. Thin film surfaces for the experiments incorporating an HPLC separation step were prepared in a different way. First, 1 mM individual stock solutions of rhodamines B and 6G were prepared in 50/50 (v/v) MeOH/water. A 20 μM solution of this dye mixture for HPLC separation optimization was prepared by dilution of the stock solutions with 50/50/0.1% (v/v/v) ACN/water/FA. In addition, a 0.5 mM solution of this dye mixture in 50/50 (v/v) MeOH/water was prepared to make the mixed dye thin film. The thin films were created by spotting 10 μL of this solution onto a glass microscope slide treated with Rain-X, and allowing the slides to dry in an oven at 90°C for 5 min. This created a spot about 1 mm in diameter corresponding to about 6.4 nmol/mm^2 for the individual dyes. Sampling solution for this surface was 50/50/0.1 (v/v/v) ACN/water/FA.

Laser Set-up. The schematic of the experimental setup is shown in Figure 37. A 10 Hz frequency doubled 532 nm Continuum Minilite Nd:YAG laser (Continuum, Santa Clara, CA) set at 50 μJ/pulse was used for all experiments. The laser beam was coupled into a 50 μm-core-diameter multimode fiber QMMJ-3S3S-UVVIS-50/125-3-2 (OZ Optics Limited, Ottawa, Canada) using a PAF-XM-7-A fiberport (Thorlabs, Newton, NJ). The fiberport was positioned on top of model 429 and 430 translation stages

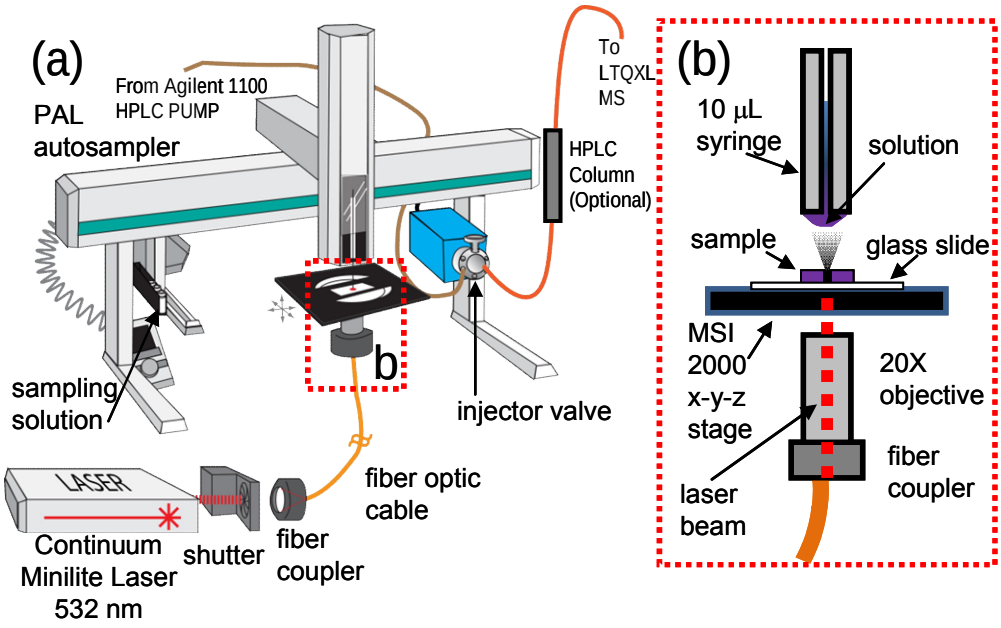

Figure 37. a) Schematic illustration of the experimental setup. b) Zoomed in region around the sample and the collection syringe needle showing laser ablation of the sample and its consequent collection in the liquid phase.

(Newport, Irvine, CA) to give *x*-*y* positioning control for laser alignment. The entrance of the laser beam into the fiberport was controlled using a SC10 shutter and shutter controller (Thorlabs). The laser output out of the fiber was focused onto the backside of the glass sample slide for transmission geometry laser ablation using a PAF-X-7-VIS fiberport (Thorlabs) and a 20X M Plano Apo SL objective (Mitutoyo, Tokyo, Japan). Both the fiberport and microscope objective were mounted on a LP-1-XYZ 3-axis lens positioner (Newport) to allow for optimal alignment of the laser beam onto the sample. The fiberport, objective, and lens positioner assembly were mounted onto a model 429 translation stage (Newport) for fine adjustment of the *z*-positioning of the objective relative to the back side of the sample. Glass microscope sample slides (VWR International, West Chester, PA) were secured to a MS2000 *x*-*y*-*z* robotic platform (Applied Scientific Instrumentation Inc., Eugene, OR). Laser power of 5 μJ/pulse was measured using a FieldMaxII laser power meter (Coherent, Santa Clara, CA) at the exit of the fiber optics setup and on the opposite side of the glass sample slide following transmission through the slide. The control software used to manipulate the sample surface relative to the stationary laser beam is described in previous work.[157] The laser spot size on the sample surface was monitored during an experiment visually using a zoom lens connected to a Costar SI-C400N CCD camera (Costar Inc., Anaheim, CA) and a Marshall V-R102DP-NDA LCD monitor with a 4:3 aspect ratio (Marshall Electronics Inc., El Segundo, CA).

Liquid Handling Instrumentation. The liquid handling setup was very similar to that used previously for liquid microjunction surface sampling coupled with HPLC for analysis of whole-body thin tissue sections.[158] Briefly, an HTC PAL autosampler (LEAP

Technologies Inc., Carrboro, NC) was used for liquid handling during the surface ablation process (Figure 37). The MS2000 *x, y, z* stage and the autosampler were both secured onto the same 24"×24" aluminum breadboard (Thorlabs). This was done to fix the position of the two *x-y-z* robots (i.e. the stage and the autosampler) relative to each other and to minimize shaking of the system during movement of the autosampler arm. Also, the vial holder of the autosampler was removed and replaced with an in-house made "needle guide stop".[158] In addition, a vial holder from an HP 1090 HPLC system was secured to the autosampler to allow rapid exchange of vials holding various sampling solutions (Figure 37). The autosampler was coupled to an Agilent 1200 HPLC system (Agilent Technologies, Santa Clara, CA) and to an LTQ XL mass spectrometer (Thermo, San Jose, CA).

Laser Ablation/Liquid Phase Collection Surface Sampling. The multi-step laser ablation and liquid phase collection process began with aspiration of 0.3 μL of sampling solution into the 10 μL autosampler syringe. Following this aspiration, the syringe moved to the "Home" position for a 20 s pause that allowed wiping the excess sampling liquid off of the outside of the syringe needle. This practice produced a dry needle surface that ensured formation of a well-defined liquid droplet at the end of the autosampler syringe needle. Note that this manual step was not needed in previous direct liquid extraction based surface sampling applications,[145,159] and might be automated or unneccesary with other syringe or probe configurations. The droplet formation step involved approaching the sample surface to within about 500 μm and pushing 0.1 μL of sampling solvent out of the capillary in 6 s at a speed of 16 nL/s. The hanging droplet did not touch the surface. The laser was then fired for about 15 s (corresponding to

approximately 150 laser shots). Some of the material ablated from the surface upward toward the hanging droplet was entrapped in the liquid. The syringe plunger was then retracted to aspirate a 0.2 μL volume (liquid and air) into the syringe. The complete sample within the syringe (0.4 μL solvent/air mixture) was then either flow injected into a stream of 80/20/0.1 (v/v/v) ACN/water/FA (thin-film surface of rhodamine 6G) or injected onto an Hydro-RP 80A HPLC column (50 x 2 mm, 4 μm particle size; Phenomenex, Torrance, CA) for a subsequent isocratic HPLC separation (thin-film surface of rhodamine B and 6G mixture) employing a 50/50/0.1 (v/v/v) ACN/water/FA eluent. Solution flow rate was 50 μL/min in both cases.

Reflection Geometry

Experimental Setup using Continuous Flow Liquid microjunction Surface Sampling Probe (LMJ-SSP). The experimental setup figure is shown in Figure 38. A 10 Hz, 337 nm nitrogen laser (MassTech, Columbia, MD) set at 100 μJ/pulse was used for all experiments. The laser beam was coupled directly from the output of the laser into a 400 μm-core-diameter multimode fiber P400-1-SR (Ocean Optics, Dunedin, FL). The laser beam was focused onto the surface at a 45° angle using a 500 mm quartz lens (MassTech, Columbia, MD). Glass microscope sample slides (VWR International, West Chester, PA) were secured to a MS2000 *x-y-z* robotic platform (Applied Scientific Instrumentation Inc., Eugene, OR). Laser power was measured using a FieldMaxII laser power meter (Coherent, Santa Clara, CA) at the exit of the quartz lens. The control software used to manipulate the sample surface relative to the stationary laser beam was equivalent to that described above. The laser spot size on the sample surface was

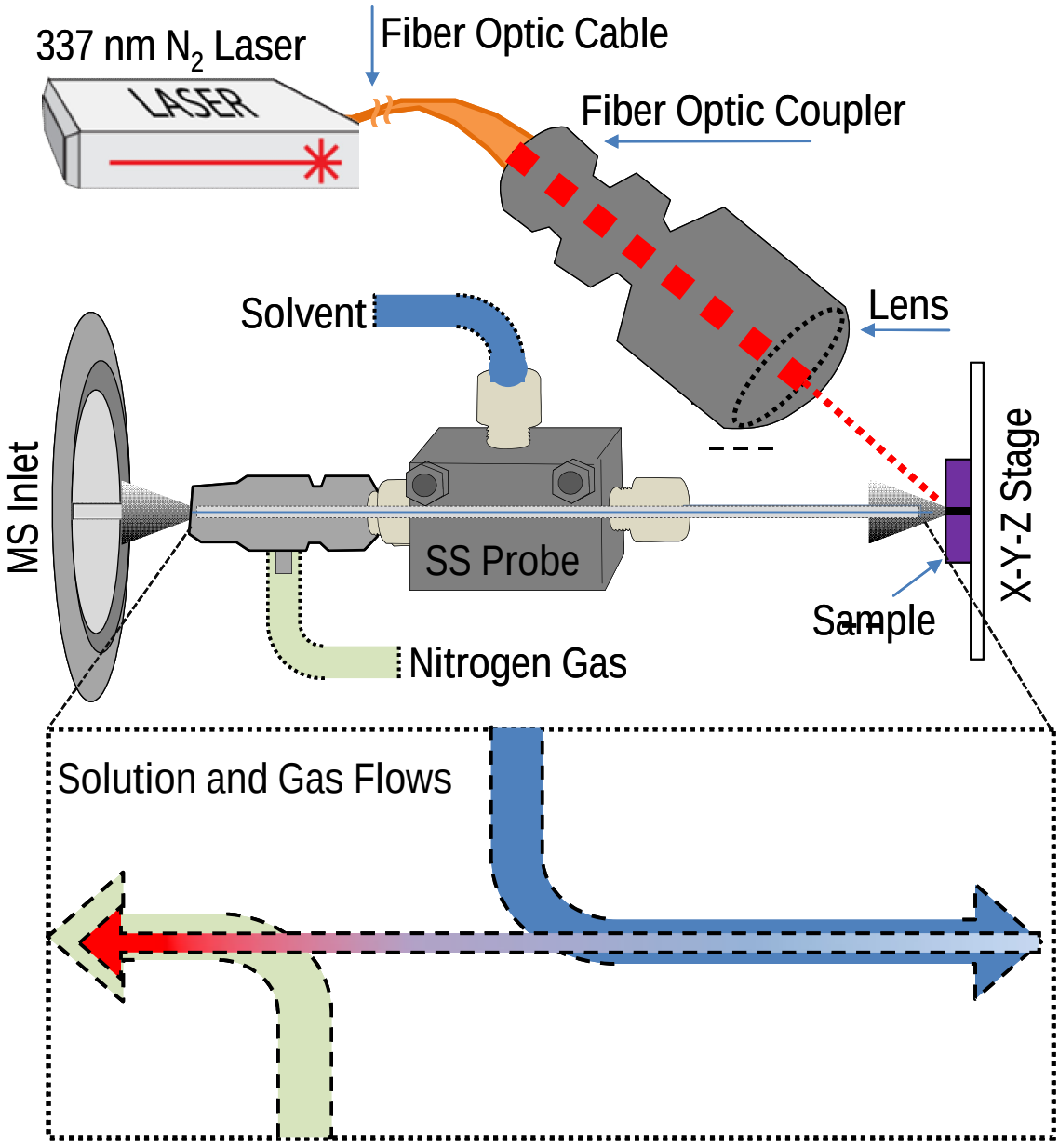

Figure 38. Schematic illustration of reflection geometry experimental setup.

measured to be 400 μm and monitored during an experiment visually using a zoom lens connected to a Costar SI-C400N CCD camera (Costar Inc., Anaheim, CA) and a Marshall V-R102DP-NDA LCD monitor with a 4:3 aspect ratio (Marshall Electronics Inc., El Segundo, CA).

A schematic of the continuous flow probe used in these experiments is show in Figure 38 and has been described in detail in previous work.[159,] **Error! Bookmark not defined.** Briefly the LMJ-SSP/ESI-MS system used here had the electrospray on-axis to the atmospheric sampling orifice of a LTQ Deca mass spectrometer (Thermo Scientific, San Jose, CA). A syringe pump (Harvard Apparatus, Holliston, MA) delivered 50/50/0.1% (v/v/v) acetonitrile/water/formic acid extraction solvent to the surface sampling probe from a 10 mL glass syringe at 10 μL/min. The gas flow into the surface sampling probe was adjusted to create a liquid meniscus as the end of the surface sampling probe, and the probe was positioned 0.5 mm from the sample surface.

RESULTS

As shown in Figure 37, the vertically aligned transmission geometry laser ablation arrangement used in these experiments allowed for direct on-axis alignment of the laser beam with the also vertically aligned autosampler syringe needle for capture of the ablated material into the suspended liquid droplet. With this geometry, a 0.1 μL volume liquid droplet could be reproducibly produced at the end of the syringe needle and positioned to be about 500 μm above, but never touch, the surface. Furthermore, this transmission geometry provided a platform for the future from which to achieve very

high spatial resolution laser ablation (e.g., 1 - 2 μm) similar, for example, to that possible with many existing laser capture microdissection devices[160,161,162,163]

The ability to capture some or all of the laser ablated sample/plume into a suspended liquid droplet was first tested in a flow injection mode using a thin film of red Sharpie ink applied to a transparent glass microscope slide. This ink contained compound **2**. Figure 39a shows the extracted ion chronogram for *m/z* 443 for the flow injection of both a 0.1 μL droplet (80/20/0.1 (v/v/v) acetonitrile/water/formic acid) that had been suspended over the ablation region and the 10 Hz laser fired for 15 s (~150 laser shots, 5 μJ/shot) to ablate the dye from the surface (time window 0-3.75 min) as well as a droplet simply suspended over the dye surface (at a different position), but with the laser turned off for the 15 s sampling time (time window 8.25-12 min). Figures 39b and 39c show the corresponding averaged mass spectra for the flow injection peaks observed at approximately 1 min and 9 min, respectively. These data clearly demonstrate that laser ablated material was successfully collected by the hanging liquid droplet and that no direct liquid extraction sampling took place. As such, the spatial resolution was determined by the size of the focused laser beam spot on the surface. In this case, as the optical image insert in Figure 39a shows, the diameter of the ablation area was about 70 μm. This ablated area was somewhat smaller than the best spot sampling size reported for direct liquid extraction surface sampling (100 μm),[150] but significantly larger than the 15 μm spot size that has been demonstrated with transmission geometry matrix assisted laser desorption (MALDI).[155] A smaller diameter fiber optic cable and improved laser

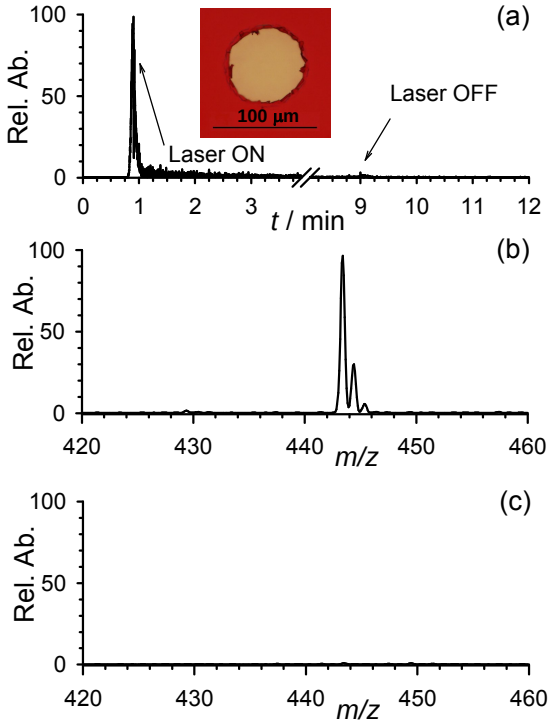

Figure 39. (a) Extracted ion chronogram generated using the ion intensity for *m/z* 443. Inset shows the approximately 70-µm-diameter ablated area after the 10 Hz laser was turned on for 15 s with an output energy of 5 µJ/pulse during the sampling process. Mass spectra in (b) correspond to the laser turned ON and in (c) to the laser turned OFF and are normalized to the highest signal in (b). The syringe needle was positioned 500 µm above the surface. A volume of 0.1 µL was used to create a droplet at the end of the syringe needle. Sampling solution was 80/20/0.1 (v/v/v) ACN/water/FA. The sample was injected into a stream of the same solvent and sprayed at a flow rate of 50 µL/min.

focusing optics incorporated into the present apparatus would reduce the size of the ablation spot achieved.

In addition to the simple flow injection type analysis just discussed, this laser ablation/liquid phase collection combination allowed for further processing of the collected sample before mass spectral analysis. To demonstrate this processing capability, we used a thin film of a mixture of the isobaric compounds 1 and 2 prepared on a glass slide. The sampling procedure was identical to that described above (except for the solvent droplet composition, 50/50/0.1 (v/v/v) acetonitrile/water/formic acid) and the ablated area was also about 70 μm in diameter. Rather than performing a simple flow injection, an Hydro-RP 80A HPLC column (50 x 2 mm, 4 μm particle size; Phenomenex, Torrance, CA) was positioned between the injector and ESI source and an isocratic separation (50/50/0.1 (v/v/v) acetonitrile/water/formic acid) of the captured ablated material was carried out at a flow rate of 50 μL/min. Figure 40a shows the extracted ion chromatogram recorded for *m/z* 443 from the 8 min HPLC-MS run. Two distinct peaks were observed in the chromatogram at 5.3 min and 6.3 min corresponding to compounds 1 and 2, respectively. Using the surface concentration of the dyes (about 6.4 nmol/mm^2 for each individual dye) and size of the ablated area (3.85 x 10^{-3} mm^2), one calculates that about 11 ng of each dye was ablated from the surface. The amount of that material collected into the drop has not been determined. However, visual observation of the plume of laser ablated material during the experiment made it apparent that not all of the material was captured. As a control experiment, Figure 40b shows the extracted ion chromatogram of *m/z* 443 under the same conditions except that the laser was not fired

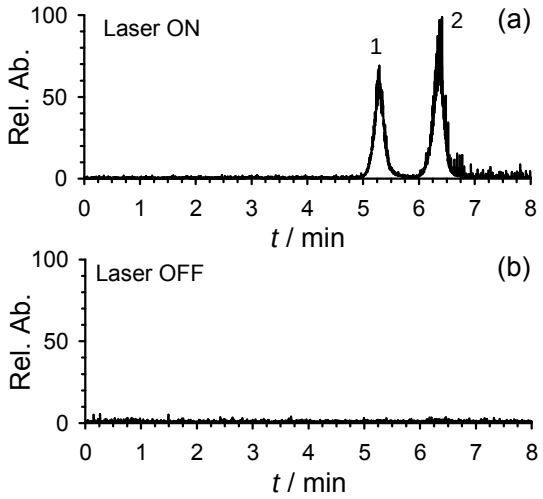

Figure 40. Extracted ion chromatograms for *m/z* 443 recorded during a 8-min HPLC-MS run with the laser turned (a) ON and (b) OFF during the sampling process. Measured signal intensities in both figures were normalized to the highest signal in (a). Output fluence of the 10 Hz laser was 5 μJ/pulse ablating an approximately 70-μm-diameter area that corresponded to about 25 pmol (about 11 ng) of both rhodamines B (compound 1) and 6G (compound 2) being removed from the glass slide surface. Sampling and isocratic HPLC eluent solutions were both 50/50/0.1 (v/v/v) ACN/water/FA. Flow rate of the HPLC separation was 50 μL/min.

when the droplet was in the sampling position. No signal corresponding to the respective dyes was observed in that case.

The data presented here prove the ability to sample analyte from a surface using laser ablation and to capture that ablated material into a suspended liquid droplet which can then be directly analyzed, or further processed, in this case by HPLC, prior to mass spectral analysis. Relative to direct liquid extraction based surface sampling approaches; the present combination offers superior sampling resolution and also avoids issues that can arise when attempting to analyze wettable surfaces. Relative to direct AP laser-based surface sampling methods, this combination provides the ability to process the sample collected prior to mass spectral analysis for enhanced analytical benefit (e.g., separation of isobaric components in a mixture). Work is under way to quantify and improve various analytical figures of merit for this new methodology including capture efficiency of the laser ablated material into the droplet, minimum sample spot size that provides detectable signal, and detection levels for various compound classes.

As additional data demonstrates, this sampling approach can be used, if desired, with a reflection geometry laser ablation or with a continuous flow LMJ-SSP. The ability to achieve the best possible spatial sampling resolution may be more difficult to obtain in reflection geometry versus the transmission geometry. The flow probe does not allow as simple a coupling for sample processing as the syringe droplet capture and injection procedure described above. But, because it is continuously sampling and ionizing collected material, it might be used as a means to increase sampling through put or even be used to provide this technique the ability for chemical imaging. Nonetheless, the fundamentals of the ablation and sample capture process are the same with either laser

ablation geometry or sampling probe type. Therefore, analyses that are successful in one configuration should be achievable in another. Thus, in addition to the rhodamine dye data focused on here, we can also report that the proteins cytochrome c and bovine insulin have been sampled and multiply charged and small fragile molecules like propranolol glucuronide successfully sampled and detected (See Figure 41, 42, and 43). In general, the laser ablation and liquid phase collection approach to surface sampling can be applied to materials that can be ablated and captured and, for the most part, dissolved in the capture solvent, then effectively ionized with the ionization source in use. Different laser wavelengths, power, pulse widths, and repetition rates and the use of surface chemistries or chemical matrices as in MALDI might be among the techniques used to improve the effectiveness of ablation for different analytes from diverse sample matrices. More nonpolar solvents might be used to capture less polar analytes in conjunction with ionization using APCI or APPI. In cases where elemental analysis is desired, one can imagine the use of acidic aqueous solutions to capture ablated materials, including particulates, which then can be delivered to an ICP for atomization and ionization prior to mass analysis.

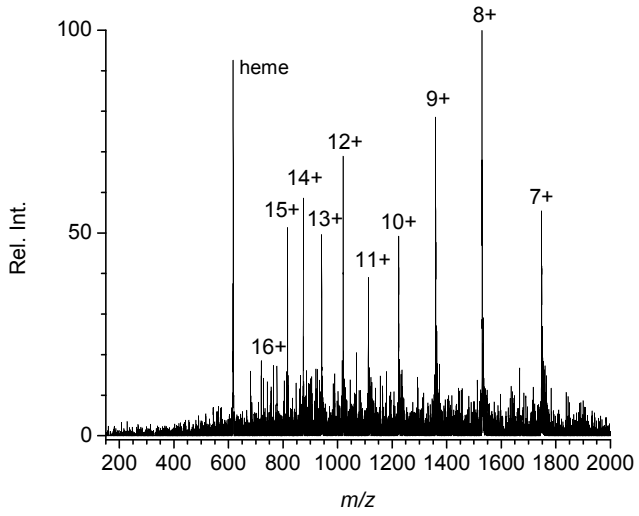

Figure 41. Averaged full scan mass spectra of 327 pmol of bovine cytochome c, MW 12224 Da, that was spotted onto a glass slide. A 337 nm nitrogen laser with a 10 Hz repetition rate, operating at 100 μJ/pulse illuminated the sample surface at a 45° angle in reflection geometry to produce the spectra. The laser spot size on the surface was 400 μm. The solvent in the LMJ-SSP was 50/50/0.1% (v/v/v) acetonitrile/water/formic acid flowing at 10 μL/min.

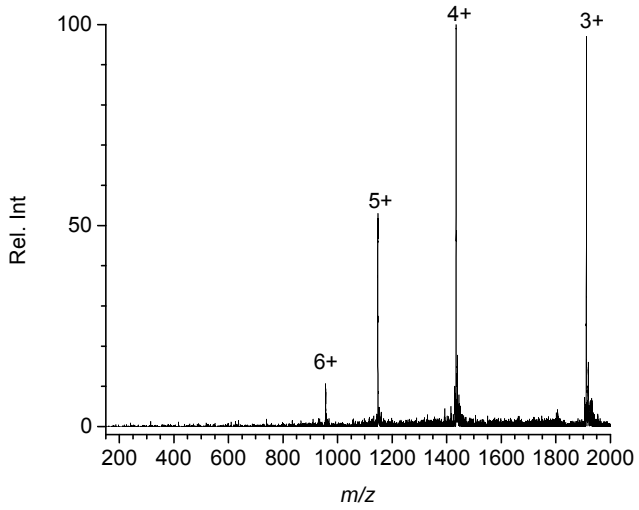

Figure 42. Averaged full scan mass spectra of 340 pmol of bovine insulin, MW 5724 Da, that spotted onto a glass slide. A 337 nm nitrogen laser with a 10 Hz repetition rate, operating at 100 μJ/pulse illuminated the sample surface at a 45° angle in reflection geometry to produce the spectra. The laser spot size on the surface was 400 μm. The solvent in the LMJ-SSP was 50/50/0.1% (v/v/v) acetonitrile/water/formic acid flowing at 10 μL/min.

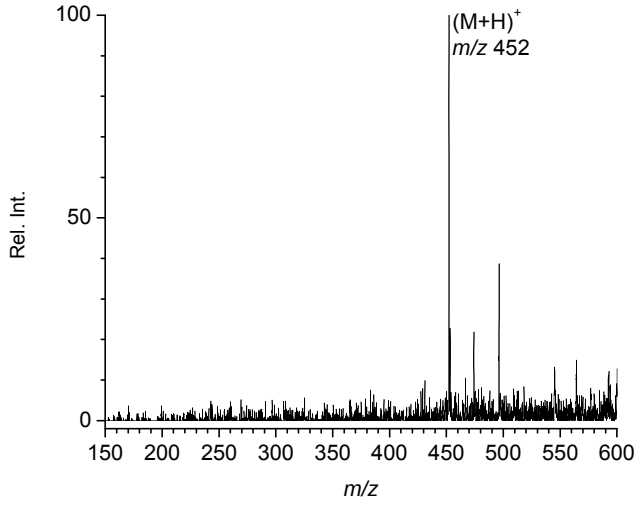

Figure 43. Averaged full scan mass spectra of 2 ng of hydroxylated propranolol glucoronide, that was spotted onto a glass slide. A 337 nm nitrogen laser with a 10 Hz repetition rate, operating at 100 μJ/pulse illuminated the sample surface at a 45° angle in reflection geometry to produce the spectra. The laser spot size on the surface was 400 μm. The solvent in the LMJ-SSP was 50/50/0.1% (v/v/v) acetonitrile/water/formic acid flowing at 10 μL/min.

CHAPTER V
CONCLUSIONS AND FUTURE PROSPECTS

The efficacy of studies of materials and systems is dependent on available technologies. The push towards studying materials and systems in the nanoscale range creates the opportunity for many new discoveries. However, currently available techniques that allow nanometer resolution studies are limited in the amount of chemical information provided. Atmospheric pressure (AP) techniques like atomic force microscopy (AFM) that allow for spatial imaging resolution of 1 nm or better provide almost no chemical information about the sample. In contrast AP mass spectrometry based chemical imaging is able to provide chemical information about a sample on the molecular level but is not capable of imaging with submicron resolution. Therefore, the coupling the of AFM and mass spectrometry is the next stage in scientific progress towards the development of new methods for studying systems such as cell walls, membrane proteins, material junctions etc. that require both nanoscale spatial resolution as well as high chemical specificity.

An analytical tool with high sensitivity that can provide detailed molecular information with high spatial resolution has been the goal behind the development of different chemical imaging techniques. In order to provide chemical and topographic information at the nanometer scale, work has been done by several groups to couple mass spectrometry with near field near-field tip enhanced laser desorption. These techniques rely on using tip-enhanced laser ablation to create submicron sized ablation craters varying in size from (~200 nm – 50 nm) in a surface and sample the ablated material into a mass spectrometer for ionization and detection, the ionization of the ablated material

has been accomplished in these cases using electron ionization (EI), inductively coupled plasma (ICP) or direct laser desorption ionization (LDI). These experiments demonstrated the potential of acquiring mass spectrometric data from nanometer sized craters in vacuum and at atmospheric pressure as well as obtaining structural surface information through the use of scanning probe microscopy (SPM). However, due to the difficult nature of tip-enhanced laser desorption experiments and the inability to effectively extract and detect material from submicron craters produced through the tip-enhanced laser desorption at atmospheric pressure, more recent attempts have been made to combine AFM and MS for multimodal chemical and topographic imaging with a 1 μm spatial resolution using direct laser desorption/ionization (LDI) on a AFM platform.

Outside of the laser based techniques another approach to high resolution surface sampling at atmospheric pressure that combines the chemical specificity of mass spectrometry with the physical characterization allowed by atomic force microscopy has been demonstrated by the use of local thermal desorption from Wollaston wire AFM tips. In their work Reading et al use Wollaston wire AFM tips, that have a tip radius of 5 μm microns to carry out local thermal desorption on a surface and then to analyze the desorbed material, from polymers, plant tissue, as well as pharmaceuticals using gas-chromatography mass spectrometry (GC/MS). Using this set-up they were able to desorb material from craters that were conical in shape and approximately 6 μm wide by 1.7 mm deep. Their work demonstrated the potential for a nanometer spatially resolved TD-based mass spectrometry surface analysis technique.

This dissertation describes research towards a novel set of techniques, using atmospheric pressure hybrid proximal probe topography chemical imaging, where a mass spectrometer is coupled with a state of the art atomic force microscope (AFM). These techniques use AFM probes to desorb material from a surface and then analyze the desorbed gas phase material with a mass spectrometer. These techniques have broad application for studying systems such as cell walls, material junctions, etc. where enhanced or high spatial resolution chemical information is required. Laser desorption/ablation and thermal desorption with a secondary ionization are the two main routes for analyzing surfaces with mass-based chemical imaging that have been developed as part of the research discussed in this thesis for simultaneous topographical imaging. However, other forms of nanoscale surface sampling that could be used on a combined AFM-MS platform such as nano-liquid surface sampling are potential areas of research that could also be added to the current portfolio of AFM-MS techniques.

The further development of all the combined AFM-MS techniques could be envisioned to encompass a multimodal imaging platform where the AFM is used to provide physical information about the surface like topography, bulk modulus stiffness, melting point and glass transition information and the mass spectrometer will serve as the ultimate tool for spatially resolved chemical characterization of the material. The coupling of both laser and thermal desorption approaches with different atmospheric pressure ionization mechanisms like ESI, APCI, APPI or ICP will allow for the detection of compounds with desperate properties as well as for elemental analysis. The research and development of a platform that will allow for a combined AFM/MS platform for nanoscale chemical imaging using proximal probe thermal desorption with a secondary

ionization is currently under discussion with industry partners both in mass spectrometry and scanning probe microscopy community. We can envision that this close interaction will help us get one step closer to a commercially available nanometer scale chemical imaging system. However, there still remains a substantial amount of investigation with using this combination to realize the true potential of a simultaneous mass-based chemical imaging and topographical imaging system at atmospheric pressure.

One particular future research direction for combined AFM, nanoscale TD-MS chemical imaging is a target application to co-register local nanomechanical measurements of plant cells using AFM with mass spectrometry-based chemical imaging of plant growth regulators within those cells. This information is of vital importance in understanding plant productivity on the molecular level. Auxins and gibberellins, for example, are responsible for plant development (growth), and are found in higher concentration in areas of buds, roots, and stem shoots[1]. Chemical imaging of targeted molecules responsible for plant development like gibberellic acid and plant hormone indole-3-acetic acid in areas of interest, i.e. roots, shoots and buds, can lead to understanding of transport of these molecules, which can lead to a better understanding of plant growth. Nanomechanical studies of cells can reveal information about cell stiffness and defects. Cell stiffness is an indication of cell growth because cell stiffness decreases as cells expand. This information can be correlated with chemical information obtained from MS data on targeted molecules in individual plant cells. The central objective of this research would be to demonstrate chemical imaging of biological surfaces with nanometer spatial resolution under ambient conditions accompanied by nanometer resolved topographic information as well as nanomechanical information about the

material. This method would illustrate promise for the advancement of imaging based techniques by combining a scanning probe technique with the high chemical information technique of mass spectrometry.

Another research direction briefly mentioned earlier is the use of nanoscale liquid sampling through an AFM liquid delivery probe coupled with MS. This approach would allow for the use liquid extraction surface sampling in the nanoscale regime. The use of AFM cantilevers as the delivery system for the liquid would allow for surface mapping of the sample with nanoscale resolution in regards to topography and other physical surface characterization like stiffness, and at the same time allow to collect chemical information about the sample as well. Using liquid extraction would expand on the classes of molecules that currently can be sampled from the surface by nano-TD to thermally labile compounds and large biomolecules like proteins. Capturing analyte into a liquid allows for the opportunity to easily capture and store the liquid in some other fashion to allow for analysis at a later period in time. For example placing the liquid in a well array, or onto a microfluidic lab on a chip to be analyzed later by conventional MS means are some of the possibilities. This type of system would open up the possibly to study biological systems on the sub-cellular level and identify metabolites that are extremely fragile. One example would be a cell to cell study of animal tissue dosed with a particular drug and the presence of the parent drug as well the fragile phase I and phase II metabolites of the drug.

The main scientific driver behind this research would be expanding liquid surface sampling into the nanoscale regime and its application to the study of animal and plant metabolism on the sub-cellular lever. The ability to chemically and physically

differentiate between healthy and tumor cell on a cell by cell basis is one clear application for the technique.

The other obvious application of liquid extraction is expanding of the current laser ablation into a liquid droplet experiment for the online study of biological plant and animal tissue. Mass spectrometric chemical imaging of targeted molecules responsible for plant productivity can lead to the understanding of transport of these molecules, which can lead to a better understanding of plant growth, drought resistance, and plant-bacterial signaling critical to the development of biofuel research. Using a laser micro-dissection instrument coupled with an online liquid phase collection surface sampling followed by sample clean-up with high performance liquid chromatography would allow for spatially resolved studies of targeted compound in plant tissue used for biofuel research. Ideally, the spatially resolved sub-cellular chemical information obtained will be combined with other direct infusion mass spectrometric data obtained via gas chromatography mass spectrometry (GC-MS) and fluorescence imaging data to providing a direct correlation between chemical structure and cellular functionality.

Keeping with the topic of liquid extraction another direction that could have a large impact on the scientific community is the ability of liquid extraction to sample and extract insoluble and inorganic materials. This could potentially be accomplished by using the laser ablation of material into a liquid. However, to increase sample capture a liquid junction could now be made with the surface and the laser would fire directly into the liquid and ablate the sample. This approach to laser ablation of materials in liquid has been around since the 1960 and most recently has been used for the production of nanoparticles.[164] Since the material is not soluble in the liquid the spatial resolution

would be defined by the spot of the laser on the sample which could potentially be submicron when using UV lasers with wavelengths in the 200 nm range. This type of approach to surface sampling would allow for almost total sample collection with little to no carry over to adjacent sampling areas because the material is being caught in a liquid and carried away. Also, since the ablated material is being collected into a small volume there is a large concentration effect. The collected liquid could then be post processed using traditional analytical techniques as well as the analyte could be ionized in a variety of ways including inductively couple plasma (ICP) for subsequent analysis by mass spectrometry for elemental analysis of inorganic materials used for energy capture and storage i.e. thin film organic photovoltaics, thin film lithium ion batteries and thin film fuel cells.

The capability of mass spectrometry to examine structure and chemical composition from mesoscopic to atomic scales makes it the ultimate characterization tool in chemistry and materials science. Laser ablation inductively coupled plasma mass spectrometry (LA-ICP-MS) is an established technique that allows spatially resolved studies of elemental composition in inorganic materials. The implementation of such a system for the study energy storage and conversion devices seems an ideal companion to the laser ablation of material into liquid with analysis by ICP-MS. Ideally, structural information obtained via LA-ICP-MS imaging can be synergistically combined with other spectroscopic data, providing a direct correlation between structure and electronic functionality. Characterization of optical and chemical properties of materials on the micro and nano scale is a high priority direction within the Department of Energy. In particular using laser desorption coupled with mass spectrometry as a source of spatially

resolved highly specific chemical information from materials and material junctions for energy storage and conversion materials.

By broadening the scope of and generating new technologies, the work described in this dissertation has made possible new discoveries contingent on spatially resolved chemical information. These approaches to multimodal imaging platforms open up avenues to studying materials with various tools simultaneously and extracting both physical and chemical information about the sample. These techniques hold the potential to solving some basic questions regarding the chemical composition of materials on the submicron scale in a variety of systems ranging from biological plant and animal tissue to materials systems for energy storage and conversion.

LIST OF REFERENCES

[1] Teale, W. D.; Paponov, I. A.; Palme, K. "Auxin in action: signaling, transport and the control of plant growth and development." *Nature Rev. Mol. Cell Bio.* **2006**, *7*, 847-859.

[2] Ng, C. K. Y.; Carr, K.; McAinsh, M. R.; Powell, B.; Hetherington, A. M. "Drought-induced guard cell signal transduction involves sphingosine-1-phosphate." *Nature* **2001**, *410*, 596-599.

[3] Becker, J. S.; Zoriy, M.; Becker, J, Su.; Pickhardt, C.; Przybylsky, J. "Determination of phosphorus and metal in human brain proteins after isolation be gel electrophoresis by laser ablation inductively coupled plasma source mass spectrometery." *J. Anal. Atom. Spectrom.* **2004***, 19*, 149-152.

[4] Rasmussen A.; Deckert, V. "New dimension in nano-imaging: breaking through the diffraction limit with scanning near-field optical microscopy." *Anal. Bioanal. Chem.* **2005**, *381*, 162-172.

[5] Craig, D. Q. M.; Kett, V. L.; Andrews, C. S.; Royall, P. G. "Pharmaceutical applications of micro-thermal analysis." *J. Pharm. Sci.* **2002**, *91*, 1201-1213.

[6] Winograd, N. "The magic of cluster SIMS." *Anal. Chem.* **2005**, *77,* 142A-149A.

[7] Todd, P.J.; Schaaff, T.G.; Chaurand, P.;Caprioli, R.M "Organic ion imaging of biological tissue with MALDI and SIMS." *J. Mass Spectrom.* **2001**, *36,*, 355-369.

[8] Cornett, D. S.; Reyzer, M. L.; Chaurand, P.; Caprioli, R. M. "MALDI imaging mass spectrometry: molecular snapshots of biochemical systems." *Nature Methods* **2007**, *4,* 828-833.

[9] Bennighoven, A.; Rudenuer, F. G.; Werner, H. W. *Secondary Ion Mass Spectrometry*; John Wiley & Sons: New York, 1987.

[10] Schweiters, J.; Cramer, H-G.; Heller, T.; Jurgens, U.; Niehuis, Rulle, H.; Heller, T.; Zehnpfennig, J. F.; Bennighoven, A. *Secondary Ion Mass Spectrometry Proceeding of the Eight International Conference(SIMS VIII)*. John Wiley & Sons: Chichester, England, 1992; p. 497.

[11] Horning, E. C.; Horning, M. G.; Carroll, D. I; Dzidic, I.; Stillwell, R. N. "New pictogram detection system based on a mass spectrometer with an external ionization source at atmospheric pressure." *Anal. Chem.* **1973,** *45*, 936-943.

[12] Fenn, J. B.; Mann, M.; Meng, C. K.; Wong S. F.; Whitehouse, C. M. "Electrospray ionization for mass spectrometry of large biomolecules." *Science* **1989**, *246*, 64-71.

[13] Gray, A. L.," Solid sample introduction by laser ablation for inductively coupled plasma source-mass spectrometry." *Analyst* **1985,** *110*, 551-556

[14] Novotny, L.; Stranick, S. J.; "Near-field optical microscopy and spectroscopy with pointed probes." *Annu. Rev. Chem.* **2006**, *57*, 303-331.

[15] Price, D. M.; Reading, M.; Hanniche, A.; Pollock, H. M. "Micro-thermal analysis: scanning thermal microscopy and localized thermal analysis." *Int. J. Pharm.* **1999**, *192*, 85-96.

[16] McDonnell, L.A.; Heeren, R.M.A. "Imaging mass spectrometry." *Mass Spectrom. Rev.*, 2007, **26**, 606-643.

[17] Pacholski, M.L.; Winograd, N. "Imaging with mass mpectrometry." *Chem. Rev.*, 1999, **99**, 2977-3005.

[18] Amstalden van Hove, E.R.; Smith, D.F.; Hereen, R.M.A. "A concise review of mass spectrometry imaging." *J. Chrom. A*, 2010, **25**, 3946-3954.

[19] Van Berkel, G.J.; Pasilis, S.P.; Ovchinnikova, O. "Established and emerging atmospheric pressure sampling/ionization techniques for mass spectrometry." *J. Mass. Spectrom*., 2008, **43**, 1161-1180.

[20] Harris, G. A.; Nyadong, L; Fernandez, F. "Recent developments in ambient ionization techniques for analytical mass spectrometry." *Analyst* **2008**, *133*, 1297-1301.

[21] Venter, A.; Nefliu, M.; Cooks, R. G. "Ambient Desorption Ionization Mass Spectrometry." *Trends Anal. Chem.* **2008**, *27*, 284-290.

[22] Chughtai, K.; Hereen, R.M.A. "Mass spectrometric imaging for biomedical tissue analysis." *Chem. Rev.*, 2010, **110**, 3237-3277.

[23] Wiseman, J.M.; Ifa, D.R.; Zhu, Y.; Kissinger, C.B.; Manicke, N.E.; Kissinger, P.T.; Cooks, R.G. "Desorption electrospray ionization mass spectrometry: Imaging drugs and metabolites in tissue." *Proc. Natl. Acad. Sci.*, 2008, **105**, 18120-18125.

[24] Ifa, D.R.; Jackson, A.U.; Paglia, G.; Cooks, R.G. "Forensic applications of ambient mass spectrometry." *Anal. Bio. Chem.*, 2009, **394**, 1995-2008.

[25] Ifa, D.R.; Gumaelius, L.M.; Eberlin, L.S.; Manicke, N.E.; Cook, R.G. "Forensic analysis of inks by imaging desorption electrospray ionization (DESI) mass spectrometry." *Analyst*, 2007, **132**, 461-467.

[26] Ifa, D.R.; Wiseman, J.M.; Song, Q.Y.; Cooks, R.G. "Development of capabilities for imaging mass spectrometry under ambient conditions with desorption electrospray ionization (DESI)." *Int. J. Mass Spectrom.*, 2007, **259**, 8-15.

[27] Kertesz, V.; Van Berkel, G. J. "Improving imaging resolution in desorption electrospray ionization mass spectrometry." *Rapid Commun. Mass Sprectrom*. 2008, **22**, 2639-2644.

[28] Liu, Y.; Ma, X.; Lin, Z.; He, M.; Han, G.; Yang, C.; Xing, Z.; Zhang, S.; Zhang, X. "Imaging mass spectrometry with a low-temperature plasma probe for the analysis of works of art*." Angew. Chem. Int. Ed.*, 2010, **49**, 4435-4437.

[29] Li, Y.; Shrestha, B.; Vertes, A. "Atmospheric pressure molecular imaging by infrared MALDI mass spectrometry." *Anal. Chem.*, 2007, **79**, 523-532.

[30] Nemes, P.; Vertes, A. "Laser ablation electrospray ionization for atmospheric pressure, in vivo, and imaging mass spectrometry." *Anal. Chem.* 2007, **79**, 8098-8106.

[31] Nemes, P.; Barton, A.A.; Vertes, A. "Three-dimensional imaging of metabolites in tissue under ambient conditions by laser ablation electrospray ionization mass spectrometry." *Anal. Chem.* 2009, **81**, 6668-6675

[32] Coello, Y.; Jones, A. D.; Gunarante, T.C.; Dantus, M. "Atmospheric pressure femtosecond laser imaging mass spectrometry." *Anal. Chem.,* 2010, **82**, 2753-2758.

[33] Bradshaw, J.A.; Ovchinnikova, O.S.; Meyer, K.A.; Goeringer, D.E. "Combined chemical and topographic imaging at atmospheric pressure via microprobe laser desorption/ionization mass spectrometry-atomic force microscopy." *Rapid Commun. Mass Spectrom.,* 2009, **23**, 3781-3786.

[34] Chen, L.C.; Yoshimura, K.; Yu, Z.; Iwata, R.; Ito, H.; Suzuki, H.; Mori, K.; Ariyada, S.T.; Kubota, T.; Hiraoka, K. "Ambient imaging mass spectrometry by electrospray ionization using solid needle as sampling probe." *J. Mass. Spectrom.*, 2009, **44**, 1469-1477.

[35] Vastola F. J,; Mumma R. O.; Pirone A. J., "Analysis of organic salts by laser ionization." *Organic Mass Spectrometry* **1970**, *3*, 101-1004.

[36] Gross, J. "Matrix-assisted laser desorption/ionization" In *Mass Spectrometry a Textbook;* Springer: Heidelberg, 2004, pp 411-440.

[37] Gunther, D.; Hattendorf, B., "Solid sample analysis using laser ablation inductively coupled plasma mass spectrometry". *Trac-Trends in Analytical Chemistry* **2005,** *24*, 255-265.

[38] Mokgalaka, N. S.; Gardea-Torresdey, J. L., Laser ablation inductively coupled plasma mass spectrometry: Principles and applications. *Applied Spectroscopy Reviews* **2006,** *41*, 131-150.

[39] Becker, J. S.; Zoriy, M.; Becker, J. S.; Dobrowolska, J.; Matusch, A., Laser ablation inductively coupled plasma mass spectrometry (LA-ICP-MS) in elemental imaging of biological tissues and in proteomicsw. *Journal of Analytical Atomic Spectrometry* **2007,** *22*, 736-744.

[40] Zoriy, M. V.; Becker, J. S., "Imaging of elements in thin cross sections of human brain samples by LA-ICP-MS: A study on reproducibility". *International Journal of Mass Spectrometry* **2007,** 264, (2-3), 175-180.

[41] Zoriy, M. V.; Dehnhardt, M.; Reifenberger, G.; Zilles, K.; Becker, J. S., "Imaging of Cu, Zn, Pb and U in human brain tumor resections by laser ablation inductively coupled plasma mass spectrometry." *International Journal of Mass Spectrometry* **2006,** 257, (1-3), 27-33.

[42] Chery, C. C.; Gunther, D.; Cornelis, R.; Vanhaecke, F.; Moens, L., "Detection of metals in proteins by means of polyacrylamide gel electrophoresis and laser ablation-inductively coupled plasma-mass spectrometry: Application to selenium."*Electrophoresis* **2003,** 24, (19-20), 3305-3313.

[43] Wind, M.; Feldmann, I.; Jakubowski, N.; Lehmann, W. D., "Spotting and quantification of phosphoproteins purified by gel electrophoresis and laser ablation-element mass spectrometry with phosphorus-31 detection." *Electrophoresis* **2003,** 24, (7-8), 1276-1280.

[44] Coon, J. J.; Steele, H. A.; Laipis, P. J.; Harrison, W. W., "Laser desorption-atmospheric pressure chemical ionization: a novel ion source for the direct coupling of polyacrylamide gel electrophoresis to mass spectrometry." *Journal of Mass Spectrometry* **2002,** 37, (11), 1163-1167.

[45] Coon, J. J.; Harrison, W. W., "Laser desorption-atmospheric pressure chemical ionization mass spectrometry for the analysis of peptides from aqueous solutions." *Analytical Chemistry* **2002,** 74, (21), 5600-5605.

[46] Coon, J. J.; McHale, K. J.; Harrison, W. W., "Atmospheric pressure laser desorption/chemical ionization mass spectrometry: a new ionization method based on existing themes." *Rapid Communications in Mass Spectrometry* **2002,** 16, (7), 681-685.

[47] Coon, J. J.; Steele, H. A.; Laipis, P. J.; Harrison, W. W., "Direct atmospheric pressure coupling of polyacrylamide gel electrophoresis to mass spectrometry for rapid protein sequence analysis." *Journal of Proteome Research* **2003,** 2, (6), 610-617.

[48] Turney, K.; Harrison, W. W., "Corona discharge secondary ionization of laser desorbed neutral molecules from a liquid matrix at atmospheric pressure." *Spectrochimica Acta Part B-Atomic Spectroscopy* **2006,** 61, (6), 634-641.

[49] Shiea, J.; Huang, M. Z.; Hsu, H. J.; Lee, C. Y.; Yuan, C. H.; Beech, I.; Sunner, J., "Electrospray-assisted laser desorption/ionization mass spectrometry for direct ambient analysis of solids." *Rapid Comm. Mass Spectrom.* **2005,** 19, (24), 3701-3704.

[50] Huang, M. Z.; Hsu, H. J.; Lee, J. Y.; Jeng, J.; Shiea, J., "Direct protein detection from biological media through electrospray-assisted laser desorption ionization/mass spectrometry." *J. Proteome Res.* **2006,** 5, (5), 1107-1116.

[51] Doroshenko, V. M.; Laiko, V. V.; Taranenko, N. I.; Berkout, V. D.; Lee, H. S., "Recent developments in atmospheric pressure MALDI mass spectrometry." *International Journal of Mass Spectrometry* **2002,** 221, (1), 39-58.

[52] Li Y.; Shrestha B.; Vertes A., "Atmospheric pressure infrared MALDI imaging mass spectrometry for plant metabolomics." *Anal. Chem.,* **2008**, *80*, 407-420.

[53] Williams, J. P.; Scrivens, J. H. "Rapid and accurate mass desorption electrospray ionisation tandem mass spectrometry of pharmaceutical samples." *Rapid Commun. Mass Spectrom.* **2005**, *19*, 3643-3650.

[54] Cooks, R. G.; Gologan, B.; Takats, Z.; Wiseman, J. M; Cotte-Rodriguez, I. "Method and system for desorption atmospheric pressure chemical ionization." US Patent Application US2007/0187589A1, August 16, 2007.

[55] Song, Y.; Cooks, R. G. "Atmospheric pressure ion/molecule reactions for the selective detection of nitroaromatic explosives using acetonitrile and air as reagents." *Rapid Commun. Mass Spectrom.* **2006**, *20*, 3130-3138.

[56] Haapala, M.; Pol, J.; Saarela, V.; Arvola, V.; Kotiaho, T.; Ketola, R. A.; Franssila, S.; Kauppila, T. J.; Kostiainen, R. "Desorption atmospheric pressure photoionization." *Anal. Chem.* **2008**, *79*, 7867-7872.

[57] Cody, R.B.; Laramée, J. A.; Durst, H. D. "Versatile new ion source for the analysis of materials in open air under ambient conditions." *Anal. Chem*. **2005**, *77*, 2297-2302.

[58] Bell, K. L.; Dalgarno, A.; Kingston, A. E. "Penning ionization by metastable helium atoms." *J. Phys. B (Proc. Phys. Soc.)* **1968**, *1*, 18-22.

[59] McEwen, C. N.; Gutteridge, S. "Analysis of the inhibition of the ergosterol pathway in fungi using the atmospheric solids analysis probe (ASAP) method." *J. Am. Soc. Mass Spectrom.* **2007**, *18*, 1274-1278

[60] McEwen, C. N.; McKay, R. G.; Larsen, B. S. "Analysis of solids, liquids, and biological tissues using solids probe introduction at atmospheric pressure on commerical LC/MS instruments." *Anal. Chem.* **2005**, *77*, 7826-7831.

[61] Stockle, R.; Setz, P.; Deckert, V.; Lippet, T.; Wokaun, A.; Zenobi, R. "Nanoscale atmospheric pressure laser ablation-mass spectrometry." *Anal. Chem.* **2001**, *73*, 1399–1402.

[62] Schmitz, T. A.; Gamez, G.; Setz, P. D.; Zhu, L.; Zenobi, R. "Towards nanoscale molecular analysis at atmospheric pressure by near-field laser ablation ion trap/time-of-flight mass spectrometer." *Anal. Chem.* **2008**, *80*, 6537-6544.

[63] Meyer, K. A.; Ovchinnikova, O.; Ng, K.; Goeringer, D. E. "Development of scanning surface probe for nanosclae tip-enhanced desorption/ablation." *Rev. Sci. Instrum.* **2008**, *79*, 123710.

[64] Becker, J. S.; Gordunoff, A.; Zoriy, M.; Izmer, A.; Kayser, M. "Evidence of near-field laser ablation inductively coupled plasma mass spectrometery (NF-LA-ICP-MS) at nanometer scale for elemental and isotopic analysis on gels and biological samples." *J. Anal. At. Spectrom.* **2006**, *21*, 19-25.

[65] Zoriy, M. V.; Kayser, M.; Becker, J. S.; Possibility of nano-local elemental analysis by near-field laser ablation inductively coupled plasma mass spectrometery (LA-ICP-MS): New experimental arrangement and first application." *Int. J. Mass Spectrom.* **2008,** *273,* 151-155.

[66] Price, D. M.; Reading M.; Smith, R. M.; Pollock, H. M.; Hammiche, A. "Localized evolved gas analysis by micro-thermal analysis." *J. Therm. Anal. Calorim.* **2001***, 64*, 309-314.

[67] Royall, P. G.; Craig, D. Q. M.; Grandy, D. B. "The use of micro-thermal analysis as a means of in situ characterization of pharmaceutical tablet coatings." *Thermochimica Acta,* **2001**, *380*, 165-173.

[68] Savina, M.R, Lykke, K.R. "Chemical imaging of surfaces with laser desorption mass spectrometry." *Trac-Trends in Anal. Chem.* **1997**, *16*, 242-252.

[69] Pacholski, M.L; Winograd N. "Imaging mass spectrometry." *Chem. Rev.,* **1999**, *99*, 2977.

[70] Todd, P.J.; Schaaff, T.G.; Chaurand, P.; Caprioli, R.M. "Organic ion imaging of biological tissue with secondary ion mass spectrometry and matrix-assisted laser desorption/ionization." *J. Mass Spectrom.* **2001**, *36*, 355-369.

[71] Rubakhin, S.S.; Jurchen, J.C.; Monroe, E.B.; Sweedler, J.V. "Imaging mass spectrometry: fundamentals and applications to drug discovery." *Drug Discovery Today*, **2005**, *10*, 823-837.

[72] McDonnell, L.A.; Heeren, R.M.A. "Imaging mass spectrometry" *Mass Spectrom. Rev.,* **2007**, *26*, 606-643.

[73] Hillenkamp, F.; Unsold, E.; Kaufmann, R.; Nitsche, R. "High-sensitivity laser microprobe mass analyzer." *App. Phys.* **1975**, *8*, 341-348.

[74] Hillenkamp, F.; Unsold, E.; Kaufmann, R.; Nitsche, R. "Laser microprobe mass analysis of organic materials." *Nature*, **1975**, *256*, 119-120.

[75] Wilk, Z.A.; Hercules, D.M. "Organic and elemental ion mapping using laser mass-spectrometry." *Anal. Chem.,* **1987**, *59*, 1819-1825.

[76] Savina, M.R.; Lykke, K.R. "Microscopic chemical imaging with laser desorption mass spectrometry." *Anal. Chem.,* **1997**, *69*, 3741-3746.

[77] Karas, M.; Bachmann, D.; Bahr, U.; Hillenkamp, F. "Matrix-assisted ultraviolet-laser desorption of nonvolatile compounds." *Int. J. Mass Spectrom. Ion Proc.,* **1987**, *78*, 53-68.

[78] Gusev AI, Vasseur OJ, Proctor A, Sharkey AG, Hercules DM. "Imaging of thin-layer chromatograms using matrix/assisted laser desorption/ionization mass-spectrometry." *Anal. Chem.,* **1995**, *67*, 4565-4570.

[79] Caprioli, R.M.; Farmer, T.B.; Gile, J. "Molecular imaging of biological samples: Localization of peptides and proteins using MALDI-TOF MS." *Anal. Chem.,* **1997**, *69*, 4751-4760.

[80] Castaing, R.; Jouffrey, B.; Slodzian, C.R. "Sur les possibilities danalyze locale dun echantillion par utilisation des son emission ionique secondaire." *Acad. Sci.* **1960**, *251*, 2696:

[81] Liebl, H. "Ion microprobe mass analyzer." *J. App. Phys.,* **1967**, *38*, 5277.

[82]Schueler BW. "Microscope imaging by time-of-flight secondary ion mass-spectrometry." *Microscopy Microanalysis Microstructures* **1992**, *3*, 119-139.

[83] Laiko, V.V.; Baldwin, M.A.; Burlingame, A.L. "Atmospheric pressure matrix assisted laser desorption/ionization mass spectrometry." *Anal. Chem.,* **2000**, *72*, 652-657.

[84] Koestler, M.; Kirsch, D.; Hester, A.; Leisner, A.; Guenther, S.; Spengler, B. "A high-resolution scanning microprobe matrix-assisted laser desorption/ionization ion source for imaging analysis on an ion trap/Fourier transform ion cyclotron resonance mass spectrometer." *Rapid Commun. Mass Spectrom.,* **2008**, *22*, 3275-3285.

[85] Luxembourg, S.L.; Mize, T.H.; McDonnell, L.A.; Heeren, R.M.A. "High-spatial resolution mass spectrometric imaging of peptide and protein distributions on a surface." *Anal. Chem.,* **2004**, *76*, 5339-5344.

[86] McDonnell, L.A.; Mize, T.H.; Luxembourg, S.L.; Koster, S.; Eijkel, G.B.; Verpoorte, E.; de Rooij, N.F.; Heeren, R.M.A. "Using matrix peaks to map topography: Increased mass resolution and enhanced sensitivity in chemical imaging." *Anal. Chem.,* **2003**, *75*, 4373-4381.

[87] Guilliot, S.; Chaurand, P.; Stoeckli, M. In Topographic Imaging Using Time-of-Flight Mass Spectrometry, 47th ASMS Conference, 47th ASMS Conference, Dallas, TX, 1999; 47th ASMS Conference, Dallas, TX, 1999.

[88] Kossakovski, D.A.; O'Connor, S.D.; Widmer, M.; Baldeschwieler, J.D.; Beauchamp, J.L. "Spatially resolved chemical analysis with an NSOM-based laser desorption microprobe." *Ultramicroscopy,* **1998**, *71*, 111-115.

[89] Lin, B.W.; Sunner, J. "Ion-transport by viscous-gas flow-through capillaries." *J. Am. Soc. Mass Spectrom.,* **1994**, *5*, 873-885.

[90] Tan, P.V.; Laiko, V.V.; Doroshenko, V.M. "Atmospheric pressure MALDI with pulsed dynamic focusing for high-efficiency transmission of ions into a mass spectrometer." *Anal. Chem.,* **2004**, *76*, 2462-2469.

[91] Jurchen, J.C.; Rubakhin, S.S.; Sweedler, J.V. "MALDI-MS imaging of features smaller than the size of the laser beam." *J. Am. Soc. Mass Spectrom.,* **2005**, *16*, 1654-1659.

[92] Dreisewerd, K.; Schurenberg, M.; Karas, M.; Hillenkamp, F. "Influence of the laser intensity and spot size on the desorption of molecules and ions in matrix-assisted laser-desorption ionization with a uniform beam profile." *Int. J. Mass Spectrom.,* **1995**, *141*, 127-148.

[93] Zhigilei, L.V.; Leveugle, E.; Garrison, B.J.; Yingling, Y.G.; Zeifman, M.I. "Computer simulations of laser ablation of molecular substrates." *Chem. Rev.* **2003**, *103*, 321-347.

[94] Binning, G.; Rohrer, H.; Gerber, C.; Weibel, E., "Surface studies by scanning tunneling microscopy." *Phys. Rev. Lett.,* **1982**, *49,* 57-61.

[95] Binnig, G.; Quate, C.F.; Gerber, C. "Atomic force microscope." *Phys. Rev. Lett.,* **1986**, *56***,** 930-933.

[96] Inouye, Y.; Kawata, S. "Near-field scanning optical microscope with a metallic probe tip." *Optics Lett.*, **1994**, *19*, 159-161.

[97] Zenhausern, F.; Oboyle, M. P.; Wickramasinghe, H. K. "Apperatureless near-field optical microscope." *Appl. Phys. Lett.,* **1994**, *65*, 1623-1625.

[98] Downes, A.; Salter, D.; Elfick, A."Finite element simulations of tip-enhanced Raman and fluorescence spectroscopy." *J. Phys. Chem. B*, **2006**, *110*, 6692-6698.

[99] Sanchez, E. J.; Novotny, L.; Xie, X. S. "Near-field fluorescence microscopy based on two-photon excitation with metal tips." *Physical Review Letters* **1999,** 82, 4014-4017.

[100] Hartschuh, A.; Anderson, N.; Novotny, L. "Near-field Raman spectroscopy using a sharp metal tip." *Journal of Microscopy-Oxford* **2003,** 210, 234-240.

[101] Knoll B.; Keilmann, F. "Near-field probing of vibrational absorption for chemical microscopy." *Nature* **1999,** *399,* 134-137.

[102] Becker, J. S.; Gorbunoff, A.; Zoriy, M.; Izmer, A.; Kayser, M. "Evidence of near-field laser ablation inductively coupled plasma mass spectrometry (NF-LA-ICP-MS) at nanometre scale for elemental and isotopic analysis on gels and biological samples." *J. Anal. At. Spectrom.* **2007,** *22*, 222-222.

[103] Downes, A.; Salter, D.; Elfick, A. "Heating effects in tip-enhanced optical microscopy." *Optics Express* **2006,** 14, 5216-5222.

[104] Busch, K. L. "Mass spectrometric detection for thin-layer chromatographic separations." *Tr. Anal. Chem.* **1992**, *11*, 314-324.

[105] Busch, K. L. "Mass spectrometric detectors for samples separated by planar electrophoresis." *J. Chrom. A* **1995**, *692*, 275-290.

[106] Wilson, I. D.; Morden, W. "Advance in applications in the use of HPTLC-MS-MS," *J. Planar Chromatogr.* **1996**, *9*, 84-91.

[107] Wilson, I. D. "The state of the art in thin-layer chromatography-mass spectrometry: A critical appraisal." *J. Chromatogr. A* **1999**, *856*, 429-442.

[108] Gusev, A. I. "Interfacing matrix-assisted laser desorption/ionization mass spectrometry with column and planar separation." *Fresen. J. Anal. Chem.* **2000**, *366*, 691-700.

[109] Busch, K. L. "Planar separations and mass spectrometric detection." *J. Planar Chromatogr.* **2004**, *17*, 398-403.

[110] Fuchs, B.; Süß, R.; Nimptsch, A.; Schiller, J. "MALDI-TOF-MS directly combined with TLC: A review of the current state." *Chromatographia Supplement* **2009**, *69*, S95-S105.

[111] Gocan, S. "Hyphenated techniques in thin-layer chromatography." In: *Advances in Chromatography*, Grushka, E.; Grinberg, N., Eds.; CRC Press, Boca Raton, 2009, Vol 47, pp. 354-444.

[112] Chang, T. T.; Lay, J. O.; Francel R. J. "Direct analysis of thin-layer chromatography spots by fast atom bombardment mass-spectrometry." *Anal. Chem.* **1981**, *56*, 109-111.

[113] Banno, K.; Matsuoka, M.; Takahashi, R. "Quantitative-analysis of thin-layer chromatography with secondary ion mass-spectrometry." *Chromotographia*, **1991**, *32*, 179-181.

[114] Pasilis, S. P.; Van Berkel, G. J. "Atmospheric pressure surface sampling/ionization techniques for direct coupling of planar separations with mass spectrometry." *J. Chromatogr. A*, **2009**, in press.

[115] de Koning, S.; Janssen, H-G.; Brinkman, U. A. Th. "Modern methods of sample preparation for GC analysis." *Chromatographia* **2009**, *69*, S33-S78.

[116] Morlock, G.; Schwack, W. "Determination of isopropylthioxanthone (ITX) in milk, yoghurt and fat by HPTLC-FLD, HPLTLC-ESI/MS and HPTLC-DART/MS." *Anal. Bioanal. Chem.* **2006**, *385*, 586-595.

[117] Morlock, G.; Ueda, Y. "New coupling of planar chromatography with direct analysis in real time mass spectrometry." *J. Chromatogr. A* **2007**, *1143*, 243-251.

[118] Alpmann, A.; Morlock, G. "Rapid and sensitive determination of acrylamide in drinking water by planar chromatography and fluorescence detection after derivatization with dansulfinic acid." *J. Sep. Sci.* **2008**, *31*, 71-77.

[119] Smith, N. J.; Domin, M. A.; Scott, L. T. "HRMS directly from TLC slides. A powerful tool for rapid analysis of organic mixtures." *Org. Lett.* **2008**, *10*, 3493-3496.

[120] Gallagher, R. T.; Balogh, M. P.; Davey, P.; Jackson, M. R.; Sinclair, I.; Southern, L. J. "Combined electrospray ionization-atmospheric pressure chemical ionization source for use in high-throughput LC-MS applications." *Anal. Chem.* **2003**, *75,* 973-977.

[121] Douse, J.M.F. "Dynamic headspace method for the improved cleanup of gunshot residues prior to the detection of nitroglycerine by capillary column gas-chromatography with thermal-energy analysis detection." *J. Chromatogr.* **1989***, 464,* 178-185.

[122] Guardigli, A., Chow, W., Lefar, M. S. "Determination of some acidic herbicides by thin-layer chromatography." *J. Agr. Food. Chem.* **1971**, *19*, 1181-1182.

[123] Williamson, K. L. *Macroscale and Microscale Organic Experiments,* 4th ed.; Houghton Mifflin: Boston, MA, 2003, pp 160-162.

[124] Ford, M.J.; Kertesz, V.; Van Berkel G. J. "Thin-layer chromatography/electrospray ionization triple-quadrupole linear ion trap mass spectrometry system: Analysis of rhodamine dyes separated on reversed-phase C-8 plates." *J. Mass Spectrom.* **2005***, 40***,** 866-875.

[125] Inoue, H.; Hasimoto, H.; Watanabe, S.; Iwata, Y. T.; Kanamori, T.; Miyaguchi, H.; Tsujikawa, K.; Kuwayama, K.; Tachi, N.; Uetake, N. "Thermal desorption counter-flow introduction atmospheric pressure chemical ionization for direct mass spectrometry of ecstasy tablets." *J. Mass Spectrom.* **2009**, *44*, 1300-1307.

[126] Miller, J. C.; Miller, J. N. *Statistics for Analytical Chemistry,* 2nd. Ed.; Ellis Horwood Ltd: Chichester; 1988; pp. 110-115.

[127] Miller, J. M. *Chromatography Concepts and Contrasts,* 2nd ed.*,* John Wiley and Sons, Inc.: Hoboken, NJ, 2005, pp 58-59.

[128] Ovchinnikova, O. S.; Van Berkel, G. J. "Thin-layer chromatography and mass spectrometry coupled using proximal probe thermal desorption with electrospray or atmospheric pressure ionization." *Rapid Commun. Mass Spectrom.* **2010**, *24*, 1721-1729.

[129] Chen, H.W.; Gamez, G.; Zenobi, R. "What can we learn from ambient ionization techniques?" *J. Am. Soc. Mass. Spectrom.* **2009**, *20*, 1947-1963.

[130] Alberici, R. M.; Simas, R. C.; Sanvido, G. B.; Romao, W; Lalli, P. M.; Benassi, M.; Cunha, I. B. S.; Eberlin, M. N. "Ambient mass spectrometry: Bringing MS into the "Real World"." *Anal. Bioanal. Chem.* **2010**, *398*, 265-294.

[131] Huang, M. Z.; Yuan, C. H.; Cheng, S. C.; Cho, Y. T.; Shiea, J. "Ambient ionization mass spectrometry. " *Ann. Rev. Anal. Chem.* **2010**, *3*, 43-65.

[132] Weston, D. J. "Ambient ionization mass spectrometry: Current Understanding of Mechanistic Theory; Analytical Performance and Application Areas." *Analyst* **2010**, *135*, 661-668.

[133] Van Berkel, G. J.; Kertesz, V. "Automated Sampling and Imaging of Analytes Separated on Thin-Layer Chromatography Plates Using Desorption Electrospray Ionization Mass Spectrometry." *Anal. Chem.* **2006**, *78*, 4938-4944.

[134] Ovchinnikova, O.S.; Kertesz, V.; Van Berkel, G. J. "Molecular surface sampling and chemical ionization using proximal probe thermal desorption/secondary ionization mass spectrometry." *Anal. Chem.* **2011**, *83*, 598-603.

[135] Ifa, D. R.; Wu, C.; Ouyang, Z.; Cooks, R. G. "Desorption electrospray ionization and other ambient ionization methods: current progress and preview." *Analyst,* **2010**, *135*, 669-681.

[136] Chen H.W.; Hu, B.; Zhang, X. "Fundamental principles and practical applications of ambient ionization mass spectrometry for direct analysis of complex samples." *Chin. J. Anal. Chem.* **2010**, *38*, 1069-1088.

[137] Price, D.M; Reading, M.; Hammiche, A.; Pollock, H.M. "New adventures in thermal analysis."*J. Thermal Anal. Calorimetry* **2000**, *60*, 723-733.

[138] Craig, D.; Kett, V.; Andrews, C.; Royall, P.; "Pharmaceutical applications of micro-thermal analysis." *J. Pharm. Science.* **2002**, *91,* 1201-1213.

[139] Nikiforov, M.P.; Gam, S.; Jesse, S.; Composto, R.J.; Kalinin, S.V. "Morphology mapping of phase-separated polymer films using nanothermal analysis." *Macromolecules*, **2010**, *43*,6724-6730.

[140] Nikoforov, M.P; Jesse, S.; Morozovka, A.N.; Eliseec, E.A.; Germinario, L.T.; Kalinin, S.V. "Probing the temperature dependence of the mechanical properties of polymers at the nanoscale with band excitation thermal scanning probe microscopy." *Nanotechnology,* **2009**, *20*, 395709.

[141] Lee, J.; Beechem, T.; Wright, T.L.; Nelson, B.A.; Graham, S.; King, W.P. "Electrical, thermal, and mechanical characterization of silicon microcantilever heaters." *J. Microelectromech. Syst.* **2006**, *15*, 1655-1655.

[142] Wiseman, J. M.; Ifa, D. R.; Zhu, Y.; Kissinger, C. B.; Manicke, N. E.; Kissinger, P. T.; Cooks, R. G. "Desorption electrospray ionization mass spectrometry: Imaging drugs and metabolites in tissue." *Proc. Natl. Acad. Sci.* **2008**, *105*, 18120-18125.

[143] Ifa, D. R.; Jackson, A. U.; Paglia, G.; Cooks, R. G. "Forensic applications of ambient mass spectrometry." *Anal. Bio. Chem.* **2009**, *394*, 1995-2008.

[144] Van Berkel, G. J.; Sanchez, A. D.; Quirke, J. M. E. "Thin-layer chromatography and electrospray mass spectrometry coupled using a surface sampling probe." *Anal. Chem*. **2002**, *74*, 6216-6223.

[145] Van Berkel, G. J.; Kertesz, V.; King, R. C. "High-throughput mode liquid microjunction surface sampling probe." *Anal. Chem.* **2009**, *81*, 7096-7101.

[146] Kertesz, V.; Van Berkel, G. J. "Fully automated liquid extraction-based surface sampling and ionization using a chip-based robotic nanoelectrospray platform." *J. Mass Spectrom.* **2010**, *45*, 252-260.

[147] Marshall, P.; Toteu-Djomte, V.; Bareille, P.; Perry, H.; Brown, G.; Baumert, M.; Biggadike, K. "Correlation of skin blanching and percutaneous absorption for glucocorticoid receptor agonists by matrix-assisted laser desorption ionization mass spectrometry imaging and liquid extraction surface analysis with nanoelectrospray ionization mass spectrometry." *Anal. Chem.* **2010**, *82,* 7787-7794.

[148] Kertesz, V.; Van Berkel, G. J. "Liquid microjunction surface sampling coupled with high performance liquid chromatography-electrospray ionization mass spectrometry for analysis of drugs and metabolites in whole-body thin tissue sections." *Anal. Chem.* **2010**, *82*, 5917-5921.

[149] Walworth, M. J.; Stankovich, J. J.; Van Berkel, G. J.; Schulz, M.; Minarik, S.; Nichols, J.; Reich, E. "Hydrophobic treatment enabling analysis of wettable surfaces using a liquid microjunction surface sampling probe/electrospray ionization-mass spectrometry system." *Anal. Chem.* **2011**, *83*, 591-597.

[150] Van Berkel, G. J.; Kertesz, V.; Koeplinger, K. A.; Vavrek, M.; Kong, A.-N. T. "Liquid micro-junction surface sampling probe electrospray mass spectrometry for detection of drugs and metabolites in thin tissue sections." *J. Mass Spectrom.* **2008**, *43*, 500-508.

[151] Roach, P. J.; Laskin, J.; Laskin, A. "Nanospray desorption electrospray ionization: An ambient method for liquid-extraction surface sampling in mass spectrometry." *Analyst* **2010**, *135*,:2233-2236.

[152] Hecht, E. *Optics*, 4th ed.; Addison Wesley, San Fransico, CA, 2002, 595.

[153] Zeisel, D.; Dutoit, B.; Deckert, V.; Roth, T.; Zenobi, R. "Optical spectroscopy and laser desorption on a nanometer scale." *Anal. Chem.* **1997**, *69*, 749-754.

[154] Shrestha, B.; Vertes, A. "In situ metabolic profiling of Single cells by laser ablation electrospray ionization mass spectrometry." *Anal. Chem.* **2009**, *81*, 8265-8271.

[155] Inutan, E. D.; Richards, A. L.; Wager-Miller, J.; Mackie, K.; McEwen, C. N.; Trimpin, S. "Laserspray ionization - A new method for protein analysis directly from tissue at atmospheric pressure with ultra-high mass resolution and electron transfer dissociation." *Mol. Cell. Proteomics* **2011**, *10,* doi:10.1074/mcp.M110.000760.

[156] Koestler, M.; Kirsch, D.; Hester, A.; Leisner, A.; Guenther, S.; Spengler B. "A high-resolution scanning microprobe matrix-assisted laser desorption/ionization ion source for imaging analysis on an ion trap/fourier transform ion cyclotron resonance mass spectrometer" *Rapid Comm. Mass Spectrom.* **2008**, *22*, 3275-3285.

[157] Van Berkel, G. J.; Kertesz, V. "Automated sampling and imaging of analytes separated on thin-layer chromatography plates using desorption electrospray ionization mass spectrometry." *Anal. Chem.* **2006**, *78*, 4938-4944.

[158] Kertesz, V.; Van Berkel, G. J. "Liquid microjunction surface Sampling Coupled with High Performance Liquid Chromatography-Electrospray Ionization Mass Spectrometry for Analysis of Drugs and Metabolites in Whole-Body Thin Tissue Sections." *Anal. Chem.* **2010**, *82*, 5917-5921.

[159] Van Berkel, G. J.; Sanchez, A. D.; Quirke, J. M. E. "Thin-layer chromatography and electrospray mass spectrometry coupled using a surface sampling probe." *Anal. Chem*. **2002**, *74*, 6216-6223.

[160] Emmert-Buck, M. R.; Bonner, R. F.; Smith, P. D.; Chuaqui, R. F.; Zhuang, Z.; Goldstein, S. R.; Weiss, R. A.; Liotta, L. A. "Laser capture microdissection." *Science* **1996**, *274*, 998-1001.

[161] Bonner, R. F.; Emmert-Buck, M. R.; Cole, K.; Pohida, T.; Chuaqui, R. F.; Goldstein, S. R.; Liotta, L. A. "Laser capture microdissection: Molecular analysis of tissue." *Science* **1997**, *278,* 1481-1483.

[162] http://www.zeiss.de/microdissection/, last visited on January 4, 2011.

[163]http://www.leica-microsystems.com/products/light-microscopes/life-science-research/laser-microdissection/, last visited on January 4, 2011.

[164] Yang, G. W. "Laser ablation in liquids: Applications in the synthesis of nanocrystals." *Prog. Mat. Sci.* **2007**, *52*, 648-698.

APPENDIX

Solvents Dyes. The same test dye mixture used in the metric studies above containing, solvent blue 35, solvent green 3 and Sudan Red 7B was spotted as a series of tightly spaced spots containing ~ 1 μg of material per spot and separated on a normal-phase HPTLC-HLF silica gel plate. Panel (a) in Figure S1 shows a picture of the development lane on the plate with the compounds well separated. To acquire the mass spectral data shown in panels (b) – (e), the TLC plate was scanned (300 μm/s) from low to high R_F (left to right in the picture) relative to the heated proximal probe (350 ^oC) while monitoring in positive ion mode APCI the *m/z* ratios for the protonated molecules of the three dyes. The summed SIM ion current profile is shown in panel (b) and the individual SIM profiles are shown in panels (c) solvent blue 35 (*m/z* 351), (d) solvent green 3 (*m/z* 419), and (e) Sudan Red 7B (*m/z* 380). While the three compounds were present in near equal amounts on the plate, signal intensity of solvent green 3 was lower compared to the two other dyes. As the three compounds have similar volatilities Table 1, the observed signal intensity difference might relate to an ionization efficiency difference or an issue with mass spectral detection optimization.

Using this set of data, we also compared chromatographic resolutions obtained by TLC or MS. Chromatographic resolution, *R*, of two chromatographic bands was calculated using eq. 2, From the optical data obtained using the photograph of the plate in Figure 3a, the chromatographic resolution for the TLC separation of solvent blue 35 and solvent green 3 was calculated as ($R_{B/G}$) = 1.97 and for solvent green 3 and Sudan Red 7B as ($R_{G/R}$) = 1.31. From the mass spectral data in Figure 3c-e we calculated ($R_{B/G}$) = 2.13 and ($R_{G/R}$) = 1.42, or about 8% poorer apparent chromatographic resolution. This

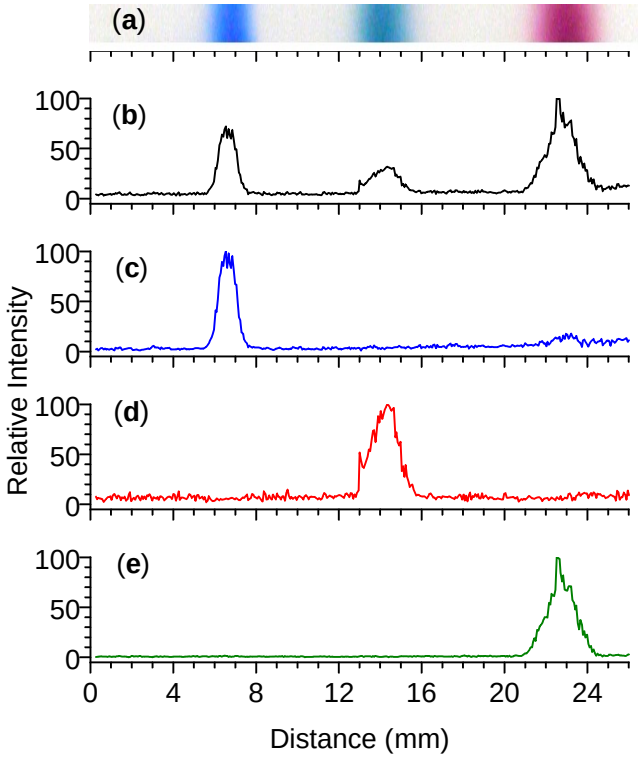

Figure S1. (a) Photograph of glass backed normal-phase silica gel plates with organic binder and UV 254 indicator (HPTLC-HLF) development lane showing the separated bands of a three component solvent dye mixture containing solvent blue 35, solvent green 3 and Sudan Red 7B. The positive ion mode APCI ion current chromatograms obtained while scanning the development lane (300 μm/s) relative to the heated probe (350 ^{o}C) are (b) the summed ion current from the SIM mass chromatograms for each of the dyes and the individual SIM chromatograms for (c) solvent blue 35 (*m/z* 351), (d) solvent green 3 (*m/z* 419), and (e) Sudan Red 7B (*m/z* 380). SIM dwell time was 100 ms for each *m/z* monitored.

was considered good agreement considering the difficultly in accurately determining the extent of the bands of the plate by simple visual observation.

Herbicides. A mixture of three structurally related herbicides, namely, 2,4-D, 2,4,5-T, and 4-(2,4-DB) was spotted in a series of closely spaced spots with 10 μg of material per spot and separated on a normal-phase HPTLC-HLF silica gel plate. Panel (a) in Figure S2 shows a picture of the development lane illustrating that only two obvious bands are visible on the plate. As the mass spectral data below show, only two bands are apparent because two of the three components did not completely separate. To acquire the mass spectral data shown in panels (b) – (e), the HPTLC plate was scanned (200 μm/s) from low to high R_F (left to right in the picture) relative to the heated probe (350 ^oC). In this case, negative ion mode APCI was used for ionization and the compounds were observed as the deprotonated molecules, $(M-H)^-$. The summed SIM ion current profile is shown in panel (b) and the individual SIM profiles are shown in panels (c) 2,4-D (*m/z* 219), (d) 2,4,5-T (*m/z* 253), and (e) 4-(2,4-DB) (*m/z* 247). The three herbicides were distinct in the mass spectral data, 2,4-D and 2,4,5-T had very similar R_f values thus appearing as one band when viewing the photograph of the development lane.

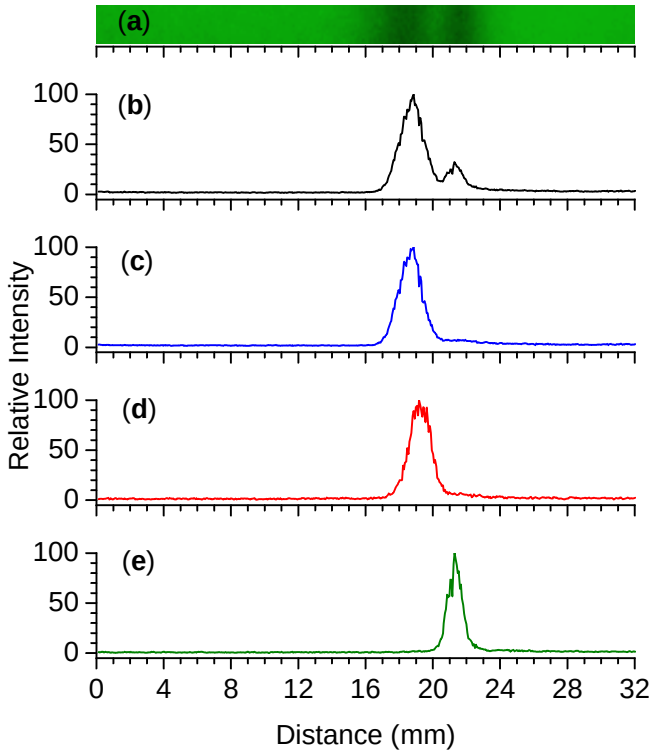

Figure S2. (a) Photograph of glass backed normal-phase silica gel plates with organic binder and UV 254 indicator (HPTLC-HLF) development lane showing the separated bands of a three component herbicide mixture containing 2,4-D, 2,4,5-T and 4-(2,4-DB). The negative ion mode APCI ion current chromatograms obtained while scanning the development lane (200 μm/s) relative to the heated probe (350 ^{o}C) are (b) the summed ion current from the SIM mass chromatograms for each of the herbicides and the individual SIM chromatograms for (c) 2,4-D (*m/z* 219), (d) 2,4,5-T (*m/z* 253), and (e) 4-(2,4-DB) (*m/z* 247). SIM dwell time was 100 ms for each *m/z* monitored.

Explosives. A mixture of three explosives, viz., HMX, RDX, and TNT, was spotted as a series of tightly spaced spots containing 1 μg of material per spot and separated on a glass backed ProteoChrom HPTLC silica gel 60 plate. Panel (a) in Figure S3 shows a picture of the development lane with three distinct bands. To acquire the mass spectral data shown in panels (b) – (e), the HPTLC plate was scanned (100 μm/s) from low to high R_F (left to right in the picture) relative to the heated probe (350 ^oC). Negative ion mode APCI was again used for detection, but in this case methylene chloride was sprayed (2 μL/min) into the source region via the ESI probe. In the APCI plasma this led to the production of Cl^- anions that were used to form the $(M + {}^{35}Cl)^-$ adducts of HMX and RDX as has been previously demonstrated.[1] TNT was detected as $(M-H)^-$. The summed SIM ion current profile for the explosives is shown in panel (b) and the individual SIM profiles are show in panels (c) HMX (*m/z* 331), (d) RDX (*m/z* 257), and (e) TNT (*m/z* 226). The most intense signal was observed for TNT, which is the most volatile of these three explosives Table 1. In contrast, HMX, the least volatile of the three explosives, showed the lowest signal intensity.

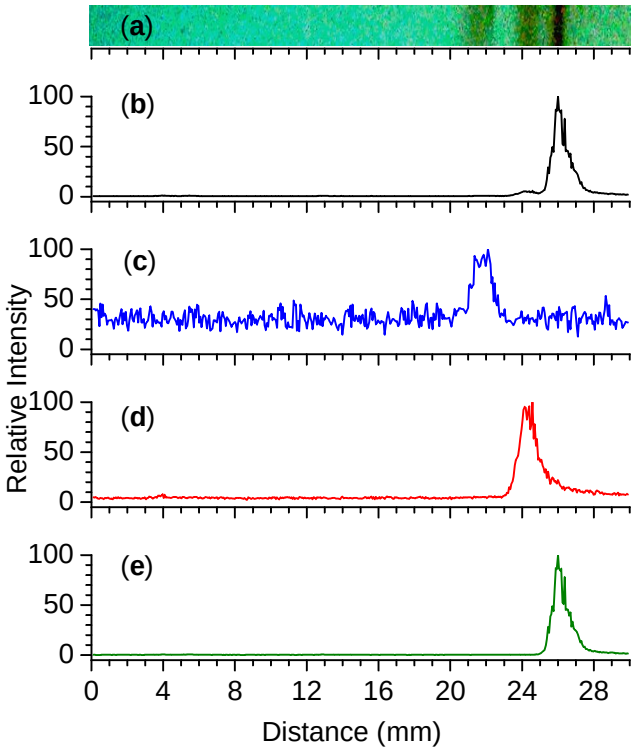

Figure S3. (a) Photograph of glass backed normal-phase HPTLC plates (ProteoChrom HPTLC silica gel 60 F_{254}) development lane showing the separated bands of a three component explosives mixture containing HMX, RDX and TNT. The negative ion mode APCI ion current chromatograms obtained while scanning the development lane (100 µm/s) relative to the heated probe (350 ^{o}C) are (b) the summed ion current from the SIM mass chromatograms for each of the explosives and the individual SIM chromatograms for (c) HMX (*m/z* 331), (d) RDX (*m/z* 257), and (e) TNT (*m/z* 226). Methelyne chloride was sprayed in at 2 µL/min. SIM dwell time was 200 ms for each *m/z* monitored.

VITA

Olga Sergeevna Ovchinnikova was born on June 16, 1983 in St. Petersburg, Russia. She moved to the United States in 1991 where she graduated from Farragut High School in Knoxville, TN in May of 2001. She then attended the University of Tennessee, Knoxville where she graduated from in May of 2005 with a Summa Cum Laude Bachelors of Science degree in Academic Physics and a Minor in Chemistry. She then attended the University of Tennessee, Knoxville graduate program in physics, where she worked under the direction of Dr. Robert N. Compton in his Chemical Physics group. She received her Masters of Science Degree in December of 2006 in Chemical Physics for her work on Photochemical Reactions of Fullerenes**.** Afterwards she began her Ph.D. research in the Organic and Biological Mass Spectrometry group at the Oak Ridge National Laboratory with Dr. Gary J. Van Berkel in the field of mass spectrometry based chemical imaging. She will receive her Ph.D. in May of 2011 in Physics with a concentration in Chemical Physics for her work on Spatially Resolved Laser and Thermal Desorption/Ionization Coupled with Mass Spectrometry.